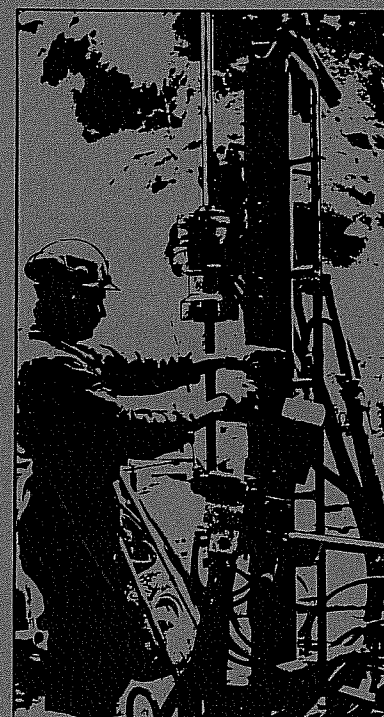


SWEDISH-AMERICAN COOPERATIVE  
PROGRAM ON RADIOACTIVE WASTE STORAGE IN  
MINED CAVERNS IN CRYSTALLINE ROCK



Technical Project Report No. 6

**A PILOT HEATER TEST IN THE  
STRIPA GRANITE**

Hans Carlsson  
Division of Rock Mechanics  
University of Luleå  
Luleå, Sweden

August 1978

A Joint Project of

Swedish Nuclear Fuel Supply Co.  
Fack 10240 Stockholm, Sweden

Operated for the Swedish  
Nuclear Power Utility Industry

Lawrence Berkeley Laboratory  
Earth Sciences Division  
University of California  
Berkeley, California 94720, USA

Operated for the U.S. Department of  
Energy under Contract W-7405-ENG-48

This report was prepared as an account of work sponsored by the United States Government and/or the Swedish Nuclear Fuel Supply Company. Neither the United States nor the U.S. Department of Energy, nor the Swedish Nuclear Fuel Supply Company, nor any of their employees, nor any of their contractors, subcontractors, or their employees, makes any warranty, express or implied or assumes any legal liability or responsibility for the accuracy, completeness or usefulness of any information, apparatus, product or process disclosed, or represents that its use would not infringe privately owned rights.

Printed in the United States of America  
Available from  
National Technical Information Service  
U.S. Department of Commerce  
5285 Port Royal Road  
Springfield, VA 22161  
Price: \$8.00 Printed Copy

A PILOT HEATER TEST IN THE STRIPA GRANITE

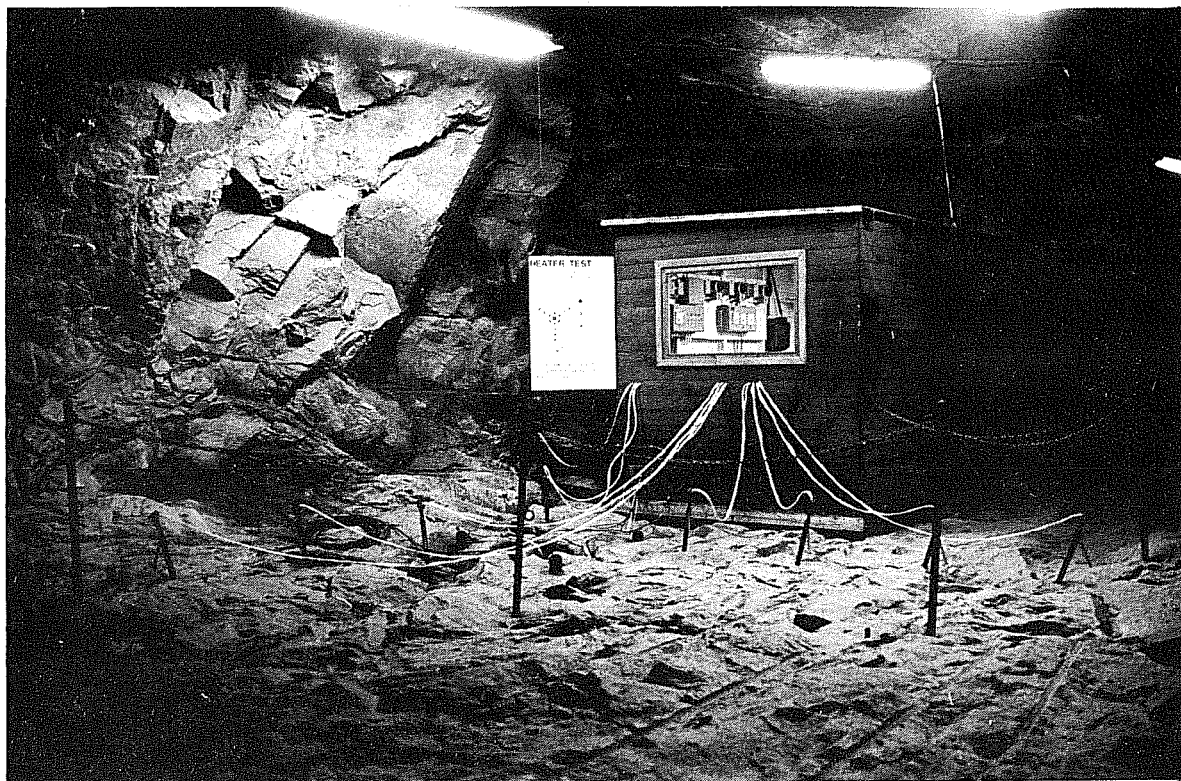
Hans Carlsson

Division of Rock Mechanics

University of Luleå

Luleå, Sweden

August 1978



XBB 788-9877



## PREFACE

This report is one of a series documenting the results of the Swedish-American cooperative research program in which the cooperating scientists explore the geological, geophysical, hydrological, geochemical, and structural effects anticipated from the use of a large crystalline rock mass as a geologic repository for nuclear waste. This program has been sponsored by the Swedish Nuclear Power Utilities through the Swedish Nuclear Fuel Supply Company (SKBF), and the U. S. Department of Energy (DOE) through the Lawrence Berkeley Laboratory (LBL).

The principal investigators are L. B. Nilsson and O. Degerman for SKBF, and N. G. W. Cook, P. A. Witherspoon, and J. E. Gale for LBL. Other participants will appear as authors of subsequent reports.

Previously published technical reports are listed below.

1. *Swedish-American Cooperative Program on Radioactive Waste Storage in Mined Caverns* by P. A. Witherspoon and O. Degerman.  
(LBL-7049, SAC-01)
2. *Large Scale Permeability Test of the Granite in the Stripa Mine and Thermal Conductivity Test* by Lars Lundström and Håken Stille.  
(LBL-7052, SAC-02)
3. *The Mechanical Properties of the Stripa Granite* by Graham Swan.  
(LBL-7074, SAC-03)
4. *Stress Measurements in the Stripa Granite* by Hans Carlsson.  
(LBL-7078, SAC-04)
5. *Borehole Drilling and Related Activities at the Stripa Mine* by P. J. Kurfurst, T. Hugo-Persson and G. Rudolph.  
(LBL-7080, SAC-05)



	CONTENTS	Page
	SUMMARY	
1	INTRODUCTION	1
2	LOCATION AND GEOLOGICAL DESCRIPTION OF THE TEST SITE	3
3	MECHANICAL AND PHYSICAL PROPERTIES OF THE STRIPA GRANITE	8
4	TECHNICAL DESCRIPTION OF THE PILOT HEATER TEST	12
4.1	General design of the heater test	12
4.2	Determination of <u>in situ</u> stresses	12
4.3	Detailed design of the heater test	15
4.4	Construction of the heaters	20
4.5	Stress measuring device	22
4.6	Temperature measuring device	27
4.7	Displacement measuring device	27
5	ACCOMPLISHMENT OF THE HEATER TEST	29
5.1	General comments	29
6	MEASURED TEMPERATURE RISE OF THE MAIN HEATER	31
6.1	Temperature as a function of time	31
6.2	Comments on measured data	31
7	MEASURED TEMPERATURE CHANGES IN THE GRANITE	34
7.1	General comments	34
7.2	Temperatures as a function of time	34

		Page
7.3	Temperatures as a function of radius from the main heater	34
7.4	Temperatures in the peripheral heater holes	40
7.5	Calculation of the heat conductivity, $\lambda$	40
7.6	Comments on measured data	41
8	MEASURED STRESS CHANGES IN THE GRANITE	44
8.1	General comments	44
8.2	Stress changes as a function of time	45
8.3	Stress changes as a function of radius from the main heater	45
8.4	Thermally induced principal stresses	45
8.5	Comments on measured data	86
9	MEASURED DISPLACEMENTS OF MAJOR FRACTURES	91
9.1	General comments	91
9.2	Displacements as a function of time	91
9.3	Comments on measured data	91
10	MEASURED WATER INFLOW IN THE PERIPHERAL HEATER HOLES	95
10.1	General comments	95
10.2	Water inflow as a function of time	95
10.3	Comments on measured data	95
11	ACKNOWLEDGMENTS	97
12	REFERENCES	98

	Page
APPENDIX I	100
The transient heat distribution from a cylindrical heater in rock	
Göran Bäckblom	
APPENDIX II	116
Predicted rock stresses for the pilot heater test at Stripa mine	
Bengt Leijon	
APPENDIX III	135
<u>In situ</u> determination of the thermal conductivity of the Stripa granite	
Bengt Leijon	



## SUMMARY

In the Stripa mine, situated in the central part of Sweden, a pilot heater test has been carried out at 348 m level. The type of rock is a granite with a rather high frequency of fractures. A central main heater with a length of 3 m, a diameter of 30 cm and a total power of 6 kW was placed at the bottom of a 10 m deep borehole. At different radial distances, varying from .85 m up to 2.95 m from the heater, stress and temperature changes were monitored. Additional measurements of movements along major fractures on the surface and changes of water inflow in boreholes were carried out.

In order to simplify the boundary conditions in a FEM-analysis, the in situ, three-dimensional, principal stresses were determined, using the Leeman over-coring method in a 20 m long borehole close to the test site. Based on the results from these measurements, all holes were drilled parallel to  $\sigma_3$ , i.e., all stress- and temperature measurements were taken in the  $\sigma_1$ - $\sigma_2$ -plane. Heating of the rock lasted for a period of 69 days, when the power was turned off to monitor the cooling effects of the rock.

The results of the heater test can be summarized as follows:

- The measured temperature distribution compares fairly well with the predicted. A maximum temperature of 333.9<sup>o</sup>C was measured on the heater just before it was turned off. The maximum temperature in the rock, as measured 0.85 m from the axis of the heater, was 102.7<sup>o</sup>C.
- The thermal isotropy is affected very little by fractures in the rock.
- By using data from the cooling period of the experiment, the thermal conductivity of the rock mass has been calculated to  $\lambda=4.8$  W/m<sup>o</sup>C.

- The thermally induced stresses in the rock mass do not correspond well with the predicted values. The predicted stresses are much higher than the measured, normally a factor of 3 to 8. A stress anisotropy is found to be prominent close to the heater.
- Results of measurements in boreholes of the in situ modulus are found to be about half of the laboratory determinations. No change in modulus is observed in either non-heated or heated rock.
- Displacements of major fractures on the floor of the test drift are very small. A maximum change in aperture of  $14 \times 10^{-6}$  m has been measured.
- Water inflow in boreholes is measured to be lower for the duration of the heater test.

## INTRODUCTION

In order to solve the problems with nuclear waste storage, the Swedish nuclear power industry organized the Nuclear Fuel Safety Company (KBS) during the late fall of 1976. Some of the research was performed at Stripa, an abandoned iron ore mine in the central part of Sweden. Adjacent to the abandoned ore is a large granite body in which all experiments have been carried out. The studies presented in this report are made for the KBS project. A cooperative program was developed when a contract between US ERDA and SKBF (Swedish Nuclear Fuel Supply Company) was signed during the spring of 1977. The Swedish part of the program was developed by KBS and the US part is carried out by LBL (Lawrence Berkeley Laboratory).

The research program is concentrated on two major tasks: a full scale heater test and a time-scaled heater test. In both cases cylindrical canisters containing electrical heater elements are used to simulate the heat output by radioactive decay of nuclear waste canisters. For a period of two years, temperature, stress and displacements will be measured in the rock. In connection with the heater tests, an extensive geophysical and hydrological program will be carried out.

A pilot heater test has been accomplished by the Division of Rock Mechanics, University of Luleå for the KBS project. The purpose of the test was to determine stress- and temperature changes around a cylindrical heater in the rock. Measurements of displacements along major fractures were also performed.

The pilot heater test was scheduled for a test period of five months, where two months were planned for heating and three for cooling.

This report contains three appendixes. The first is an analytical solution to the problem of heat distribution

from a cylindrical heater in rock, written by Göran Bäckblom. Appendix II deals with the stress distribution in the rock mass surrounding a heater, written by Bengt Leijon. The third appendix, also written by Bengt Leijon, is about the in situ determination of thermal conductivity of the Stripa granite.

## 2 LOCATION AND GEOLOGICAL DESCRIPTION OF THE TEST SITE

The Stripa test site is located in a granite which is representative for the serorogenic Precambrian granites in the Central part of Sweden.

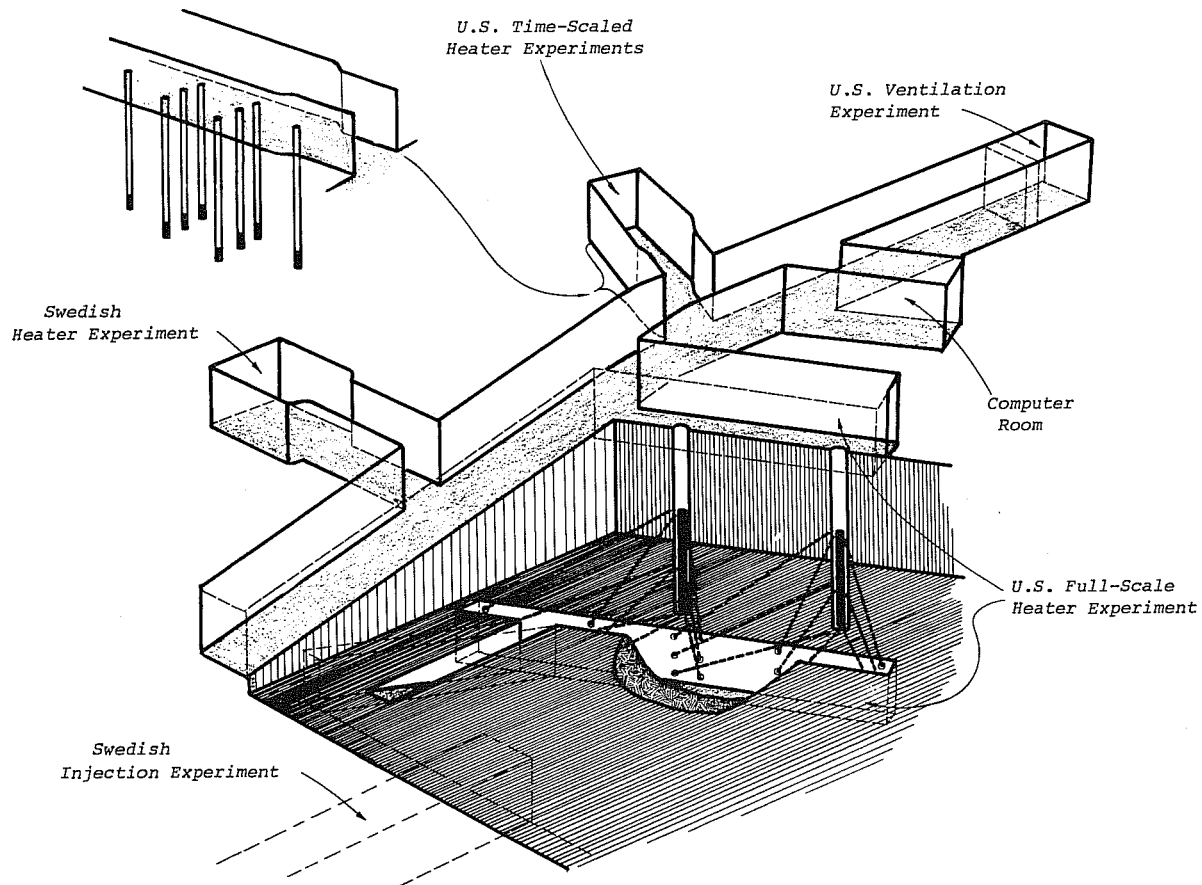
A schematic picture of the test site is shown in Fig. 2.1. All drifts have been excavated using a smooth wall blasting technique in order to minimize damage to the rock. The dimensions of the drift where the Swedish heater test was performed is 10 m x 7 m x 4 m, and its longest axis is orientated almost in the east-west direction (Fig. 2.1).

The Swedish Geological Survey (SGU) has been responsible for most of the geological investigations in the Stripa area. According to the investigations [4], the reddish type of the Stripa Granite consists of 44% quartz, 39% plagioclase, 12% microcline, 3% chlorite and 2% muscovite. The grain size is in average approximately 3 mm and varies between 1 and 5 mm.

On the southern wall of the Swedish test drift is a "lens" of syenite a few meters wide, consisting mainly of plagioclase and microcline. Accessory minerals such as chlorite, quartz and muscovite can also be observed.

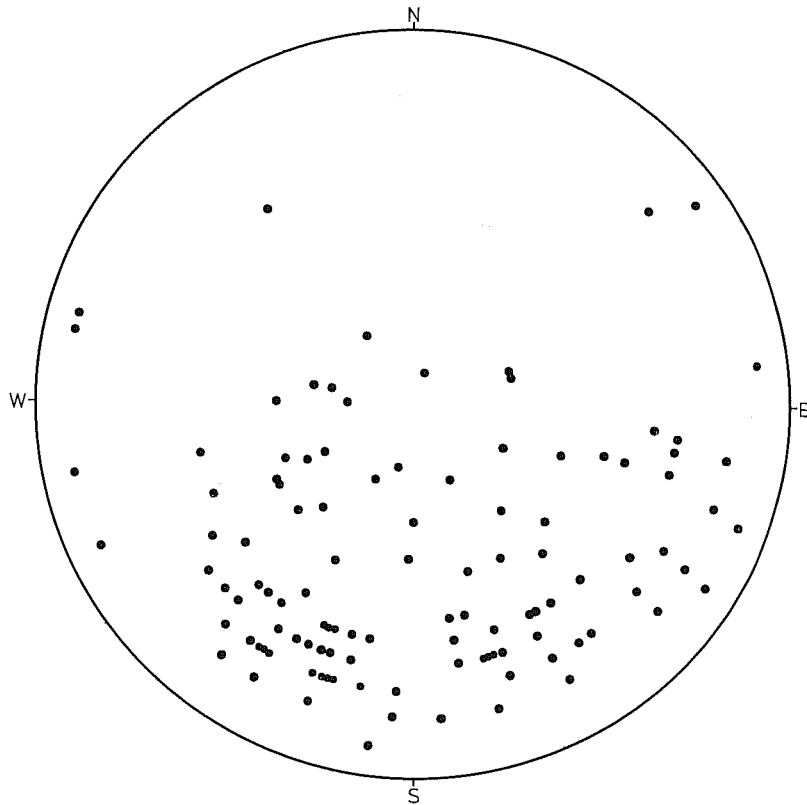
In the west rear wall of the test drift is a diabase dike with a strike of NNW. The dip is steep towards the east. In order to avoid the influence of the dike to the subsequently induced thermal stresses and displacements, the borehole configuration of the heater test was moved closer to the entrance of the drift.

Results from the fracture mapping of the main tunnel which connects the different test drifts are shown in Fig. 2.2. As can be seen in the figure, the fractures have a more or less random orientation.



XBL 7711-10802

Fig. 2.1 The test site in the Stripa granite (after Witherspoon et al.).

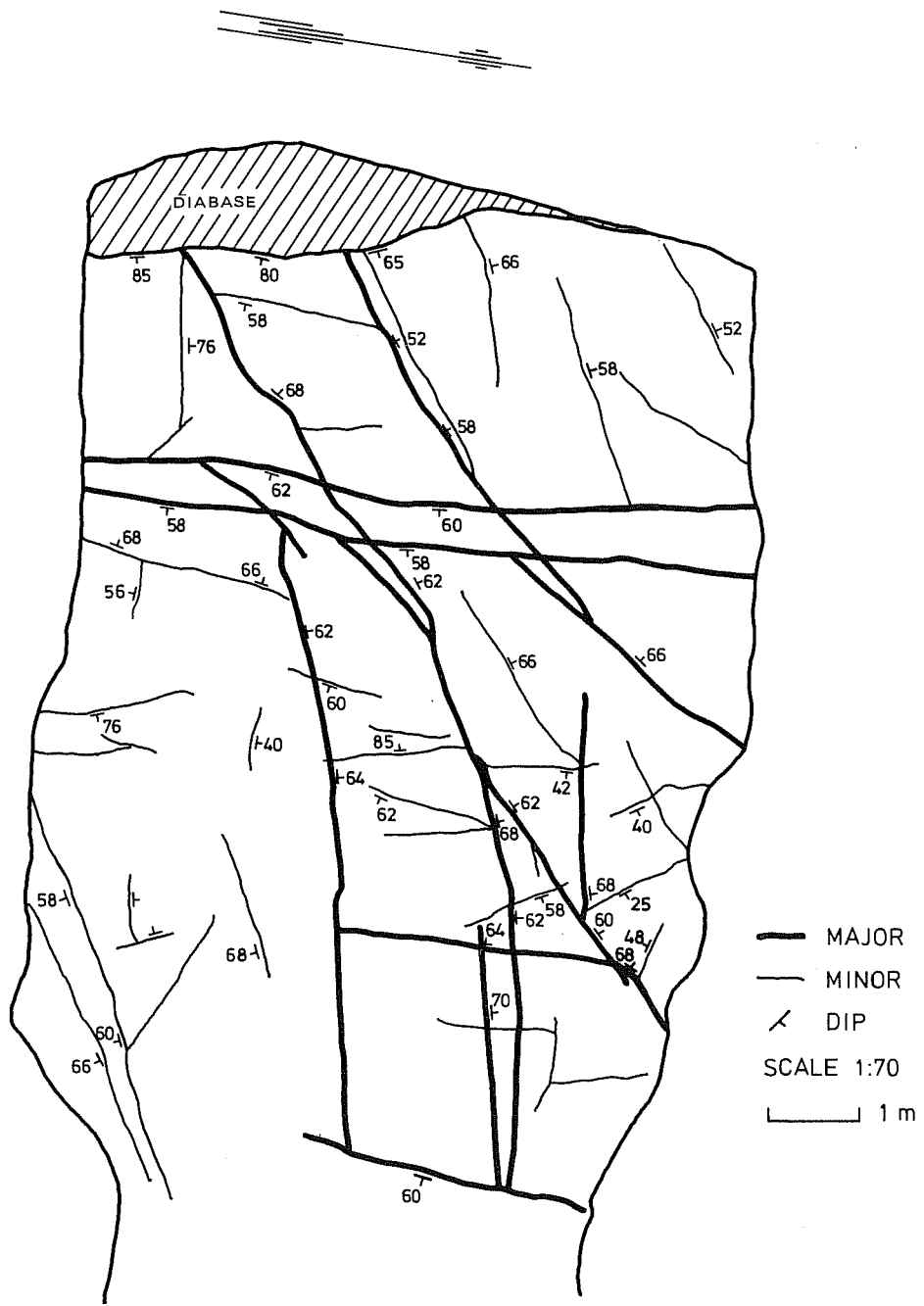


XBL 788-10151

Fig 2.2 Stereographic projection of joint surfaces from the main tunnel of the test site. (Data from Olkiewicz, et al., 1978).

A fracture map of the floor of the Swedish test drift is shown in Fig 2.3. The major fractures have a strike varying from N-S to N90E. Those fractures with a strike of NE to ENE are dipping  $60^{\circ}$ - $70^{\circ}$  towards north while the fractures with a strike in north-south are parallel to the diabase dike and the dip is essentially steep towards E.

The drill cores from drilling in the test drift show occasional highly fractured zones with mainly chlorite and calcite fillings of the joints. Open fractures can also be observed in the cores. These joints have normally a calcite or chlorite coating. In some cases epidot coating is observed. The TV- and borehole-periscope logging of the holes shows that the open fractures are very few and normally have a width of 0.2-0.6 mm. Occasionally the width reaches 1 mm. The results of the logging are described in detail in a consultant report of Hagconsult [2].



XBL 788-10152

Fig 2.3

Fractures in the floor of the heater test site.

### 3 MECHANICAL AND PHYSICAL PROPERTIES OF THE STRIPA GRANITE

The mechanical properties of the Stripa granite have been determined by the Division of Rock Mechanics, University of Luleå. The results are described in detail in a report for the KBS project [7]. Below a summary is given of Young's Modulus, Poisson's Ratio and the failure load in uniaxial compression at different temperatures.

Table 3.1 Mechanical and elastical properties of Stripa Granite

Temp [°C]	Young's Modulus [GPa]	Poisson's Ratio	Uniaxial Compressive Strength [MPa]
20	69.4	0.21	207.6
50	71.2	0.21	208.2
100	62.4	0.20	221.3
150	57.2	0.16	205.0
200	50.8	0.13	148.0

As shown in Table 3.1, the values of the parameters are lowered as the temperature is raised.

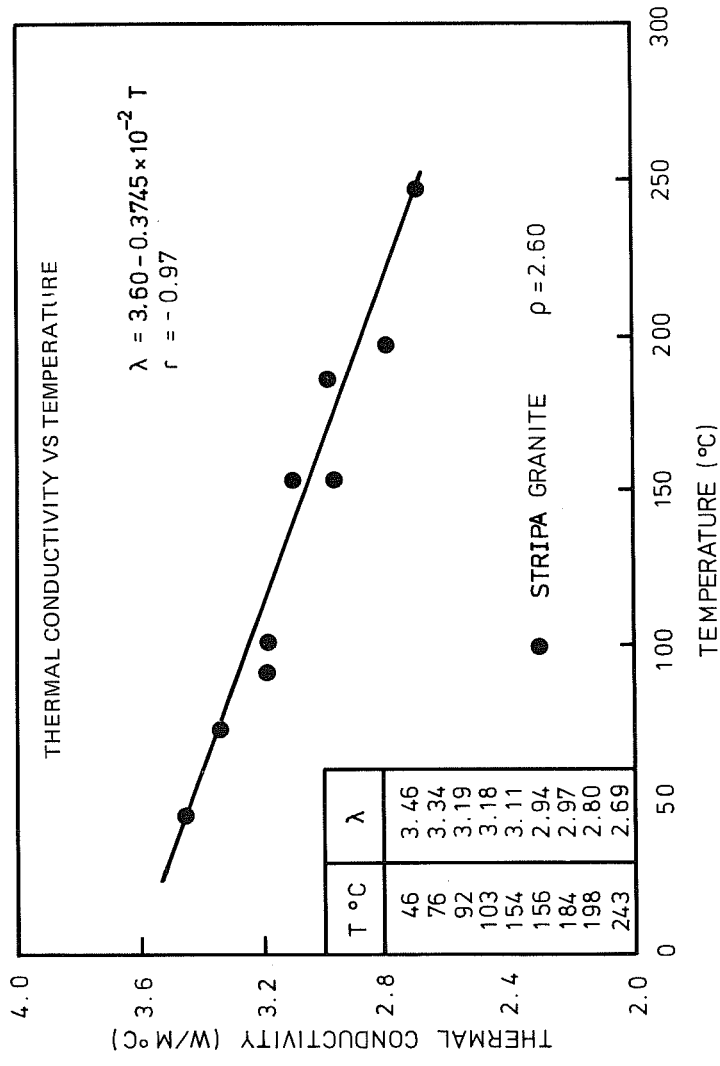
The thermal properties of the Stripa granite have been determined by TerraTek, Salt Lake City, USA as described in [5]:

Thermal conductivity,  $\lambda = 3.60 - 0.3745 \cdot 10^{-2}T$  (W/m°C),  
(see Fig 3.1).

Coefficient of thermal expansion,  $\alpha = 1.11 \cdot 10^{-5}(1/°C)$   
(see Fig 3.2)

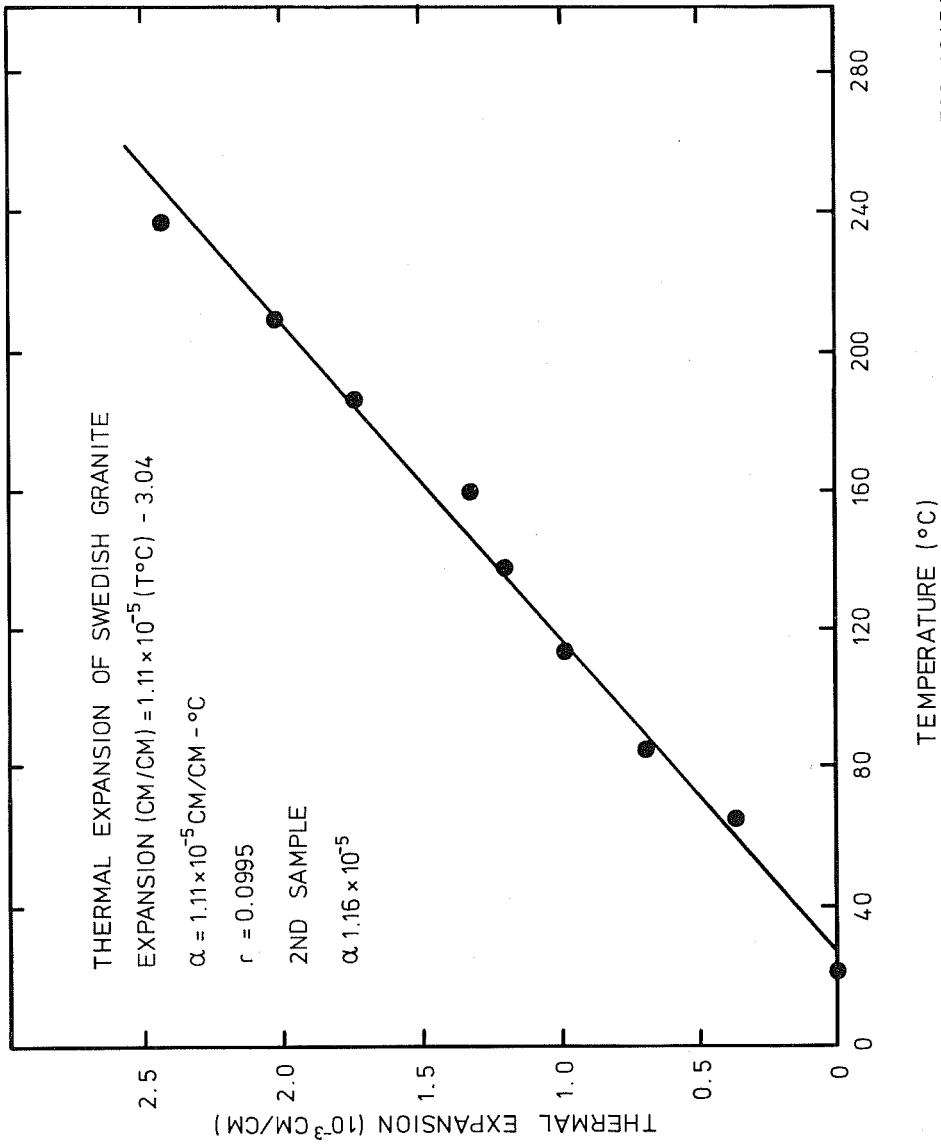
Specific heat:

$T = 113^{\circ} - 31^{\circ}C$	0.197 cal/g °C
$T = 157^{\circ} - 35^{\circ}C$	0.197 cal/g °C
$T = 230^{\circ} - 43^{\circ}C$	0.200 cal/g °C



XBL 788-10153

Fig 3.1 Thermal conductivity vs temperature of the Stripa granite (after Pratt et al., 1977).



XBL 788-10154

Fig 3.2 Thermal expansion of the Stripa granite (after Pratt et al., 1977).

Other properties of the Stripa granite are:

Density	2.600 g/cm <sup>3</sup>
Porosity	1.7 %
Permeability	< 17 · 10 <sup>-5</sup> md; laboratory determination see [5]  0.4 · 10 <sup>-10</sup> m/s at rock temp ~ +10°C 0.2 · 10 <sup>-10</sup> m/s at rock temp ~ +35°C; <u>in situ</u> determination, see [3]

## 4 TECHNICAL DESCRIPTION OF THE PILOT HEATER TEST

### 4.1 General design of the heater test

A schematic picture of the hole configuration for the heater test is shown in Fig. 4.1. Temperature and stress changes were monitored at a minimum radial distance of 0.85 m and a maximum radial distance of 2.95 m from a main heater, surrounded by three peripheral heaters.\* Measurements of displacements of major fractures on the floor surface of the test drift have also been performed.

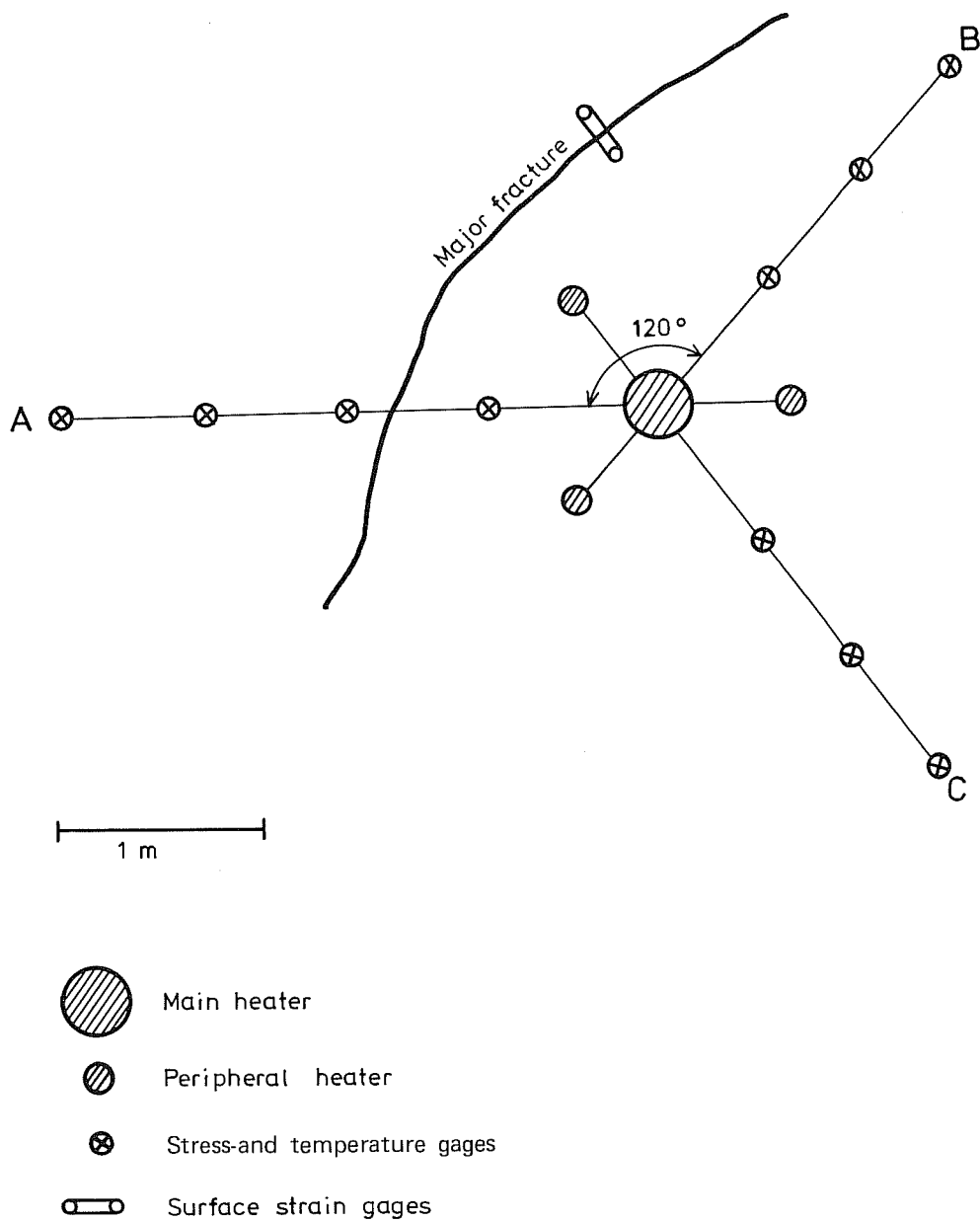
In order to determine the site isotropy of the thermal and mechanical properties, measurements of stress and temperature changes have been made in three separate radial directions from the axis of the main heater. To facilitate further discussions in this report the different directions are hereafter referred to as A, B and C respectively (see Fig 4.1).

### 4.2 Determination of in-situ stresses

In order to facilitate the boundary conditions in the numerical calculations, it was decided to orient the heater test so that all measurements were performed in the in situ  $\sigma_1$ - $\sigma_2$  plane, i.e. all boreholes should be drilled parallel to the least principal stress  $\sigma_3$ . Furthermore, it was decided to locate all measurement points in the midplane of the heater. The in situ stresses were determined by the Division of Rock Mechanics, University of Luleå. The measurements were based upon the Leeman three dimensional overcoring principle. A 20 m, subhorizontal borehole (see Fig 4.2) was used to determine the stress tensor at 19 data points along the hole. A detailed description of the results is given in [1].

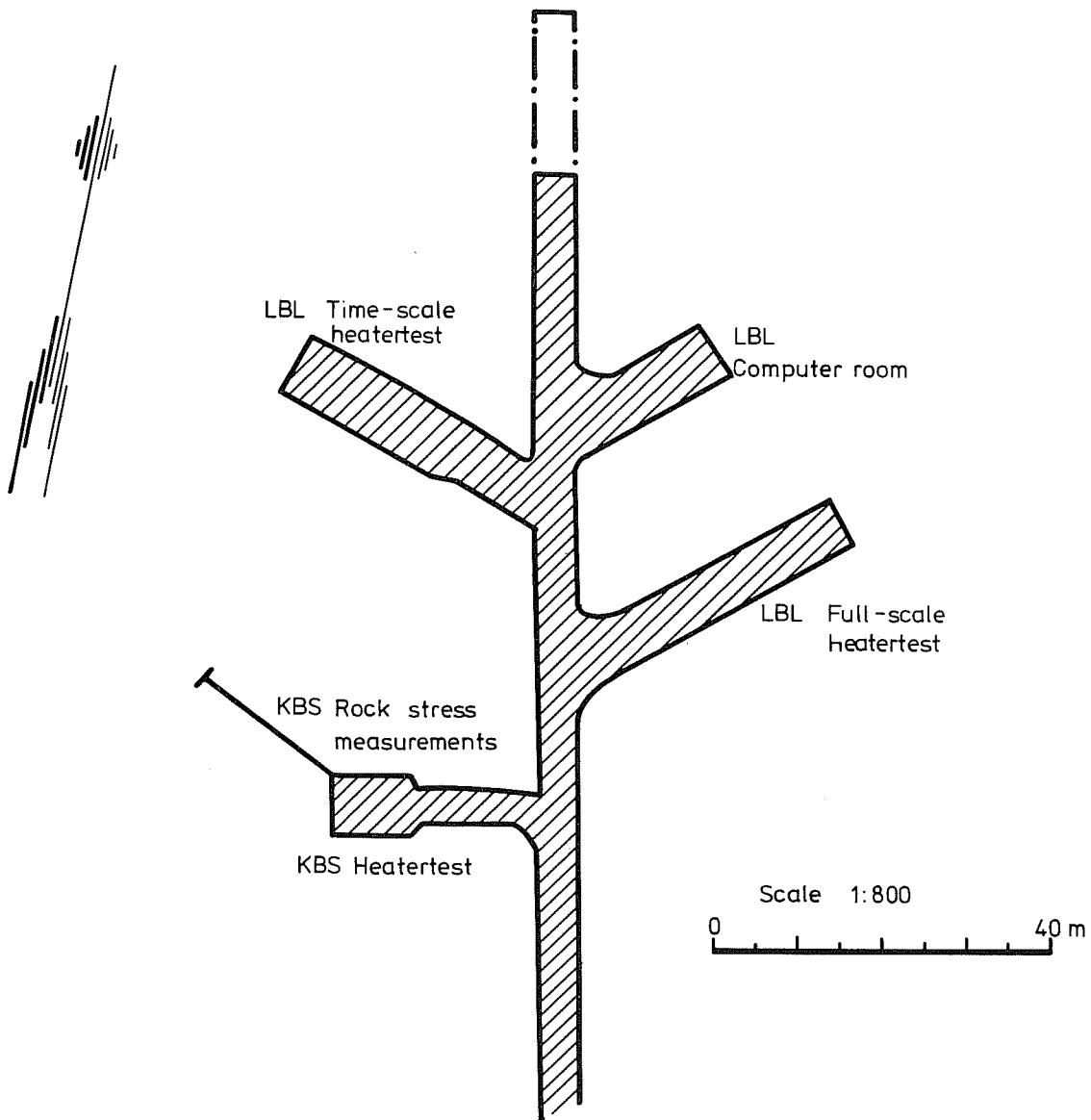
---

\*The purpose of the peripheral heaters is to heat a greater volume of the rock.



XBL 788-10155

Fig 4.1 Principal arrangement of the heater test in Stripa. Figure 5.1 relates the heater test location to the test drift and fracture network.



XBL 788-10156

Fig 4.2 Direction of the subhorizontal borehole for rock stress measurements on the 348 m level, indicating KBS test site for pilot heater test.

In summary, the following stresses were obtained:

- The main principal stress  $\sigma_1$  has a magnitude of 20.0 MPa and is dipping  $31^\circ$  in the direction of  $S68^\circ W$
- The medium principal stress  $\sigma_2$  has been computed to be 11.4 MPa and the dip is  $13^\circ$  in the direction of  $S32^\circ W$
- The minimum principal stress  $\sigma_3$  has a magnitude of 5.4 MPa and is dipping  $56^\circ$  in the direction of  $N29^\circ E$

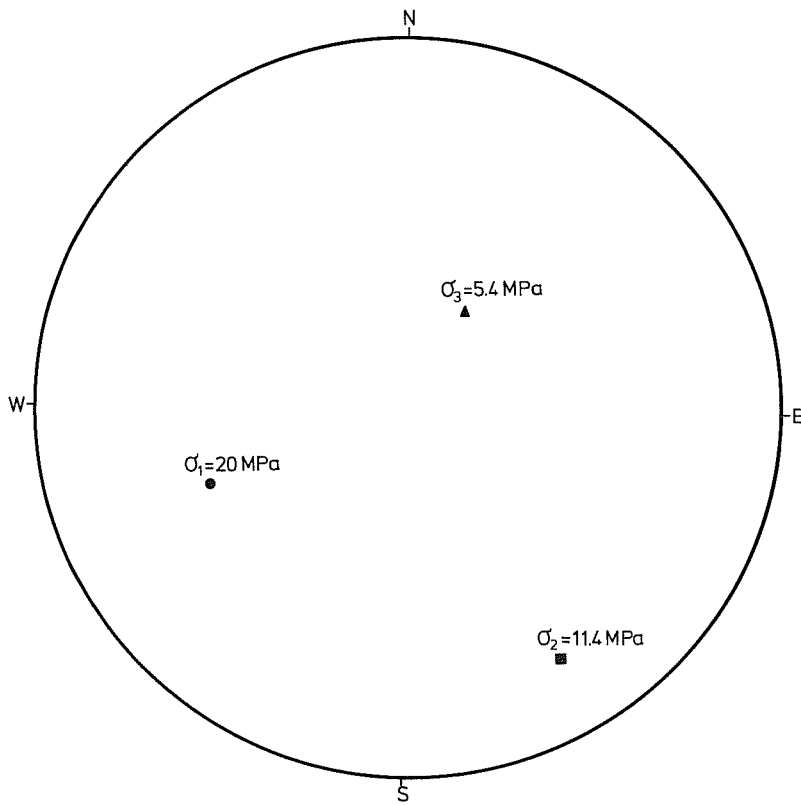
The derived principal stresses are plotted in Fig 4.3.

The measured vertical component is 9.8 MPa. With an overburden of 348 m and a density of  $2.61 \text{ g/cm}^3$ , a theoretical value of 9.1 MPa is obtained, i.e. the measured vertical component is of the same order of magnitude as predicted by theory.

#### 4.3 Detailed design of the heater test

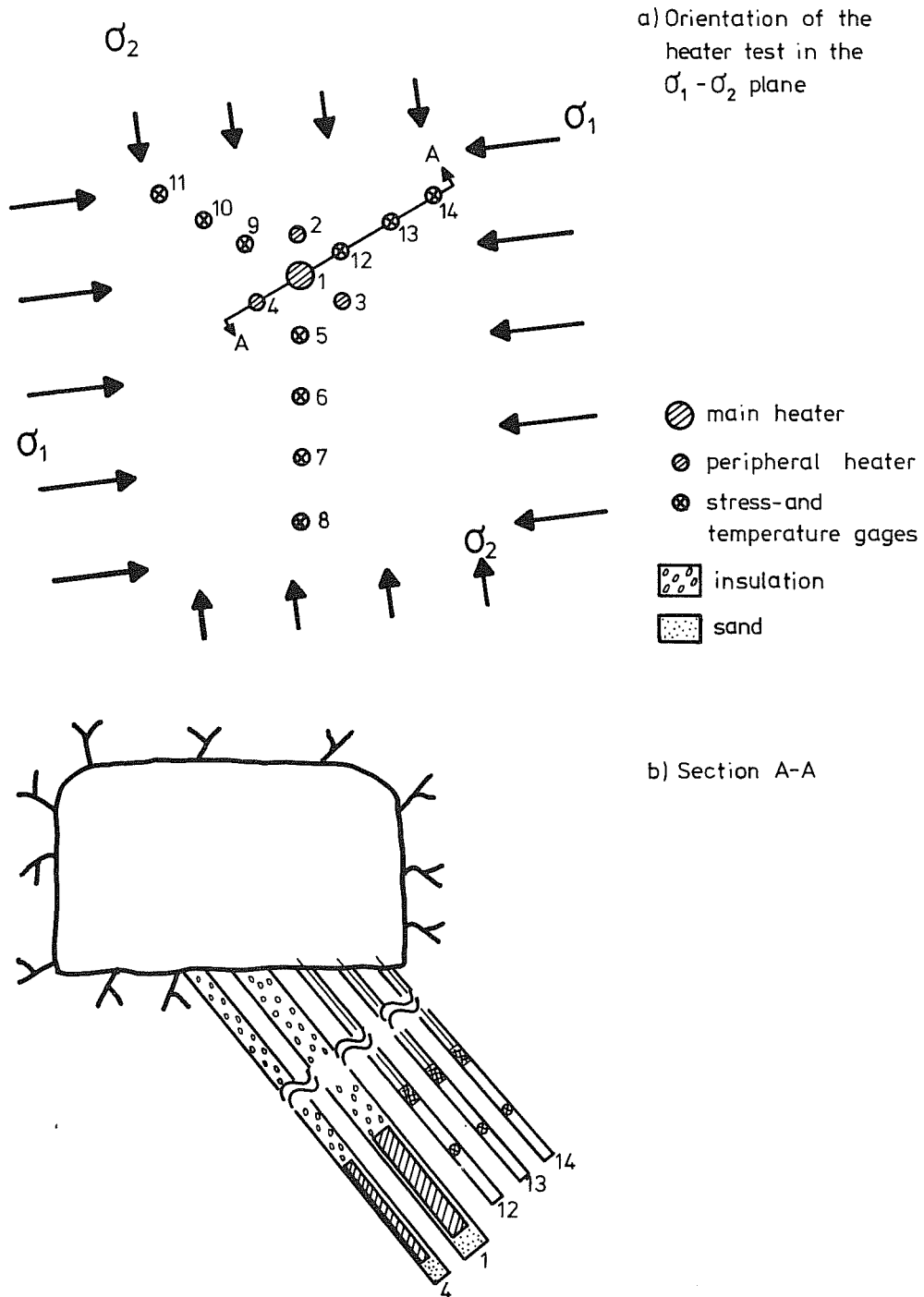
As mentioned earlier the heater test hole configuration was oriented with respect to the in situ stresses, so that all holes were drilled parallel to  $\sigma_3$ , and all measurement points were located in the midplane of the heaters. Since the maximum vertical depth was limited for practical reasons to 7.5 m, the minimal depth turned out to be 5.5 m (hole 14, see Fig 4.4). The influence of the secondary stresses caused by the drift itself is negligible at this depth. A schematic picture of the hole configuration is shown in Fig 4.4. The measured orientation and magnitude of the in situ stresses is also shown in the figure.

Detailed data about the hole configuration is given in Table 4.1.



XBL 788-10157

Fig 4.3 Principal stresses and their directions for the test site. Stripa mine, 348 m level (Carlsson, 1977).



XBL 788-10158

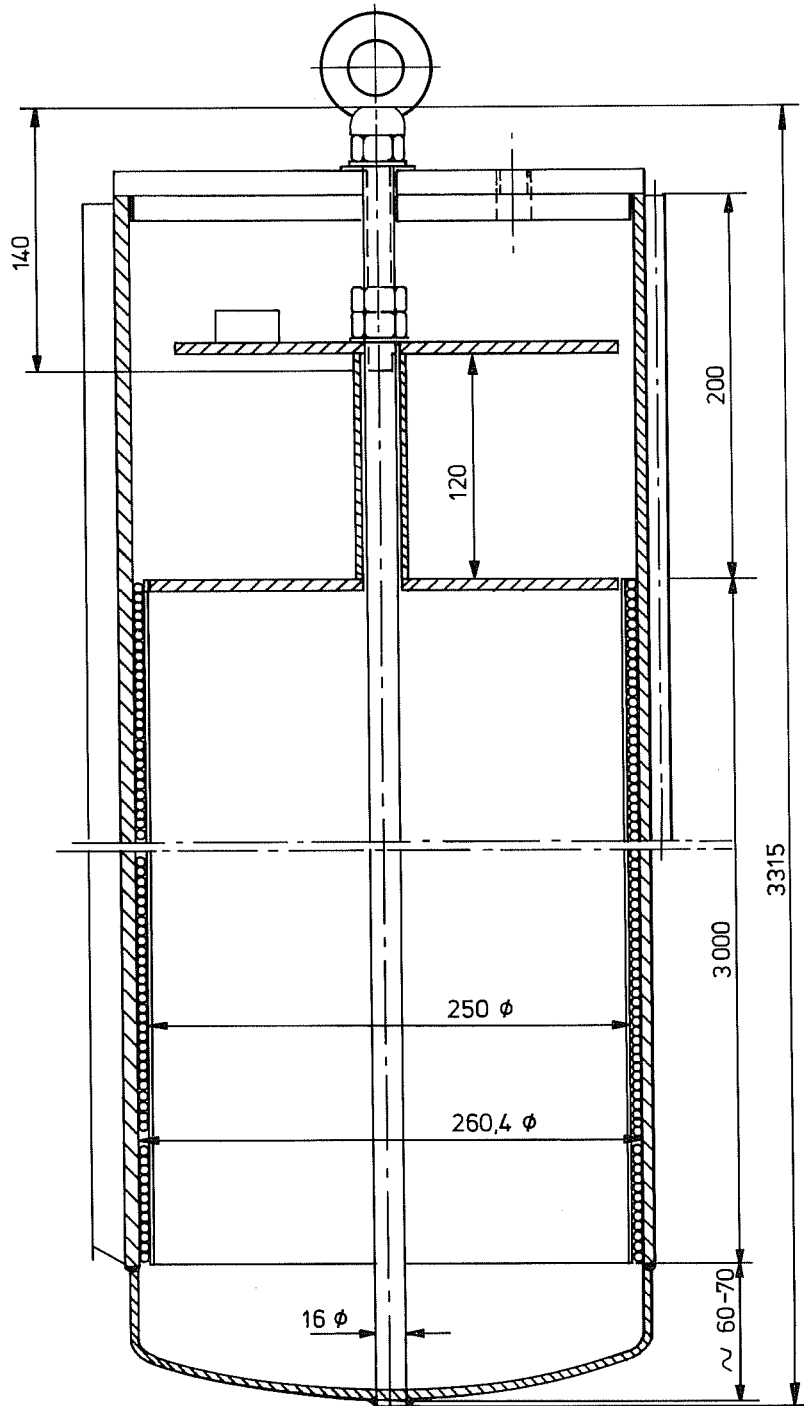
Fig 4.4 Orientation of heater test in the test drift. The numbers refer to the boreholes.

After the drilling, holes 1-4 were TV-logged and the remaining holes were logged with a borehole periscope. The results are described in [2] and will together with the results from the core logging be used in the evaluation and interpretation of the induced stress and temperature changes. The heaters

Table 4.1 Test drift drilling data

Hole no	Method of drilling	Diameter [mm]	Drill depth [m]	Depth to data point [m]	Vertical depth to data point [m]	Radial distance to main heater hole [m]
1	Percussion drilling	300	10.88	8.88	6.80	-
2	Diamond drilling	66	10.66	8.65	6.63	0.65
3	"	66	10.66	8.66	6.63	0.65
4	"	66	11.43	9.43	7.22	0.65
5	"	38	10.17	9.17	7.02	0.85
6	"	38	10.41	9.41	7.21	1.55
7	"	38	10.65	9.65	7.39	2.25
8	"	38	10.89	9.89	7.58	2.95
9	"	38	10.17	9.17	7.02	0.85
10	"	38	10.41	9.41	7.21	1.55
11	"	38	10.65	9.65	7.39	2.25
12	"	38	9.17	8.17	6.26	0.85
13	"	38	8.58	7.58	5.81	1.55
14	"	38	8.00	7.00	5.36	2.25

were constructed so that the power output of the main heater was 6 kW and for the peripheral heaters 1 kW. According to the Swedish proposal for nuclear waste storage a maximum temperature of 100°C is predicted on the surface of the waste canisters when placed in rock after thirty years of cooling. Therefore the decision was made to limit the skin temperature of the heaters to the predicted maximum temperature 100°C. Sand fill was used to properly position the heaters in the holes.



XBL 788-10159

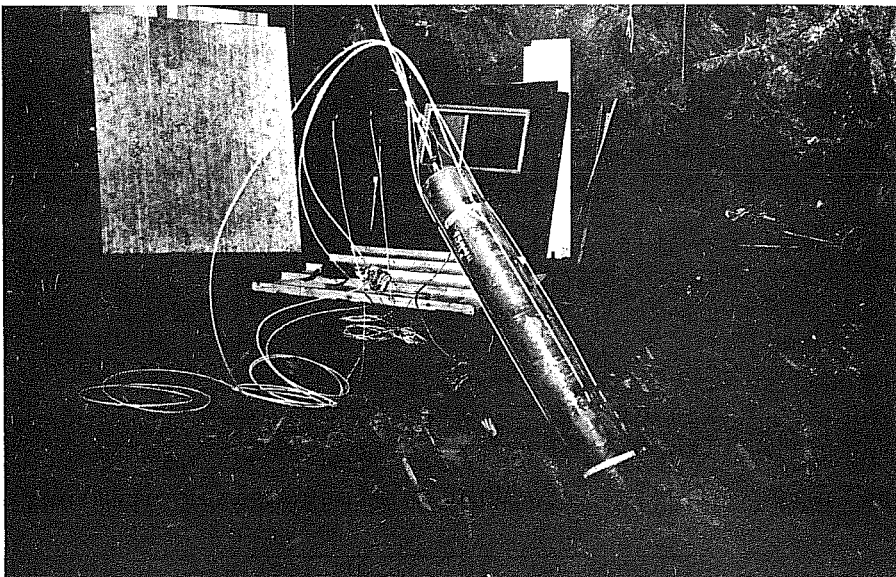
Fig 4.5 Construction of the main 6 kW heater for the KBS test site.

#### 4.4 Construction of the heaters

The main heater had a length of 3 m, a diameter of 273 mm and a maximum power output of 6 kW at 380V. In Fig 4.5 the construction of the main heater is shown in detail.

The heater was placed at a depth of 10.4 m in a 300 mm percussion drilled hole. It was centered in the hole by means of three centering devices mounted on the circumference at  $120^{\circ}$  intervals. Three thermocouples were mounted at the midplane of the heater and attached to the heater skin inside the centering devices. In addition the heater was oriented in the borehole so that the thermocouples measured in A, B and C directions respectively (see Fig. 4.1).

The accuracy of the thermocouples over the temperature range generated during this experiment was  $\pm 0.1^{\circ}\text{C}$ . Figure 4.6 shows the installation of the main heater.



XBB 788-9878

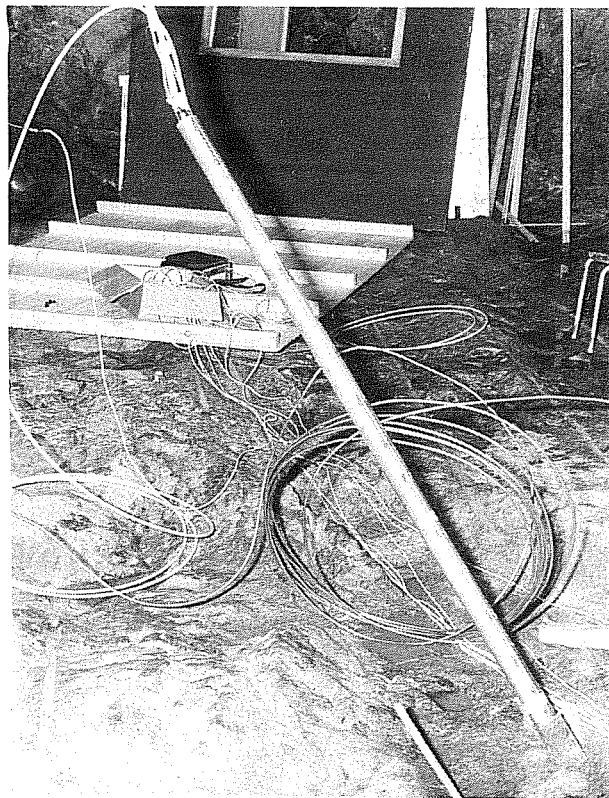
Fig 4.6 Installation of main heater.

After installation of the heater the hole was back-filled with insulation pellets. The conductivity of the pellet fill as presented by the manufacturer is  $0.23 \text{ W/m}^{\circ}\text{C}$ .

An air gap existed in the annular space between the heater and the walls of the drill hole ( $\sim 13 \text{ mm}$ ).

The peripheral heaters also had a length of 3 m. The diameter was 63 mm, and the maximum power output at 220 V was 1 kW. The temperature was monitored by a thermocouple on the heater midplane.

Figure 4.7 shows the installation of one of the peripheral heaters.



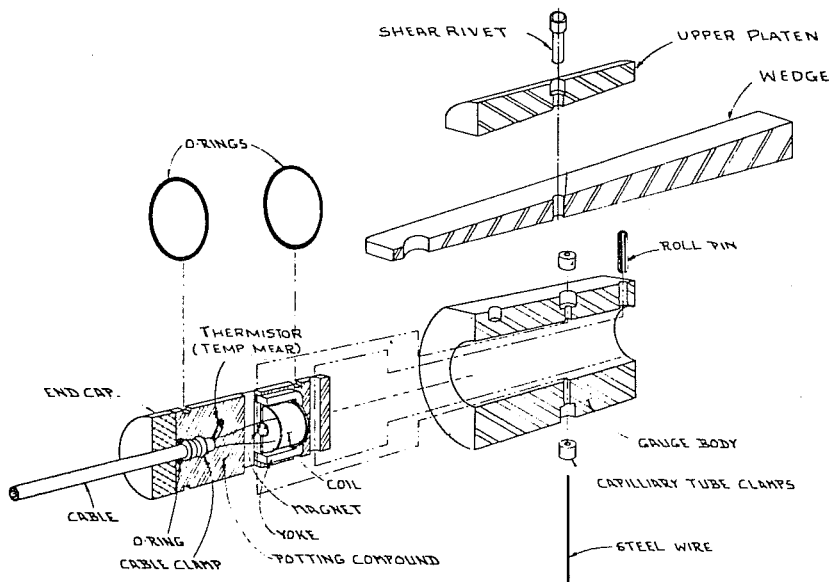
XBB 788-9879

Fig 4.7 Installation of a peripheral heater.

#### 4.5 Stress measuring device

The gages that were used for measuring stress changes for the duration of the heater test were vibrating wire stressmeters, manufactured by the American company IRAD [ 9 ] .

The gage consists of a hollow steel cylinder which is loaded diametrically in the borehole by means of a wedge and platen assembly (see Fig. 4.8). Stress changes in the rock cause changes in the natural



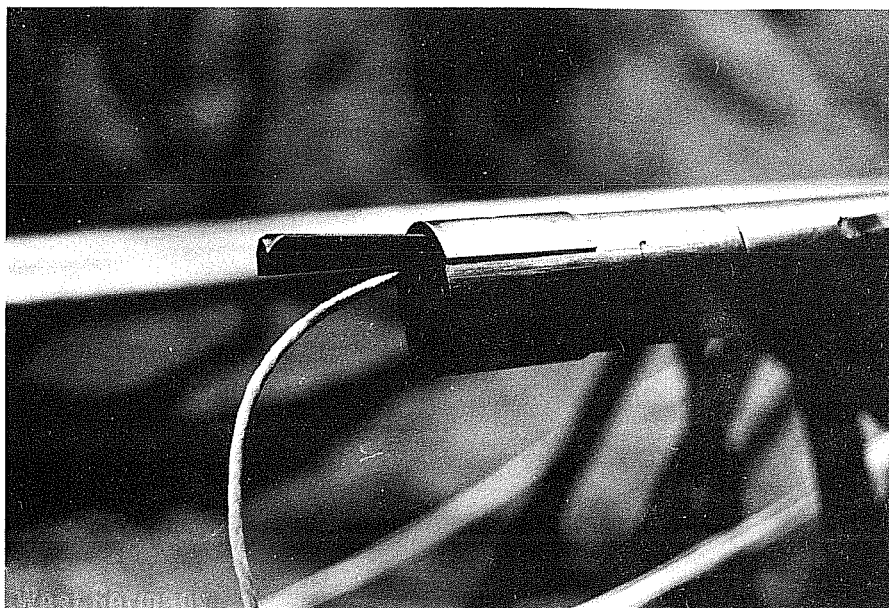
Vibrating Wire Stressmeter.  
(Section View Through Body)

XBL 788-10160

Fig 4.8 Vibrating wire stressmeter.

frequency of a highly tensional steel wire stretched diametrically across the cylinder walls in the pre-loaded direction. By calibration, changes in the wire period can be related to the magnitude of stress change in the rock. Figure 4.9 shows a gage mounted in the setting tool.

Since the gage is unidirectional, sets of three gages at specific angles to each other are needed to evaluate the stress change in the plane of a borehole.



XBB 788-9880

Fig 4.9 Gage mounted in the setting tool.

In case of a heat source in an elastic rock mass, the induced principal stress directions will be radial and tangential. Since the direction is known, only 2 gages set at the radial and tangential direction with respect to the heat source will be needed. In order to check the assumption of known principal stress directions, three gages were used in each hole in the Swedish heater test. The gages were positioned in each hole with their loading directions radial, tangential and  $45^{\circ}$  counter-clock wise (looking down hole) from radial with respect to the main heater axis. For further details about the predicted stresses see Appendix II.

A calibration of the gages set in a block of the Stripa granite has been carried out for different applied

stresses and temperatures. The calibration has been done by TerraTek in Salt Lake City, Utah and the calibration curves are shown in Fig 4.10.

The following approximations have been done for the evaluation of the induced thermal stresses:

- The thermal coefficient of expansion is the same for the gage ( $11.7 \cdot 10^{-6}$ ) as for the Stripa granite ( $11.1 \cdot 10^{-6}$ ).
- One set of calibration curves has been used for all gages (according to recommendations from the IRAD company)

The following equation has been used for the evaluation of stress changes:

$$\Delta\sigma = C_1 \frac{1}{(\underline{P} + \underline{\Delta P})^2} + C_2 \quad (4.1)$$

where

$\Delta\sigma$ =	change in stress	(MPa)
$\underline{P}$ =	period of the pretensioned wire	( $\times 10^{-7}$ sec)
$\underline{\Delta P}$ =	period offset (see Fig 4.10)	( $\times 10^{-7}$ sec)
$C_1$ =	constant varying with temperature according to	
	$C_1(T) = 1.56 \cdot 10^5(T) - 2.076 \cdot 10^8$	
$C_2$ =	constant varying with temperature according to	
	$C_2(T) = -0.0528(T) + 69.76$	

The stress changes derived by using equation 4.1 deviate by about 8% compared with hand derivation from the calibration curves directly.

In this way it is possible to calculate  $\Delta\sigma_r$ ,  $\Delta\sigma_{45}$  and  $\Delta\sigma_\phi$  as if the gage were set in the direction of a uni-axial stress.

For calculating the thermally induced principal stresses  $\sigma_1$  and  $\sigma_2$ , the following equations have to be used (Hawkes and Bailey, 1973):

$$\sigma_1 = \frac{3}{2}a + \frac{3}{4}b \quad (4.2)$$

$$\sigma_2 = \frac{3}{2}a - \frac{3}{4}b \quad (4.3)$$

where

$$a = \frac{\Delta\sigma_r + \Delta\sigma_\phi}{2} \quad (4.4)$$

$$b = [(\Delta\sigma_{45} - a)^2 + (\Delta\sigma_r - a)^2]^{1/2}. \quad (4.5)$$

The angle,  $\gamma$ , between the gage in the radial direction with respect to the main heater and the maximum principal stress  $\sigma_1$  is given by

$$\sin 2\gamma = \frac{a - \Delta\sigma_{45}}{b} \quad (4.6)$$

and

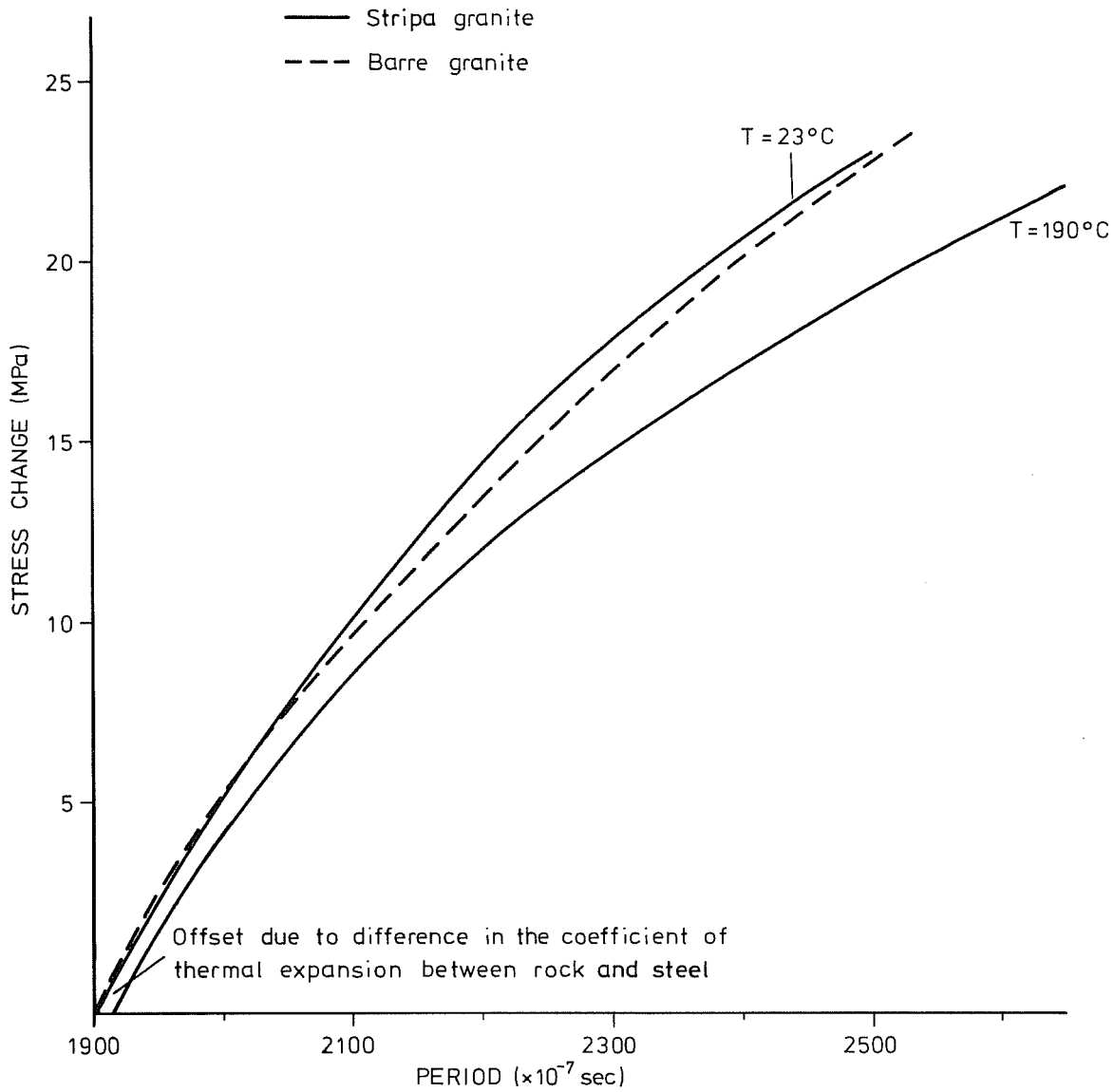
$$\cos 2\gamma = \frac{\Delta\sigma_r - a}{b}. \quad (4.7)$$

From the principal stresses  $\sigma_1$  and  $\sigma_2$ , the thermally induced radial and tangential stresses,  $\sigma_r$  and  $\sigma_\phi$  can be derived as

$$\sigma_\phi = \sigma_1 \cos^2 \gamma + \sigma_2 \sin^2 \gamma \quad (4.8)$$

$$\sigma_r = \sigma_1 \sin^2 \gamma + \sigma_2 \cos^2 \gamma. \quad (4.9)$$

If the derived angle between the radial gage and the maximum principal stress is zero, then  $\sigma_1$  is equivalent to  $\sigma_r$ , and  $\sigma_2$  is equivalent to  $\sigma_\phi$ , respectively.



XBL 788-10161

Fig 4.10 Calibration curves for the IRAD vibrating wire stressmeters, gage H 3-18.

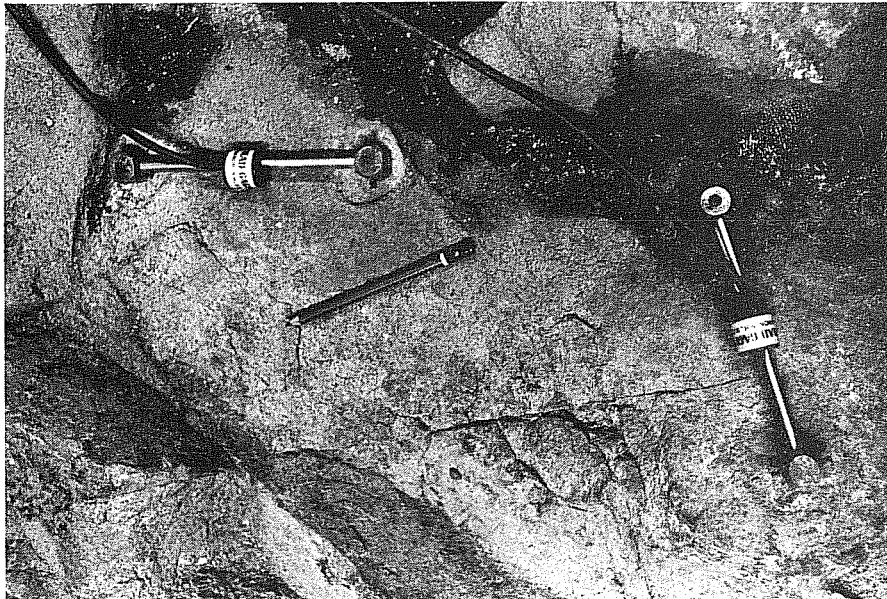
#### 4.6 Temperature measuring device

All vibrating wire stressmeters were equipped with thermistors so that all temperature measurements were carried out at the same "point" as the stress measurements. The tolerance of the thermistors used were 0.5%.

In order to prevent convection, though the measurements were carried out under water, all bore holes were scaled off with injection packers, positioned directly above the gages.

#### 4.7 Displacement measuring device

In order to check displacements of major fractures on the floor of the test site, displacement gages were



XBB 788-9881

Fig 4.11 Displacement gages mounted on the floor in the test site.

used (see Fig 4.11). In principle, these gages work in the same way as the stressmeters. A steel wire is stretched across a fracture. A change in aperture of the fracture causes a change in the length of the wire and hence a change in the natural frequency of vibration. The displacement of the fracture is derived by calibration. The accuracy of the device is  $1.5 \cdot 10^{-6} \text{m}$ .

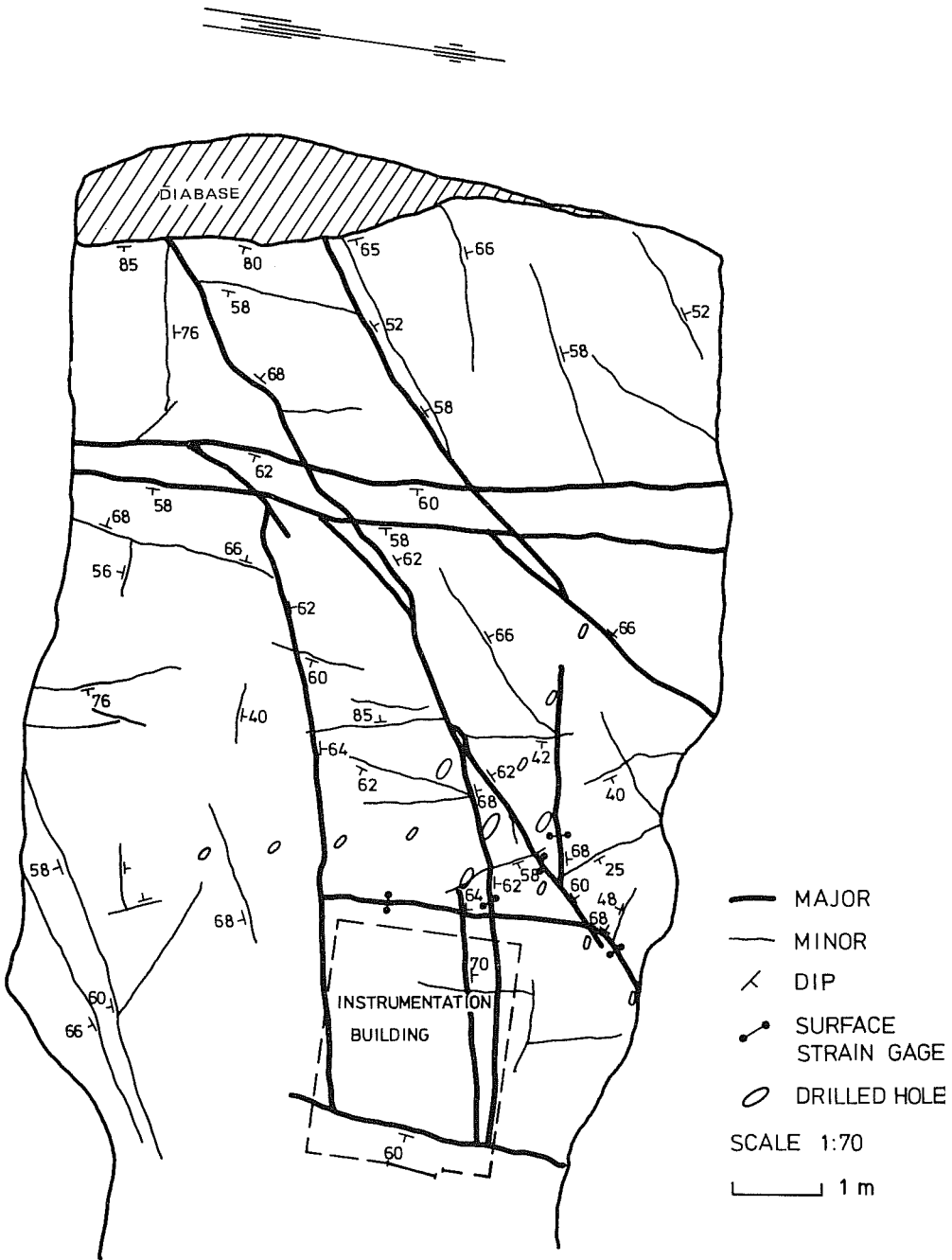
The temperature on the floor surface was monitored by a thermocouple with a accuracy of  $\pm 0.1^{\circ}\text{C}$ .

## 5 ACCOMPLISHMENTS OF THE HEATER TEST

### 5.1 General comments

The KBS heater test started in October 1977 and was completed in April 1978. As mentioned in chapter 4.3, the skin temperature of all heaters was set to reach a maximum value of 100°C. This created certain problems in operating the peripheral heaters. The heaters were not capable of keeping the holes dry since the water inflow was too great for the power output per square centimeter of the heater surface. This resulted in drastically lowered temperatures. The decision was made to control all heaters by maximum power. The higher temperature reached was then expected to dry out the holes. This change in controlling the heaters was made 6 days after the heaters had been turned on. Although the temperature on the peripheral heaters reached a maximum of 175°, this was still not enough to keep the holes dry. Practical problems also made it impossible to measure the amount of water inflow in the holes. In order to have a satisfactory check of the power used to heat the rock, it was decided to turn the peripheral heaters off and to use these three holes to measure the water inflow during the duration of the test. The peripheral heaters were turned off 19 days after the start of the heater test.

As mentioned earlier, there was no water inflow in the main heater hole, although the heater hole and the peripheral heater holes were intersected by mutually independent fractures (see Fig 5.1). This absence of water can possibly be explained by the fact that the main heater hole was percussion drilled while the peripheral heater holes were diamond drilled. This implies that the percussion drilling might have caused sealing of open fractures, as has been established elsewhere (personal communication - J. Gale, University of Waterloo).



XBL 788-10162

Fig 5.1 Orientation of heater test in the test drift.

## 6 MEASURED TEMPERATURE RISE OF THE MAIN HEATER

### 6.1 Temperature as a function of time

The total power output given to the rock was 6 kW after day 19. As shown in Fig 6.1, a steady state phase is reached after approximately 30 days, when the heater temperature was 324°C. A temperature of 333.9°C was reached 68 days after the heater was turned on. After 69 days the heater was turned off and allowed to cool in order to check the cooling properties of the rock mass. As shown in Fig 6.1, the cooling temperatures of the heater were monitored from day 69 to day 155 when the in situ experiment was finished. The last reading of the heater temperature was 14.7°C and the temperature at that time was decreasing at a rate of ~0.1°C per day.

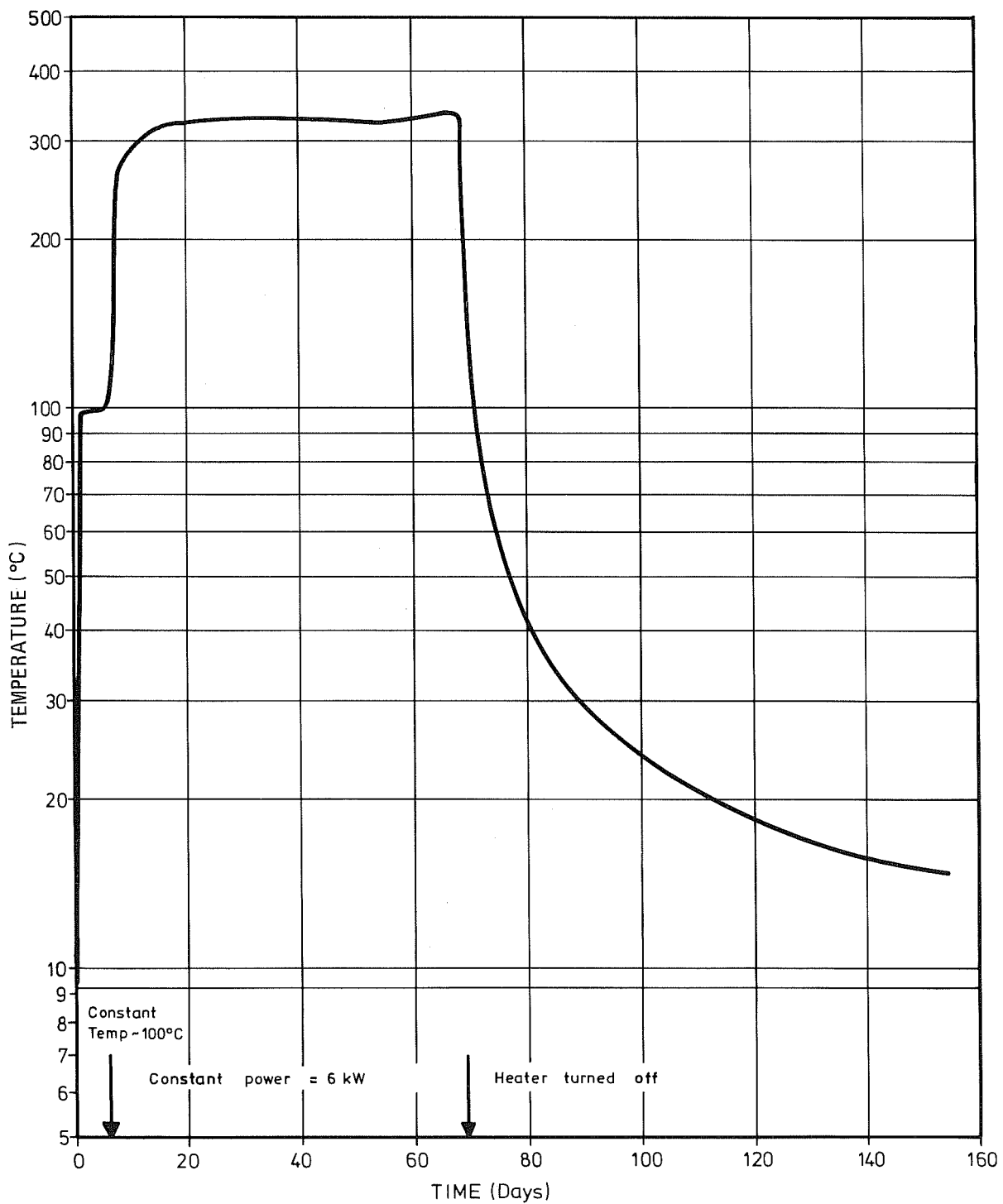
In Table 6.1 the heater temperature is given for certain days.

Table 6.1 Measured temperatures of the main heater

Day #	Temp (°C)	Day #	Temp (°C)
0	9.28	60	330.7
2	99.0	70	128.5
6	99.5	80	42.7
20	316.9	90	29.1
30	324.1	110	20.6
40	329.2	130	16.9
50	322.4	155	14.7

### 6.2 Comments on measured data

The maximum temperature of the heater skin was 333.9°C. Variation of the voltage supply caused fluctuation in heater temperature. For instance, the temperature was lowered from 329°C on day 40 to 321.1°C on day 55. The temperature was then raised to the maximum 333.9°C which was



XBL 788-10163

Fig 6.1 Main heater temperature as a function of time.

reached 69 days after the heater was turned on. These fluctuations were very clearly marked in the stress- and temperature measurements in the rock mass as will be shown in a forthcoming chapter.

The predicted temperature of the heater is slightly lower than the one measured, as shown in Figures 7.6 and 7.7. This could be explained by the annular air gas between the heater and the rock. In the analysis it is assumed that the heater is in perfect contact with the rock, and a low conductivity material such as air, would cause the heater temperature to increase. Spalling, caused by very high stress and temperature gradients, might also have occurred in the walls of the borehole, which then lowered the conductivity.

## 7 MEASURED TEMPERATURE CHANGES IN THE GRANITE

### 7.1 General comments

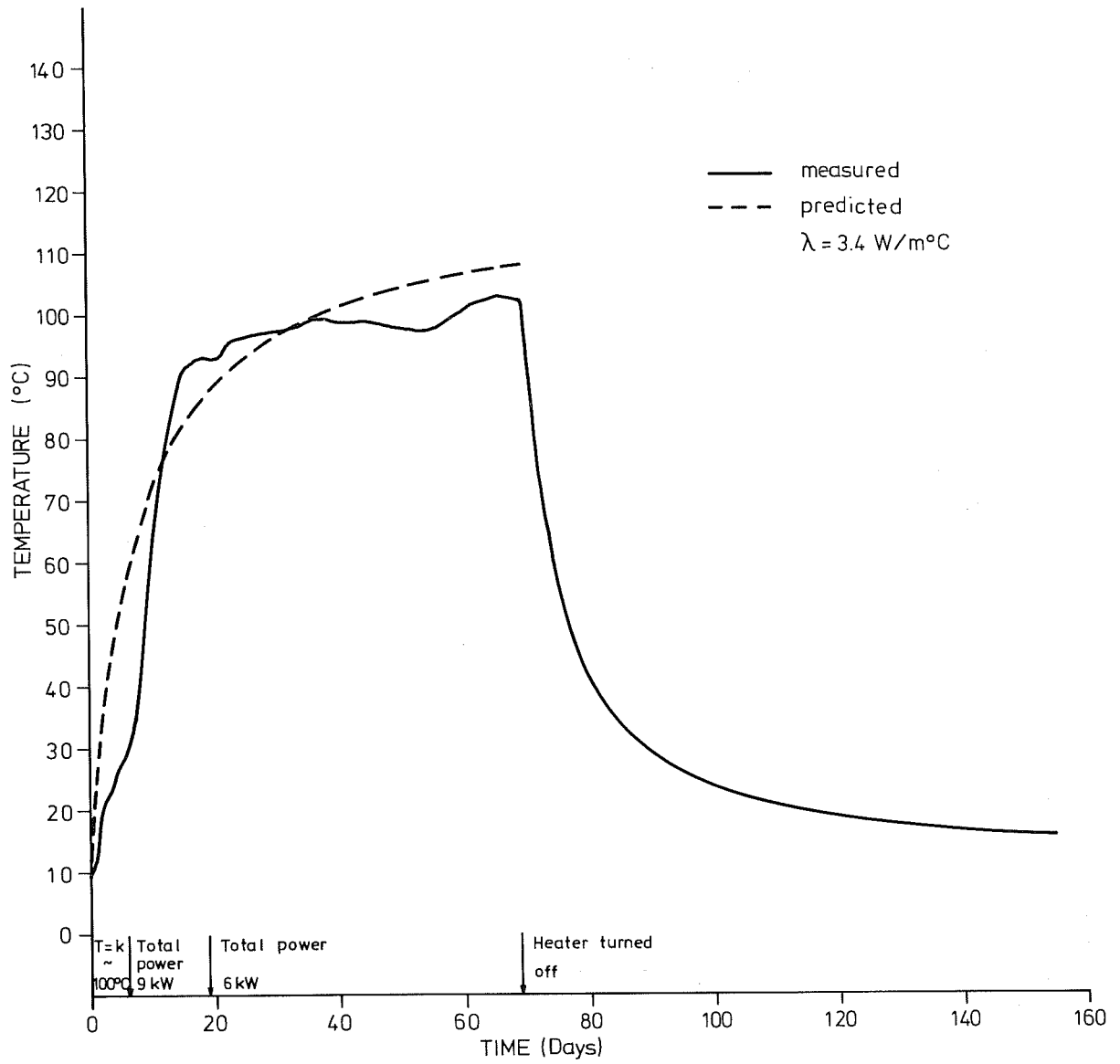
As mentioned earlier the temperature change in the rock has been monitored by thermistors. The tolerance was 0.5% and all measurements have been carried out under water. The distance from the thermistors to the center of the main heater was 0.85 m, 1.55 m and 2.25 m respectively. In order to check the thermal isotropy of the Stripa granite, measurements have been carried out along three different directions spaced at  $120^\circ$  with respect to the main heater. Additional stress and temperature measurements have been carried out at 2.95 m along the A-direction (see Fig 4.1).

### 7.2 Temperatures as a function of time

Figures 7.1 - 7.5 show the measured temperatures as a function of time along the A-direction of the test site. In the same Figures are shown the predicted temperatures from a single 6 kW heater, assuming a conductivity of  $3.4 \text{ W/m}^\circ\text{C}$  for the rock mass. In the analysis it has been assumed that the conductivity is independent of temperature, the heater is in perfect contact with the rock, and the surrounding rock is homogenous and isotropic. Furthermore, the ground water flow has not been taken into account. For further details about predicted temperatures, see Appendix I.

### 7.3 Temperature as a function of radius from the main heater

Figures 7.6 and 7.7 show the temperature as a function of radius from the main heater along the A-direction of the test site (see Fig 4.1) after 9, 14, 20 and 68 days. In the same figures are shown the calculated temperatures according to the equations presented in Appendix I.



XBL 788-10164

Fig 7.1 Temperature as a function of time at .85 m radius from the 6 kW heater, A-direction.

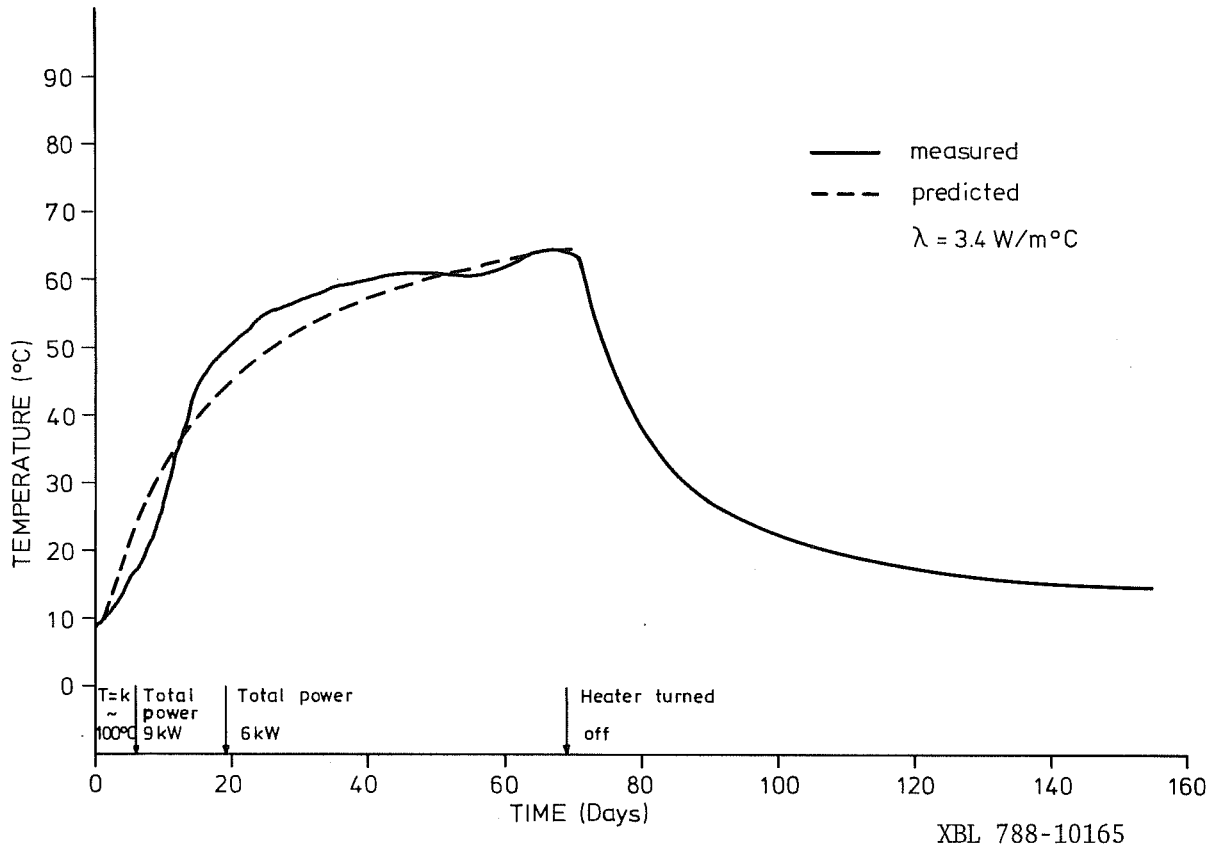


Fig 7.2 Temperature as a function of time at 1.55 m radius from the 6 kW heater, A-direction.

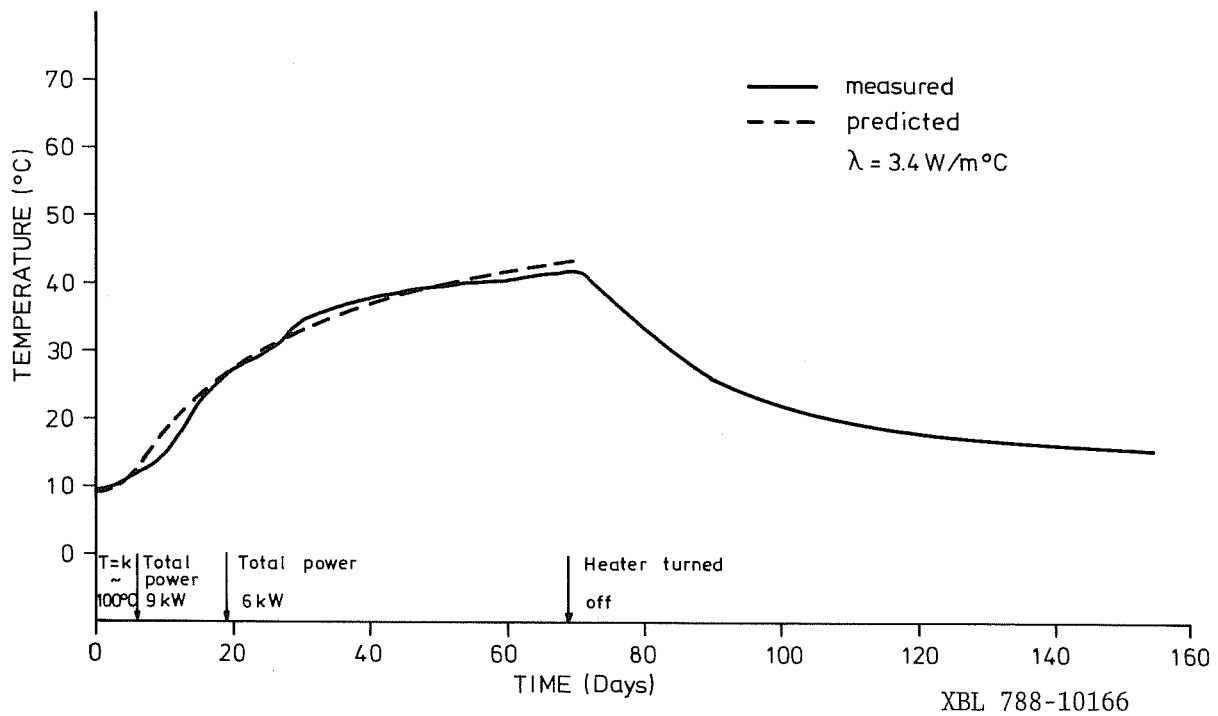


Fig 7.3 Temperature as a function of time at 2.25 m radius from the 6 kW heater, A-direction.

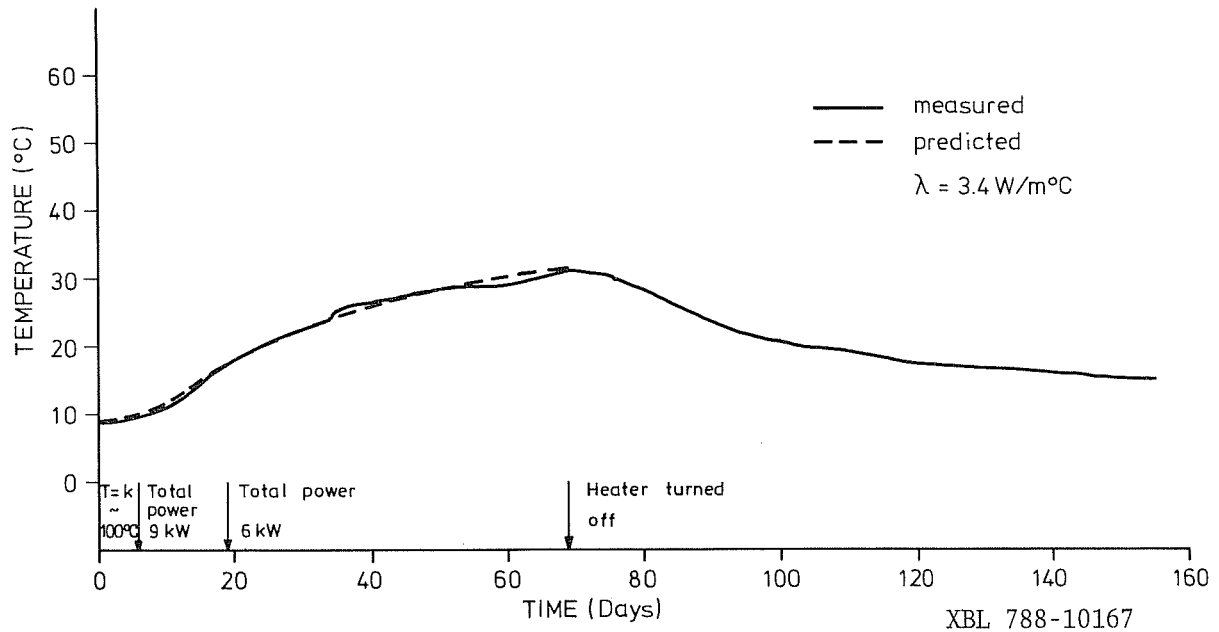


Fig 7.4 Temperature as a function of time at 2.95 m radius from the 6 kW heater, A-direction.

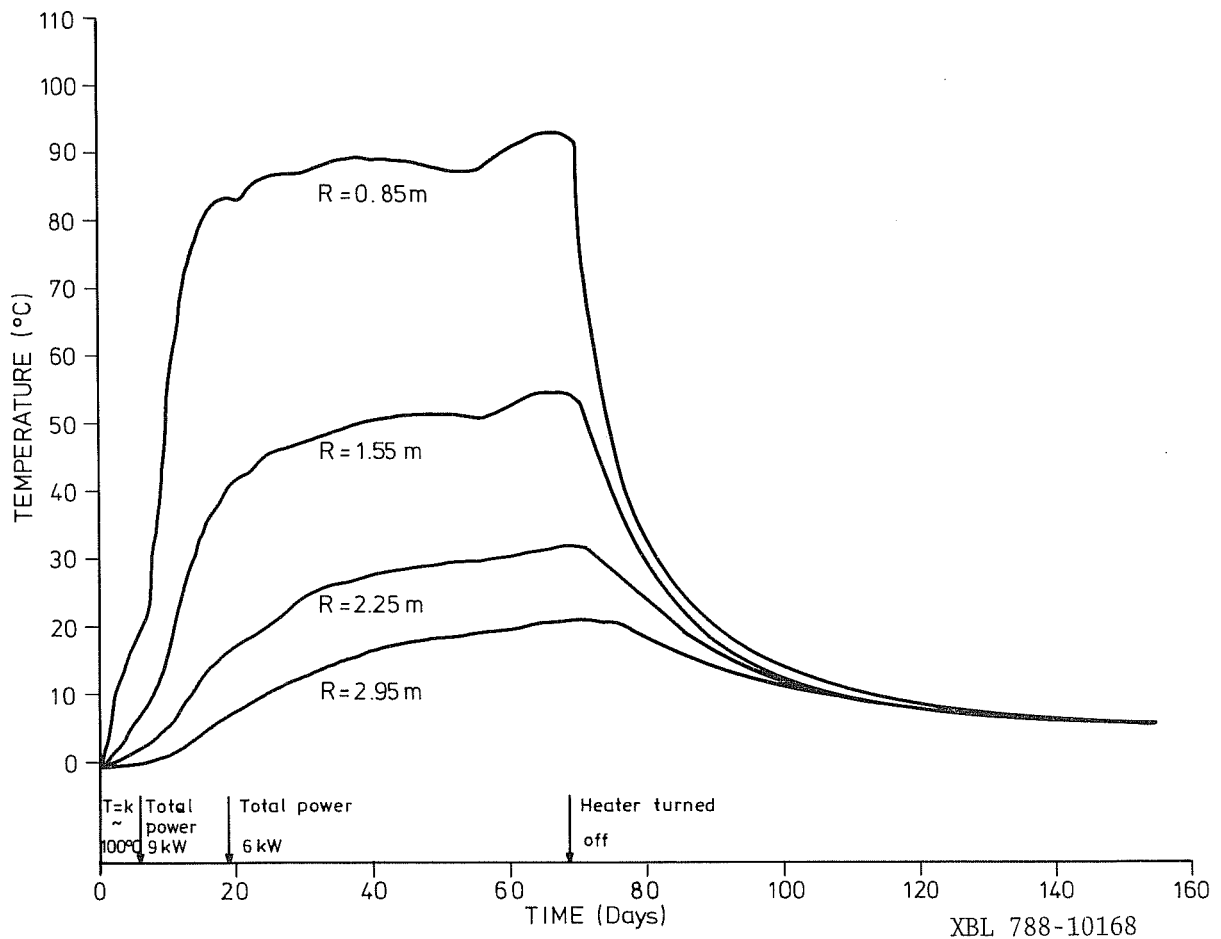
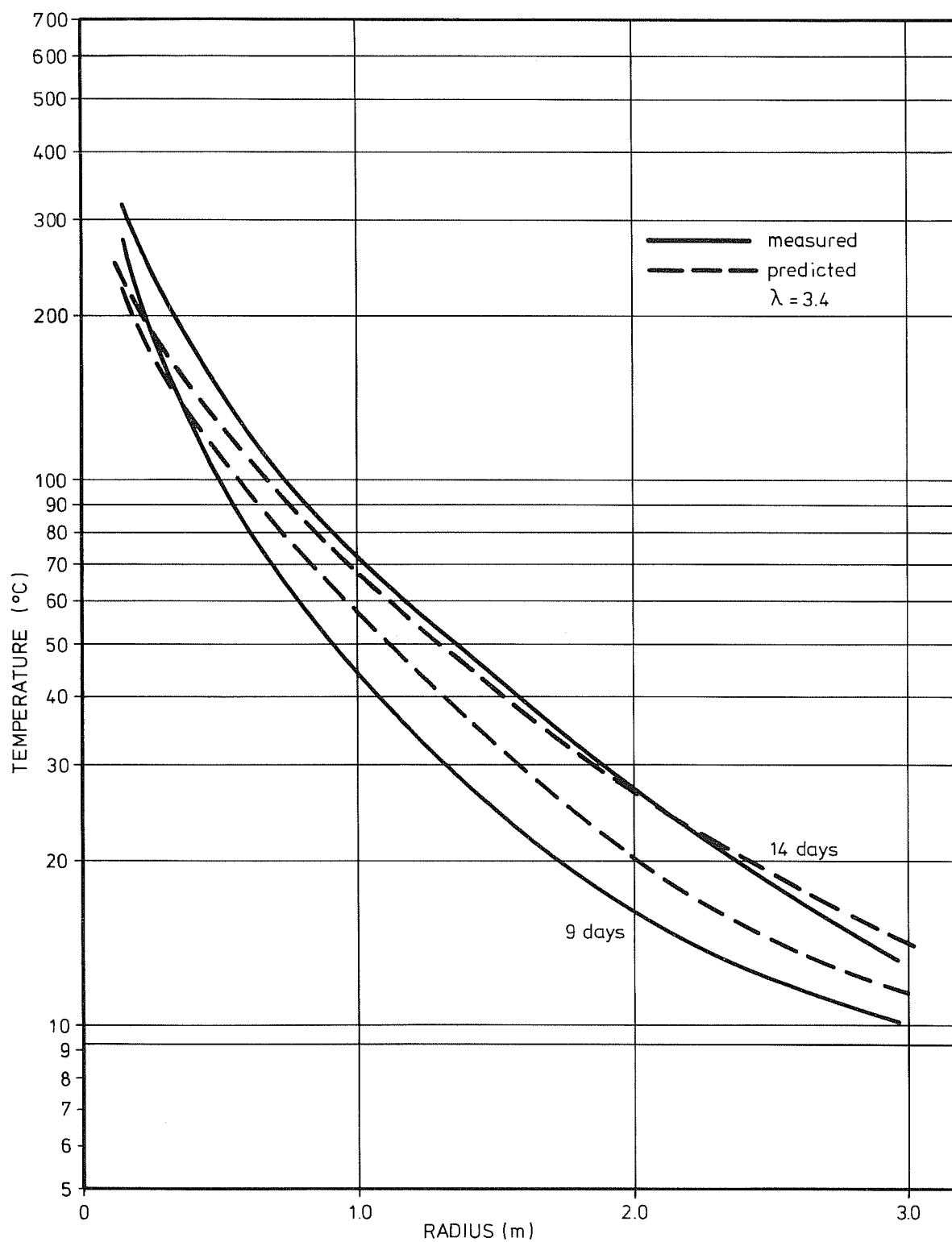


Fig 7.5 Temperature as a function of time at different radii from the 6 kW heater, A-direction.



XBL 788-10169

Fig 7.6 Temperature as a function of radius from the 6 kW heater at 9 and 14 days, A-direction.

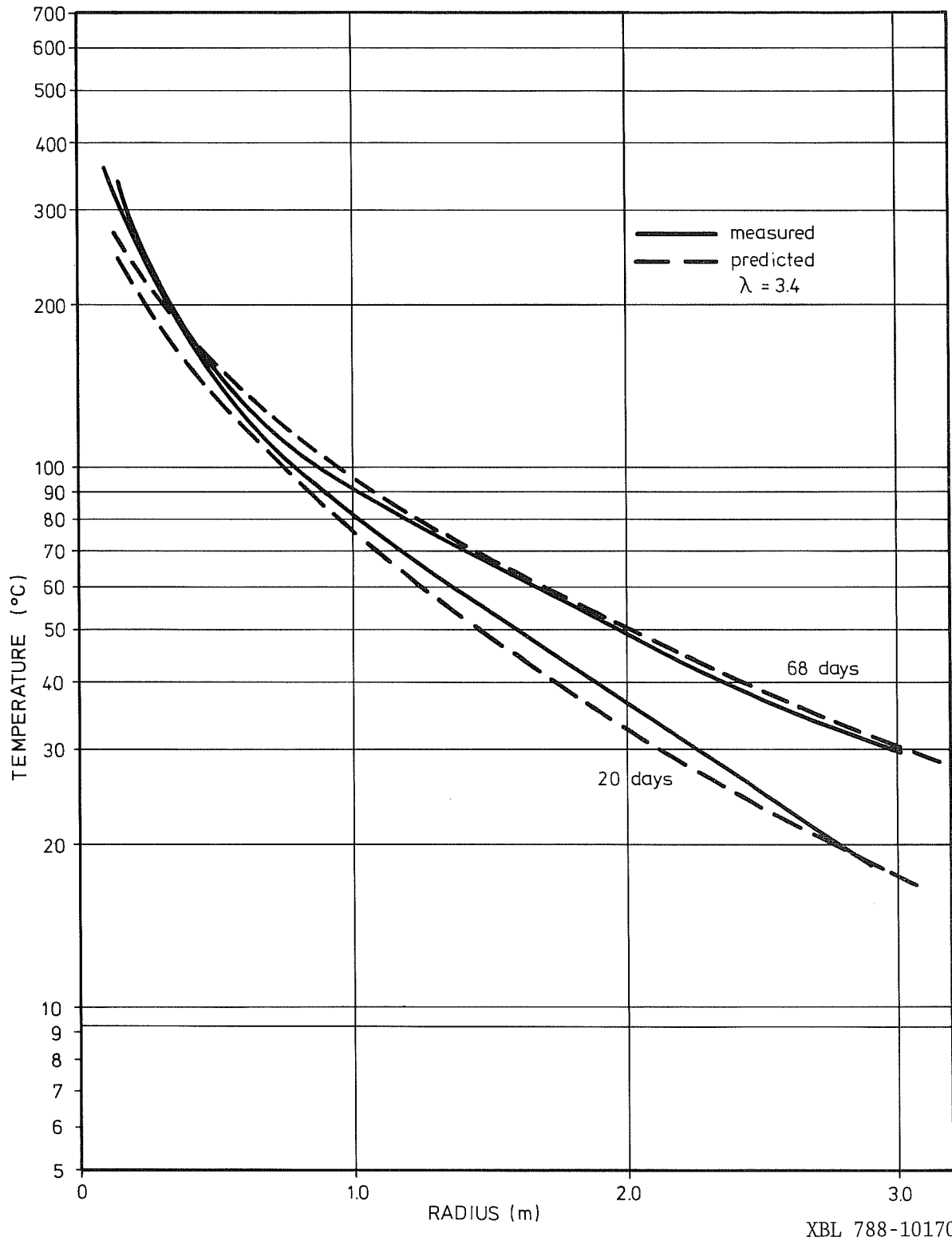


Fig 7.7 Temperature as a function of radius from the 6 kW heater at 20 and 68 days, A-direction.

#### 7.4 Temperatures in the peripheral heater holes

Additional temperature measurements were also carried out in the peripheral heater holes, Fig 7.8. The distance to the main heater is 0.65 m. A rod with a thermocouple attached to it was lowered down to the bottom of the hole. When stable readings were taken the rod was lifted 0.5 m for new recordings of temperature. Due to convection it was not possible to get stable readings above the water level in the holes.

The measurements were carried out 55 days after the heater was turned on.

#### 7.5 Calculation of the heat conductivity, $\lambda$

As already indicated and as shown in Fig 6.1, it is not suitable to use the heating period between day 0 and day 68 for calculation of heat conductivity of the rock mass. Instead, looking at the curves that represent the cooling of the rock, a much nicer course is observed.

According to Carslaw and Jaeger, 1973 [10], the temperature  $T(r, t)$  where  $r$  denotes radius from the heater and  $t$  denotes time, is supposed to satisfy

$$\frac{\partial T}{\partial t} = \frac{1}{r} \frac{\partial}{\partial r} \left( \kappa \left( 1 - \frac{1}{\gamma} T \right) \frac{\partial T}{\partial r} \right) \quad \text{where}$$

$\kappa$  and  $\gamma$  are constants.

The following basic assumptions have been made:

- The heater is a cylinder of infinite length and the heat flow is radial only

- The heater is in perfect thermal contact with the rock;
- The relation between thermal conductivity and temperature is a straight line;
- There is no flow of water in the rock;
- The surrounding rock is homogeneous and isotropic.

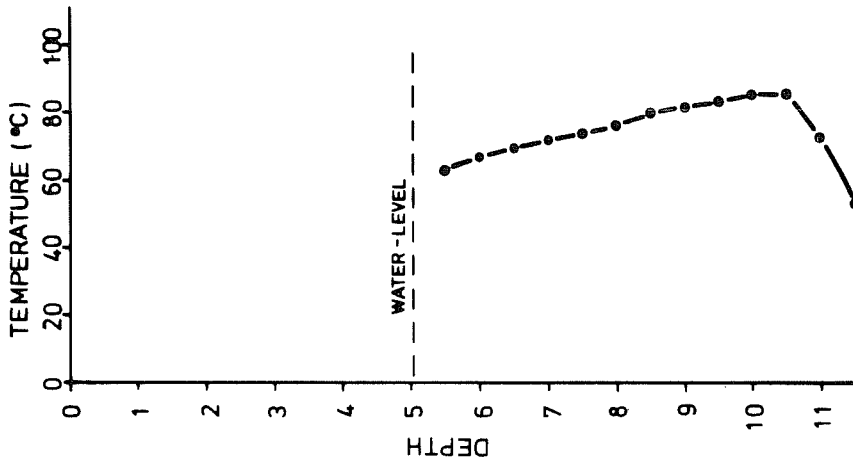
The calculations, which are shown in detail in Appendix III, give a value of the thermal conductivity for the Stripa granite of

$$\lambda = 4.8 \text{ W/m}^{\circ}\text{C}.$$

#### 7.6 Comments on measured data

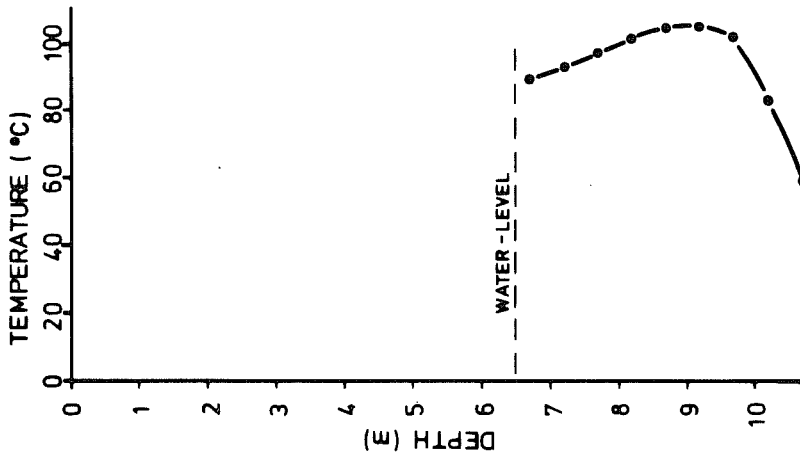
So far, only the temperatures measured along the A-direction of the borehole configuration have been presented. For comparative purposes, the measured temperatures along the B- and C-directions are listed in Table 7.1. As shown in the table, the highest temperatures are measured along the A-direction and the lowest are measured along the C-direction. According to the core logs and the logging with the borehole periscope the holes in the C-direction have the highest frequency of fractures. Furthermore, the boreholes at distances 0.85 m and 1.55 m along the B-direction and the boreholes at distances 1.55 and 2.25 along the C-direction have a very high water inflow compared to the holes in the A-direction. This implies that the water has a cooling effect on heating of the rock mass.

The predicted temperatures compare fairly well with the measured, although the water leakage and the peripheral heaters affected the temperature distribution in the rock mass. At distances far away from the heater (>1.55 m), the predicted temperatures coincide with the measured (see Figs 7.3 and 7.4).

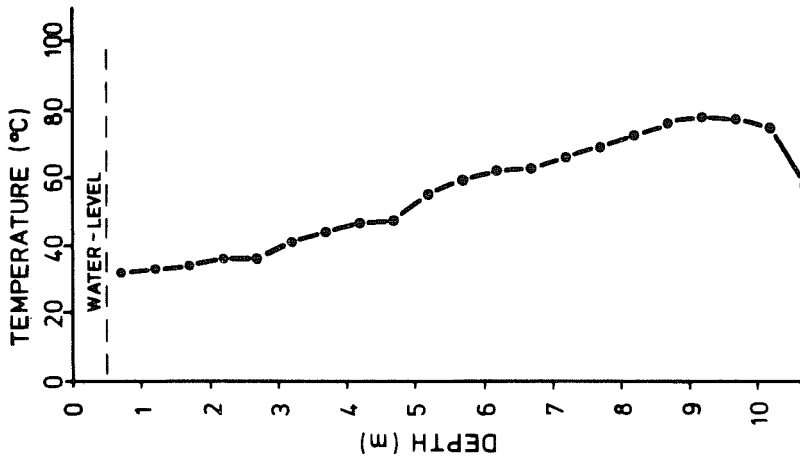


Borehole #4  
(A-direction)

XBL 788-10171



Borehole #3  
(C-direction)



Borehole #2  
(B-direction)

Fig 7.8 Temperatures as a function of depth in the water filled peripheral heater holes, day No. 55.

Table 7.1 Measured temperatures in the rock at different distances from the main heater

Day #	Direction	Measured temperatures ( $^{\circ}\text{C}$ )			
		r=0.85 m	r=1.55 m	r=2.25 m	r=2.95 m
0	A	9.28	9.35	9.35	8.90
	B	9.38	9.00	9.18	-
	C	9.27	9.20	9.00	-
2	A	18.78	10.80	9.50	8.90
	B	20.57	9.78	9.27	-
	C	14.73	9.75	9.10	-
5	A	27.43	16.38	11.00	9.28
	B	37.33	15.68	11.03	-
	C	24.82	14.05	10.40	-
9	A	55.60	23.78	13.60	10.33
	B	58.63	20.70	13.80	-
	C	42.62	17.80	12.60	-
14	A	87.50	41.78	20.50	13.20
	B	84.67	34.00	20.15	-
	C	70.03	28.70	18.35	-
20	A	92.80	51.05	26.70	17.65
	B	90.33	42.45	26.25	-
	C	80.20	39.10	24.95	-
40	A	98.40	60.10	37.50	26.44
	B	94.43	50.00	34.95	-
	C	87.73	49.78	33.78	-
60	A	100.37	62.30	40.09	29.23
	B	97.17	52.02	37.43	-
	C	89.54	49.99	36.40	-
75	A	56.90	49.50	38.60	30.45
	B	55.50	40.05	37.30	-
	C	54.88	44.10	36.35	-
90	A	28.66	27.59	25.67	23.53
	B	28.07	26.83	25.18	-
	C	28.25	26.78	25.22	-
110	A	20.40	19.94	19.51	18.79
	B	20.39	19.90	19.31	-
	C	20.28	20.01	19.39	-
155	A	15.16	14.91	15.04	14.83
	B	15.16	15.02	14.82	-
	C	15.09	15.32	15.11	-

## 8 MEASURED STRESS CHANGES IN THE GRANITE

8.1 General comments

The vibrating wire stressmeters that were used for monitoring the thermally induced stresses have never been used in an environment of both high temperature and flowing water. Although the gages were constructed in such a way that they were supposed to be high temperature resistant and waterproof, they did not fulfill these demands. For instance, leakage occurred through the teflon mantled cable thereby allowing water to come in contact with the wire and destroy the measurements. This leakage had no effect on the temperature monitoring.

Since only 50% of the gages worked properly after 25 days of the experiment, the decision was made to substitute new, modified gages for the first installed set of gages. The leakage problem did not recur to the same extent, and at the end of the test 90% of all new, modified gages worked properly.

If the rock mass is regarded as an infinite continuum, then the thermally induced stresses should not create displacements of the borehole so that the gages will loosen in the hole. Unfortunately, this assumption did not hold in the Stripa granite. In all of the holes located close to the heater ( $r=0.85$ ), at least one of the three gages loosened as the rock was heated. Since, for precise calculation, all three gages are needed for calculation of  $\sigma_r$  and  $\sigma_\psi$ , accurate derivations of radial and tangential stress changes could not be evaluated from these measurements. However, in some cases the graphs can be extrapolated if the assumption is made that the hole direction is in the line of maximum principal stress. This assumption has been made when appropriate, and these results are shown as a dashed curve in the following figures. The errors caused by this assumption are small and within a few percent.

## 8.2 Stress changes as a function of time

Figures 8.1 - 8.9 show the measured changes of stresses  $\sigma_r$  and  $\sigma_\phi$  as a function of time at different radial positions along the A-, B- and C-directions of the test.

Figures 8.10 - 8.12 show the measured radial and tangential stresses along the A-direction of the test. In the same figures are the radial and tangential stresses shown based on the predicted temperature distribution around the heater. A detailed description of the calculations is presented in Appendix II.

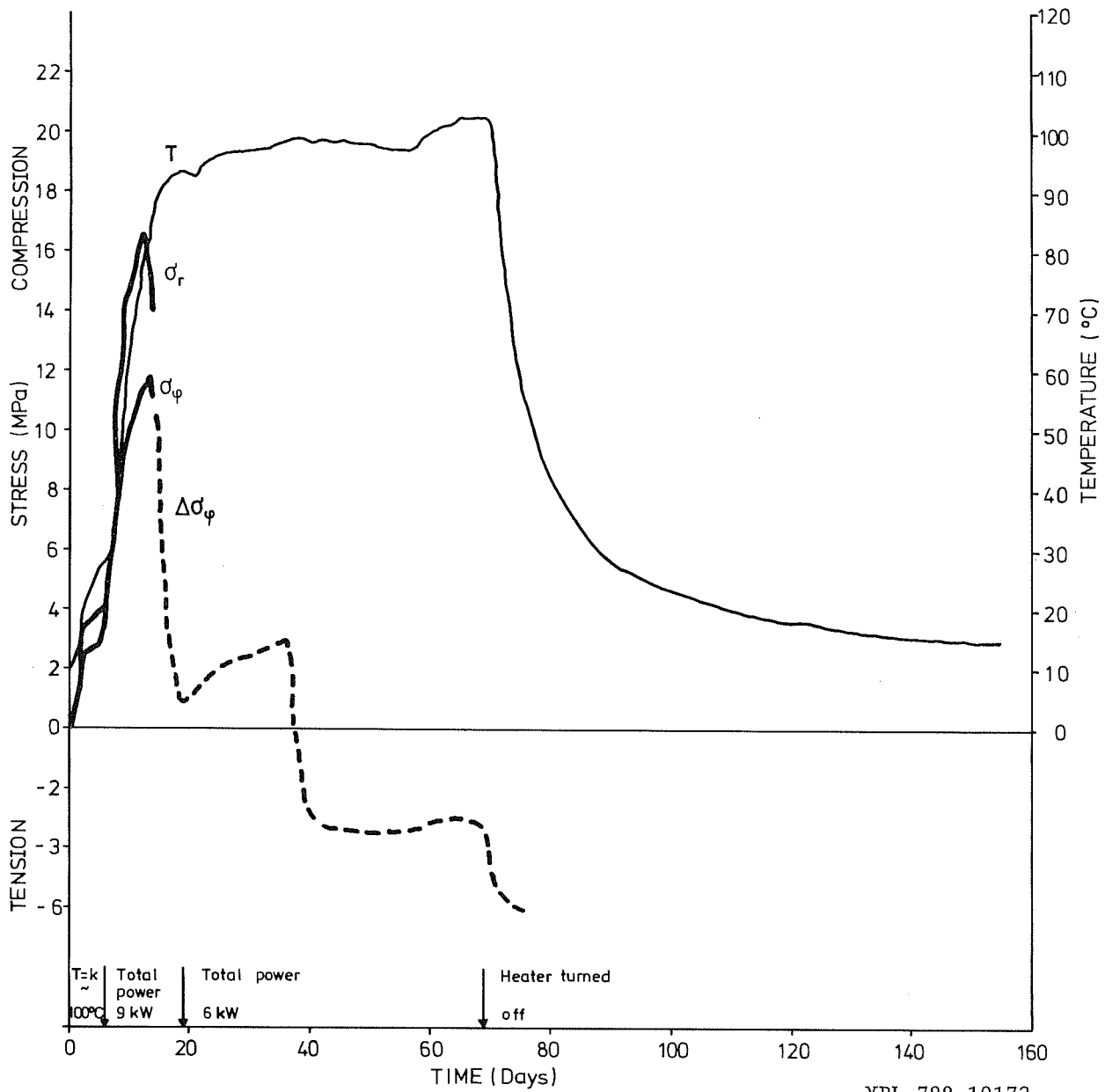
## 8.3 Stress changes at a function of radius from the main heater

Figures 8.13 - 8.29 show the measured  $\sigma_r$  and  $\sigma_\phi$  as a function of radius from the main heater. When a dashed curve occurs in the figures the stressmeter reading  $\Delta\sigma_r$  or  $\Delta\sigma_\phi$ , calculated as if the gages were set in the direction of an uniaxial stress, have been plotted to complete the curves.

Figures 8.30 - 8.37 show the measured radial and tangential stress along the A-direction. In the same figure are shown the predicted stress changes as a function of radius from the 6 kW heater.

## 8.4 Thermally induced principal stresses

The principal stresses  $\sigma_1$  and  $\sigma_2$  have been derived from the thermally induced stresses  $\Delta\sigma_r$ ,  $\Delta\sigma_{45}$  and  $\Delta\sigma_\phi$ , according to the theory developed in section 4.5. The results are shown in Figures 8.38 - 8.48. In the same Figures are shown the in situ stresses previously measured by using the overcoring technique.



XBL 788-10172

Fig 8.1

The thermally induced radial ( $\sigma_r$ ) and tangential ( $\sigma_\phi$ ) stresses as a function of time at 0.85 m radius from the 6 kW heater (A-direction).

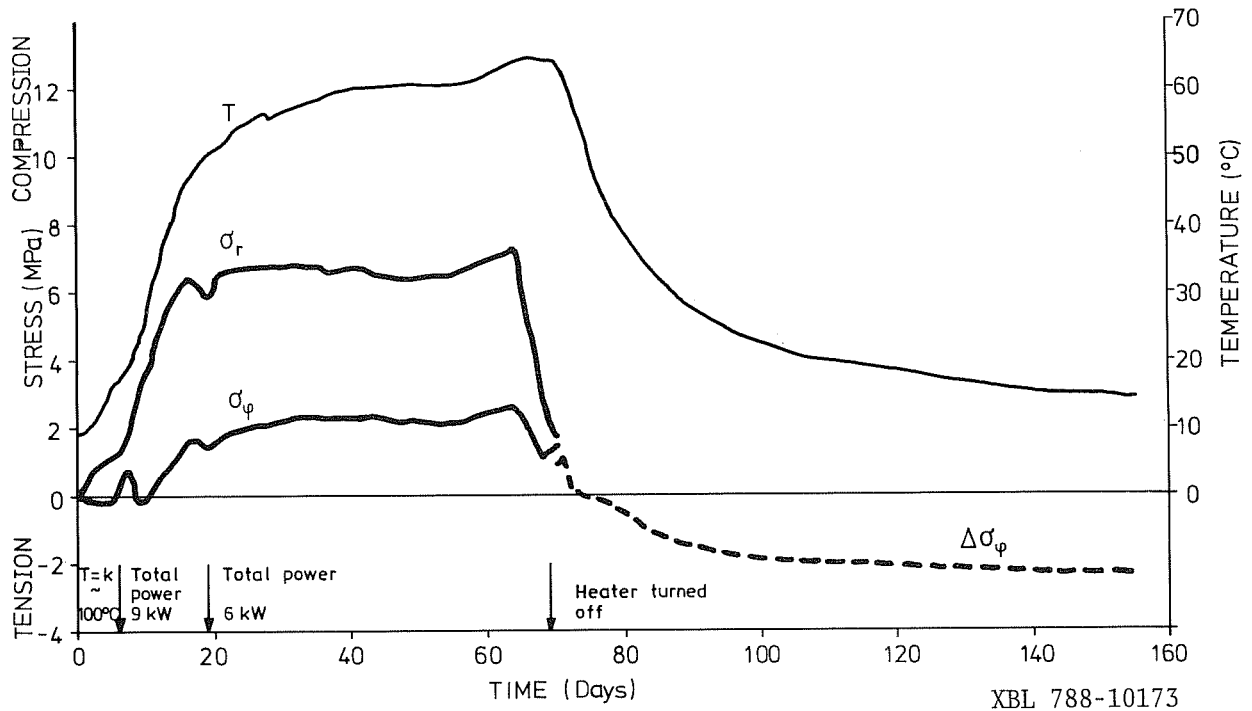


Fig 8.2 The thermally induced radial ( $\sigma_r$ ) and tangential ( $\sigma_\phi$ ) stresses as a function of time at 1.55 m radius from the 6 kW heater (A-direction).

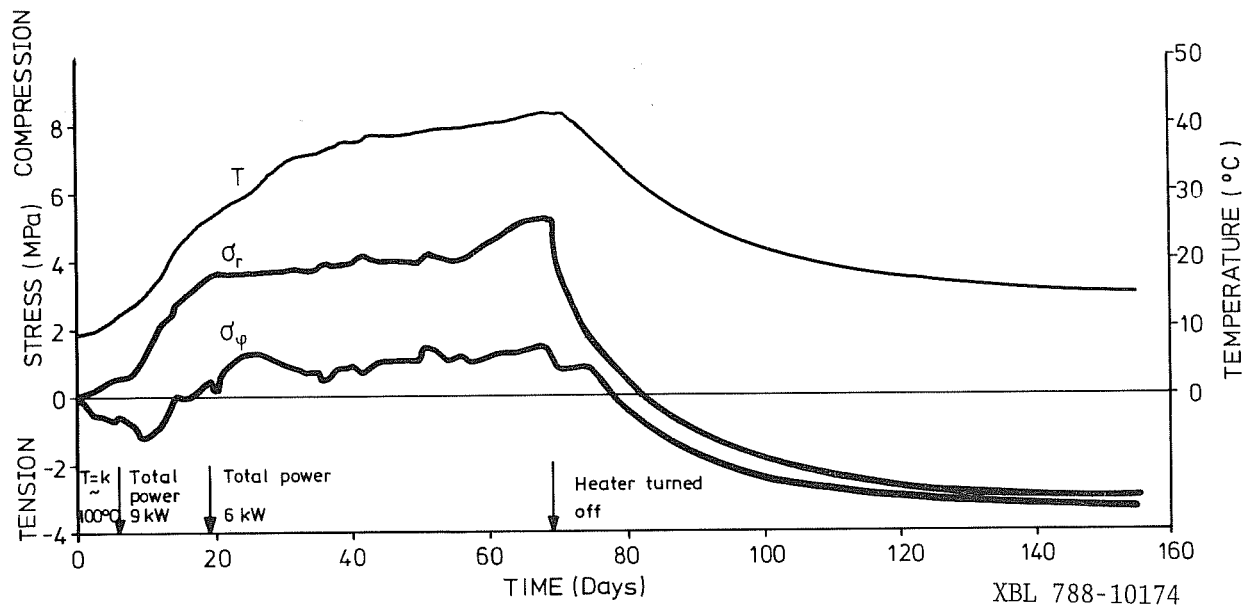
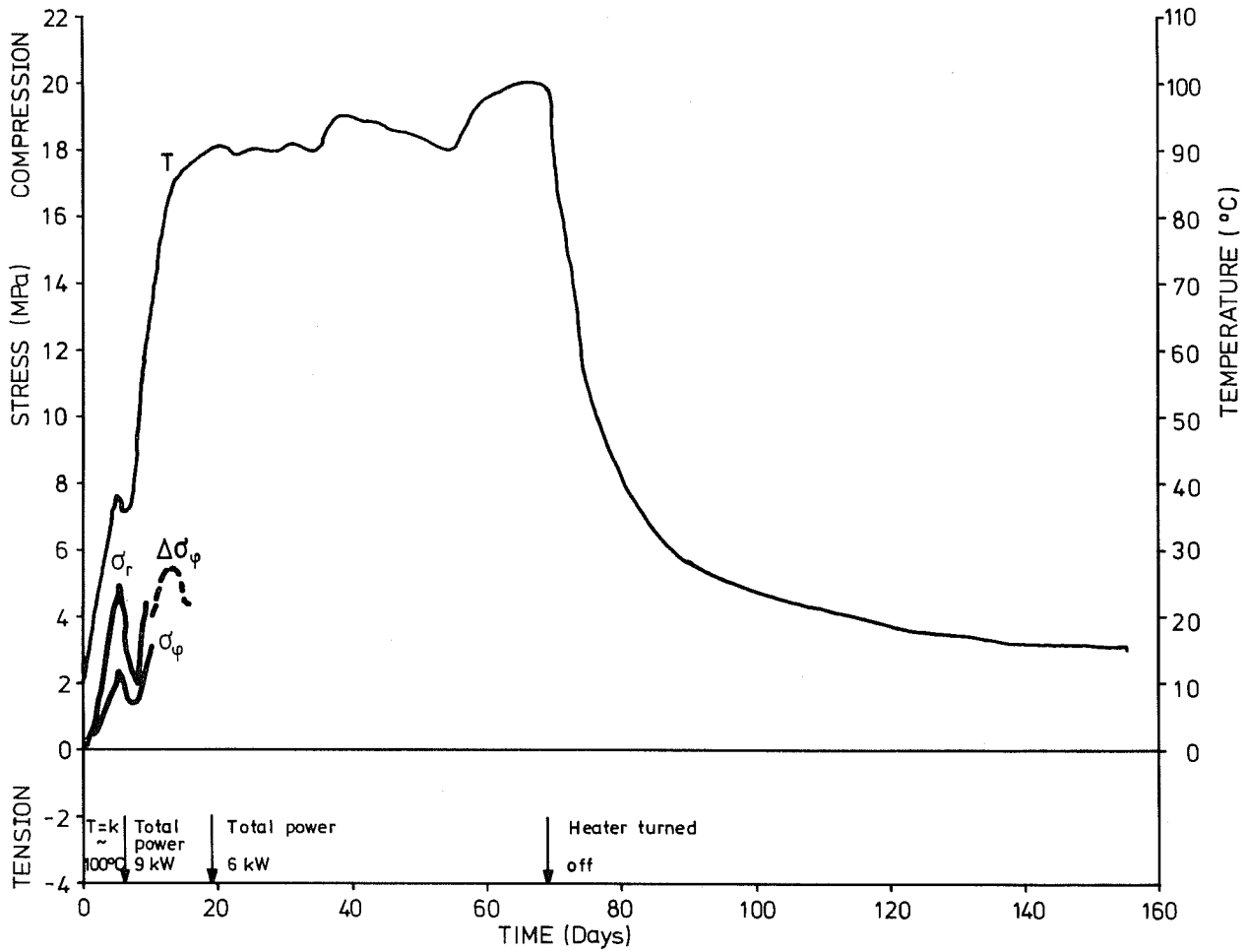


Fig 8.3 The thermally induced radial ( $\sigma_r$ ) and tangential ( $\sigma_\phi$ ) stresses as a function of time at 2.25 m radius from the 6 kW heater (A-direction).



XBL 788-10175

Fig 8.4 The thermally induced radial ( $\sigma_r$ ) and tangential ( $\sigma_\phi$ ) stresses as a function of time at 0.85 m radius from the 6 kW heater (B-direction).

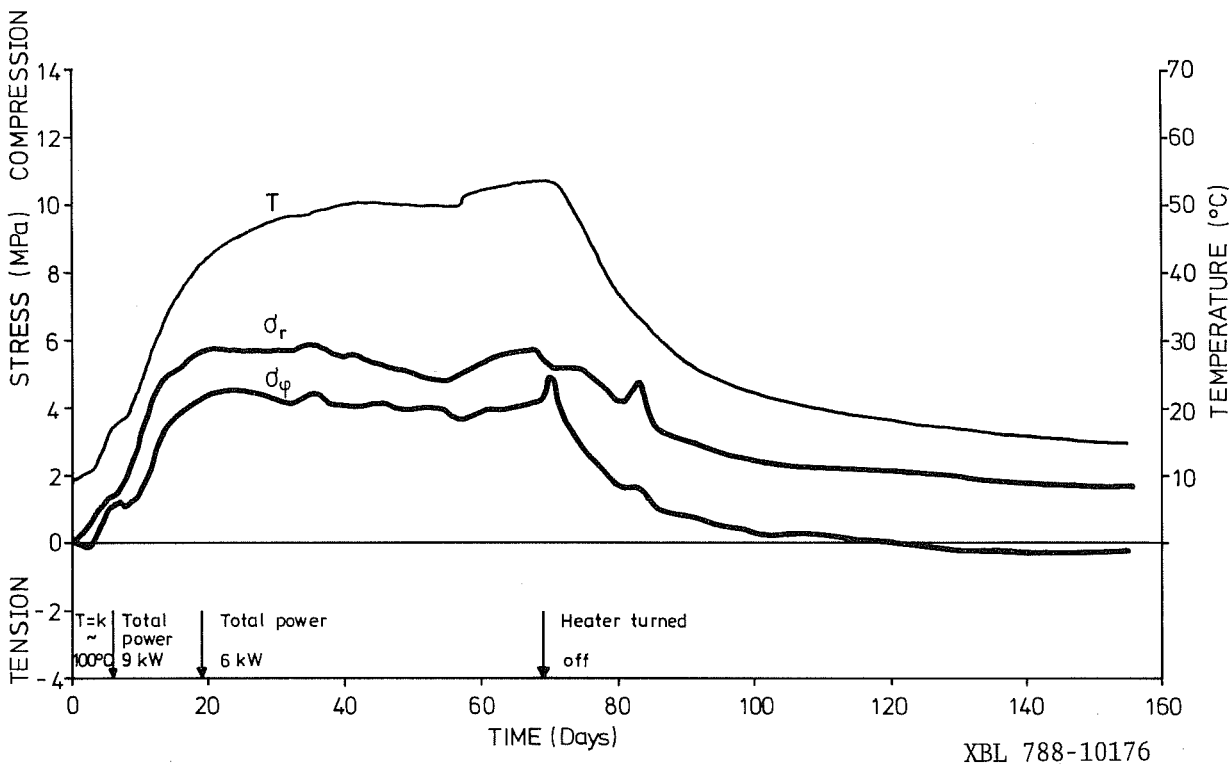


Fig 8.5 The thermally induced radial ( $\sigma_r$ ) and tangential ( $\sigma_\phi$ ) stresses as a function of time at 1.55 m radius from the 6 kW heater (B-direction).

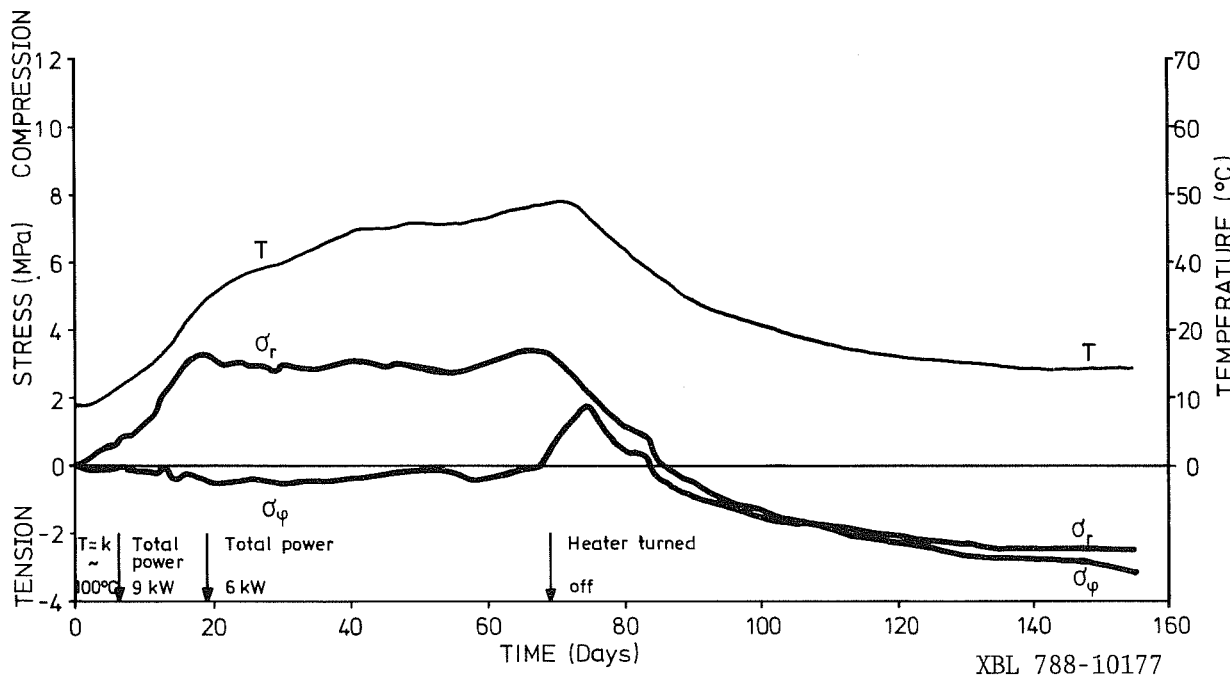
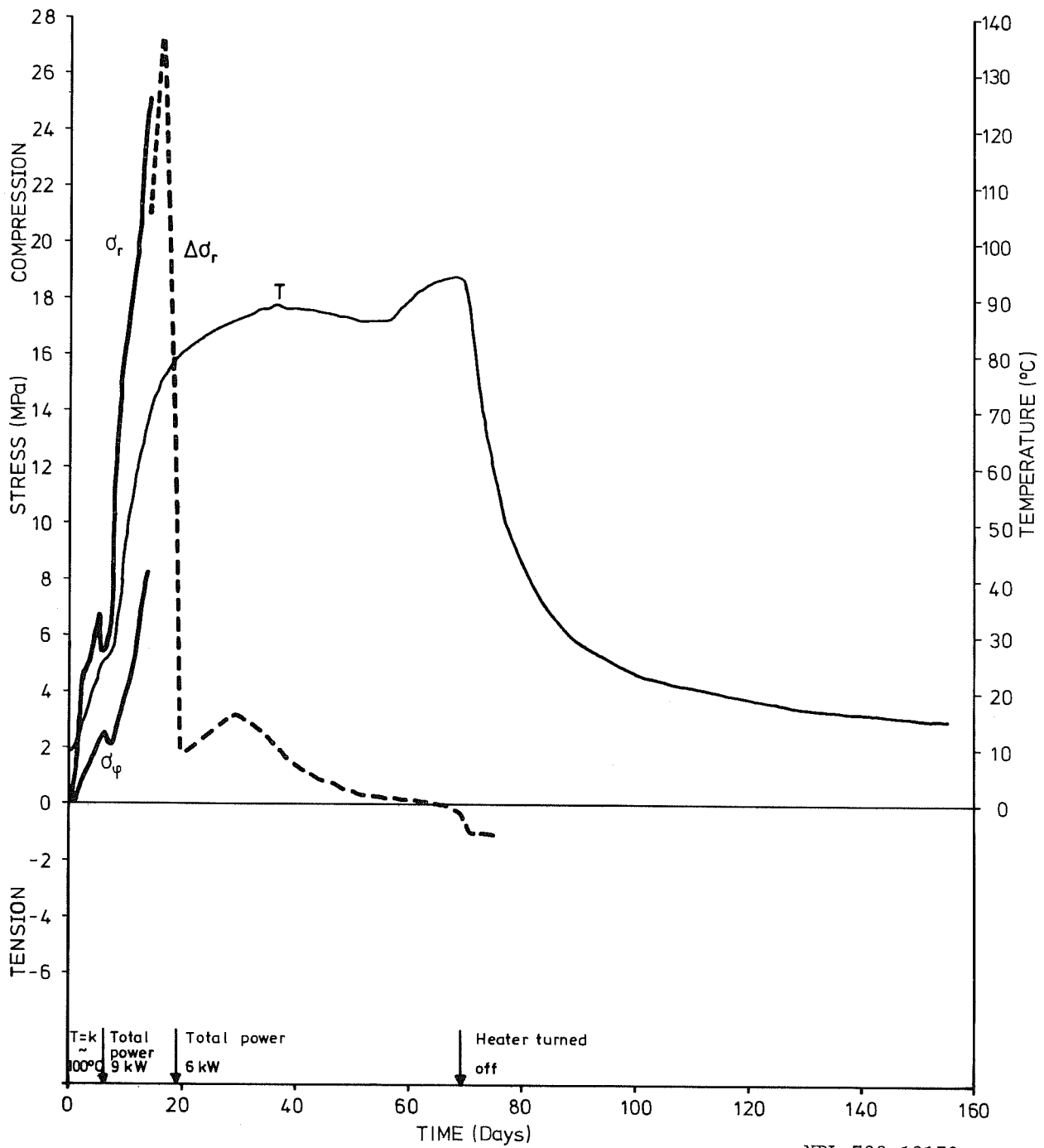


Fig 8.6 The thermally induced radial ( $\sigma_r$ ) and tangential ( $\sigma_\phi$ ) stresses as a function of time at 2.25 m radius from the 6 kW heater (B-direction).



XBL 788-10178

Fig 8.7

The thermally induced radial ( $\sigma_r$ ) and tangential ( $\sigma_\phi$ ) stresses as a function of time at .85 m radius from the 6 kW heater (C-direction).

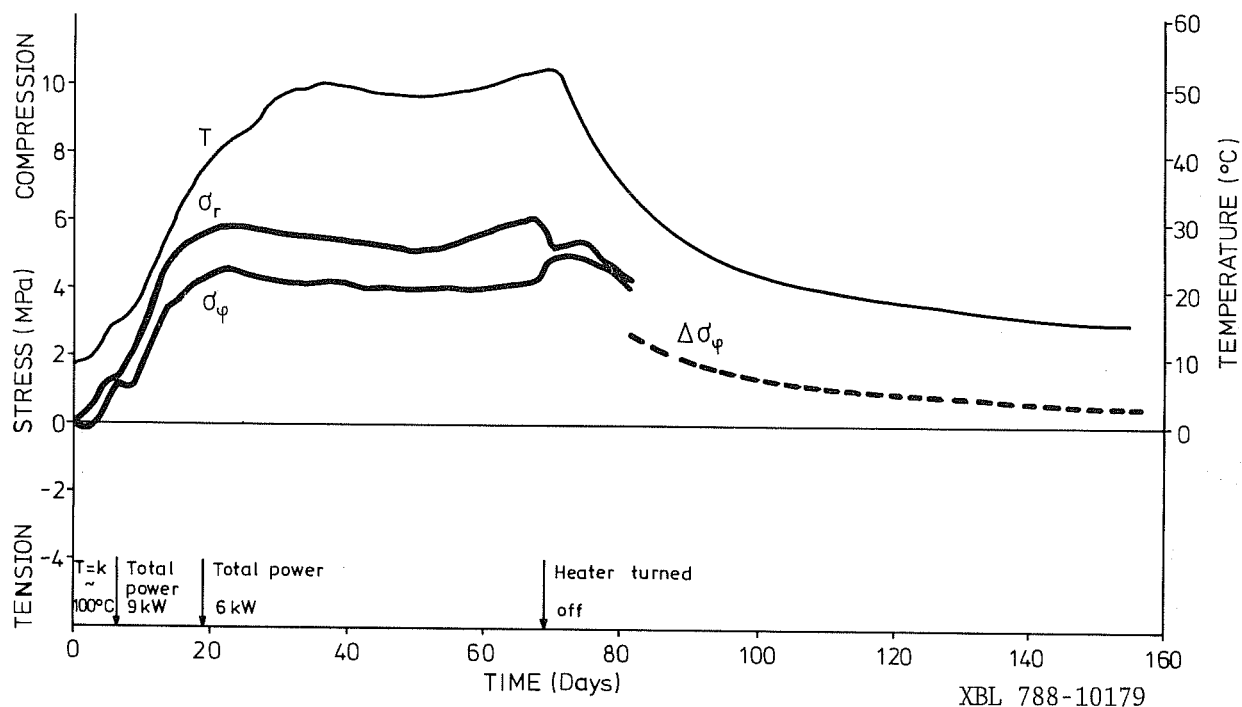


Fig 8.8 The thermally induced radial ( $\sigma_r$ ) and tangential ( $\sigma_\phi$ ) stress as a function of time at 1.55 m radius from the 6 kW heater (C-direction).

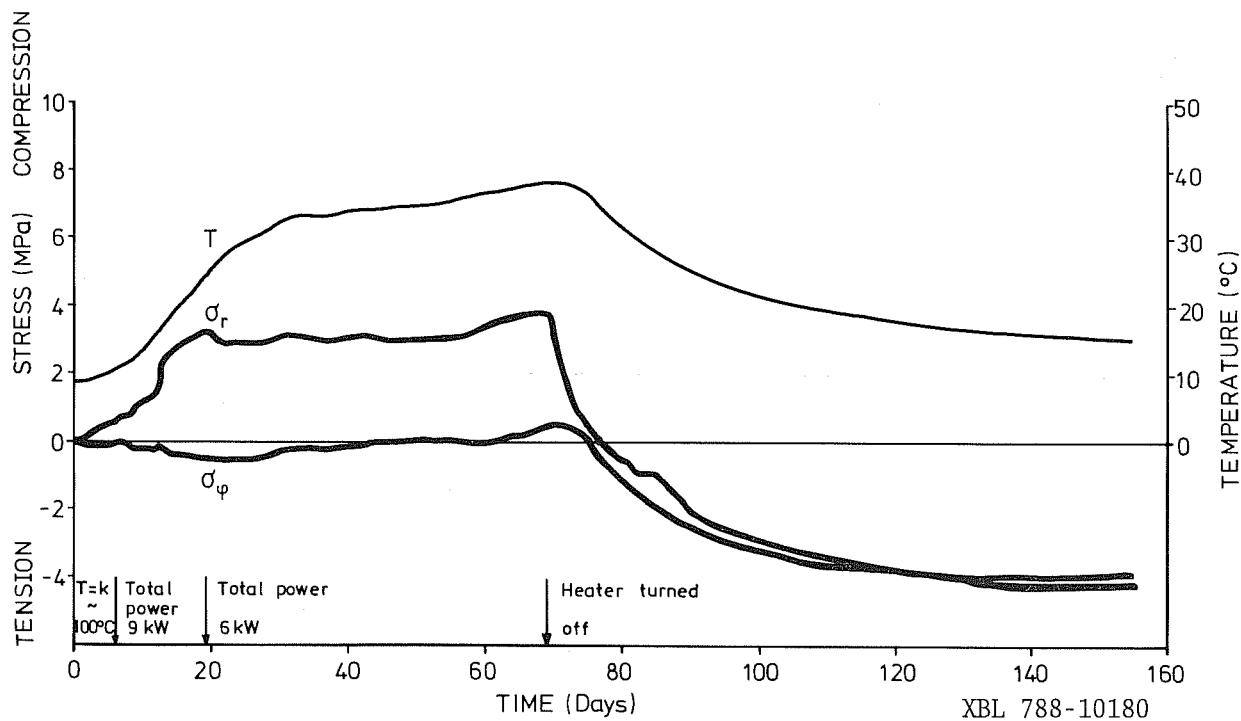
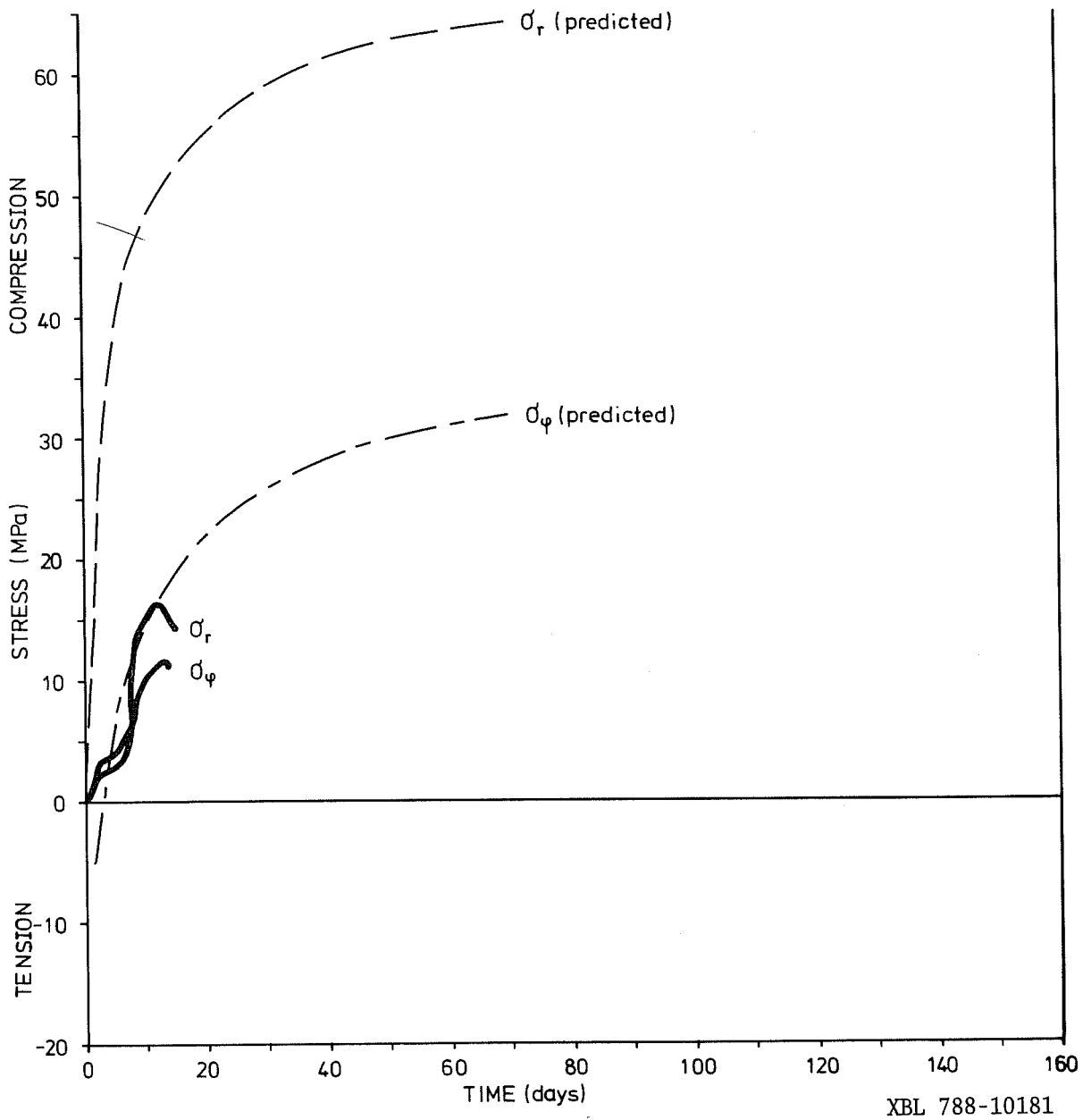


Fig 8.9 The thermally induced radial ( $\sigma_r$ ) and tangential ( $\sigma_\phi$ ) stresses as a function of time at 2.25 m radius from the 6 kW heater (C-direction).



XBL 788-10181

Fig 8.10 Measured (A-direction) and predicted stresses as a function of time at 0.85 m radius from the 6 kW heater.

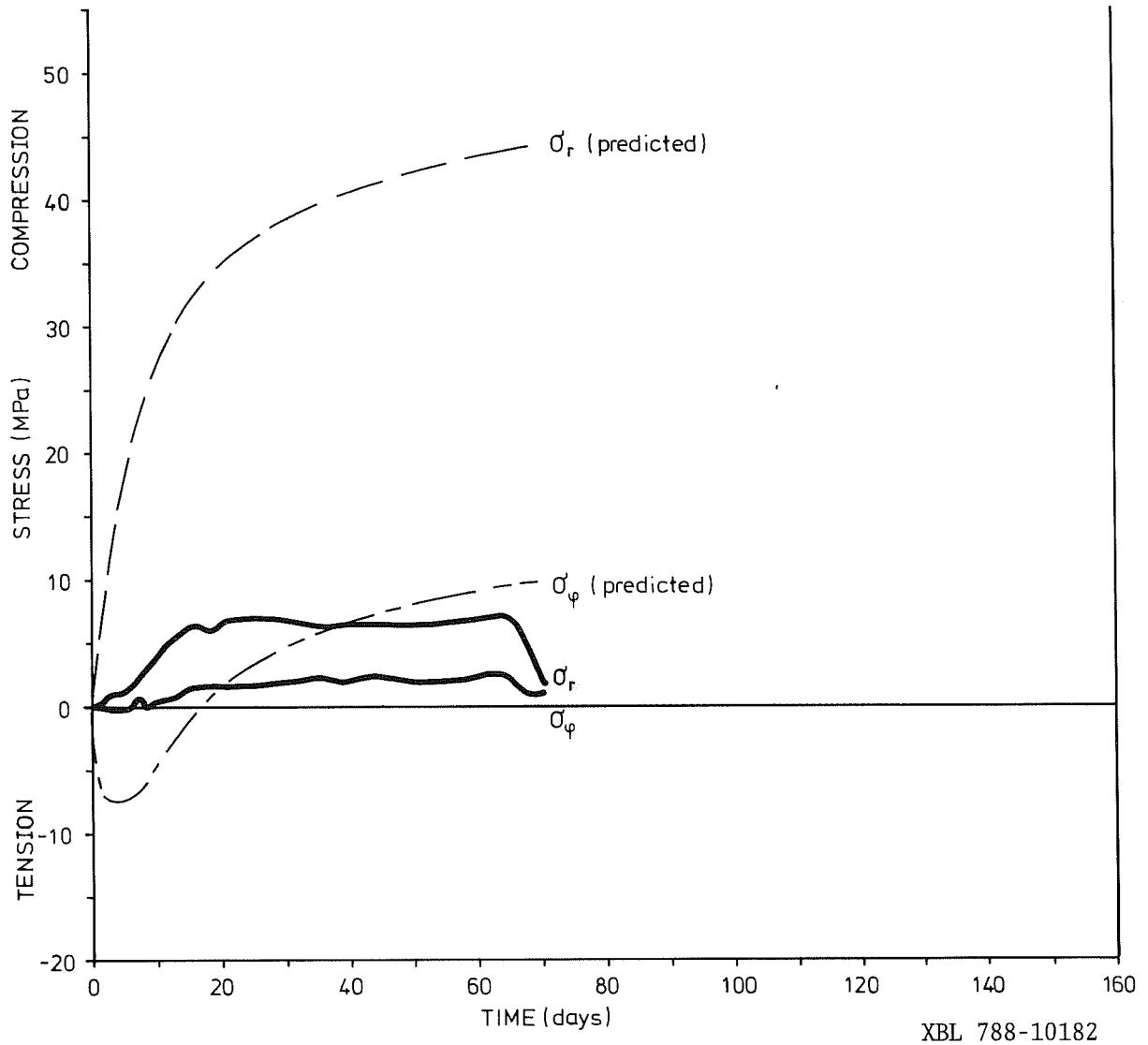


Fig 8.11 Measured (A-direction) and predicted stresses as a function of time at 1.55 m radius from the 6 kW heater.

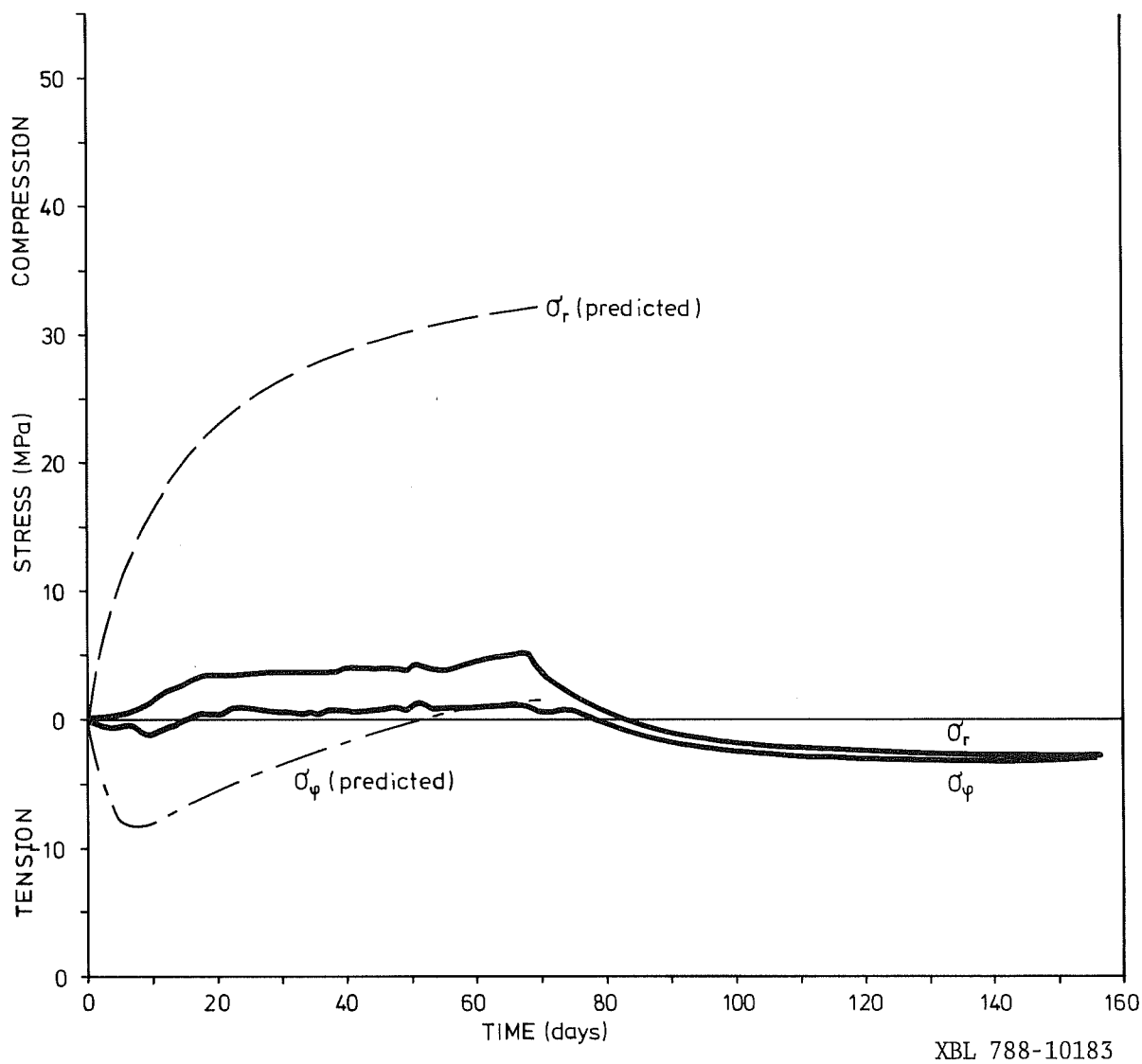


Fig 8.12 Measured (A-direction) and predicted stresses as a function of time at 2.25 m radius from the 6 kW heater.

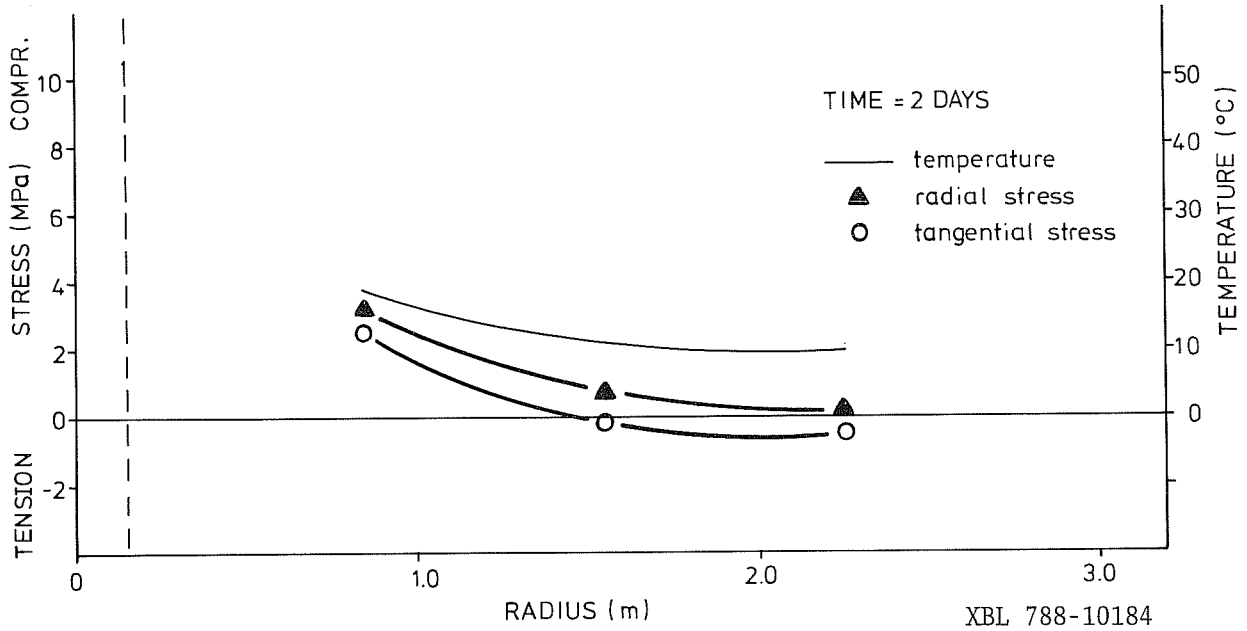


Fig 8.13 The thermally induced radial ( $\sigma_r$ ) and tangential ( $\sigma_\phi$ ) stresses as a function of radius from the 6 kW heater at 2 days (A-direction).

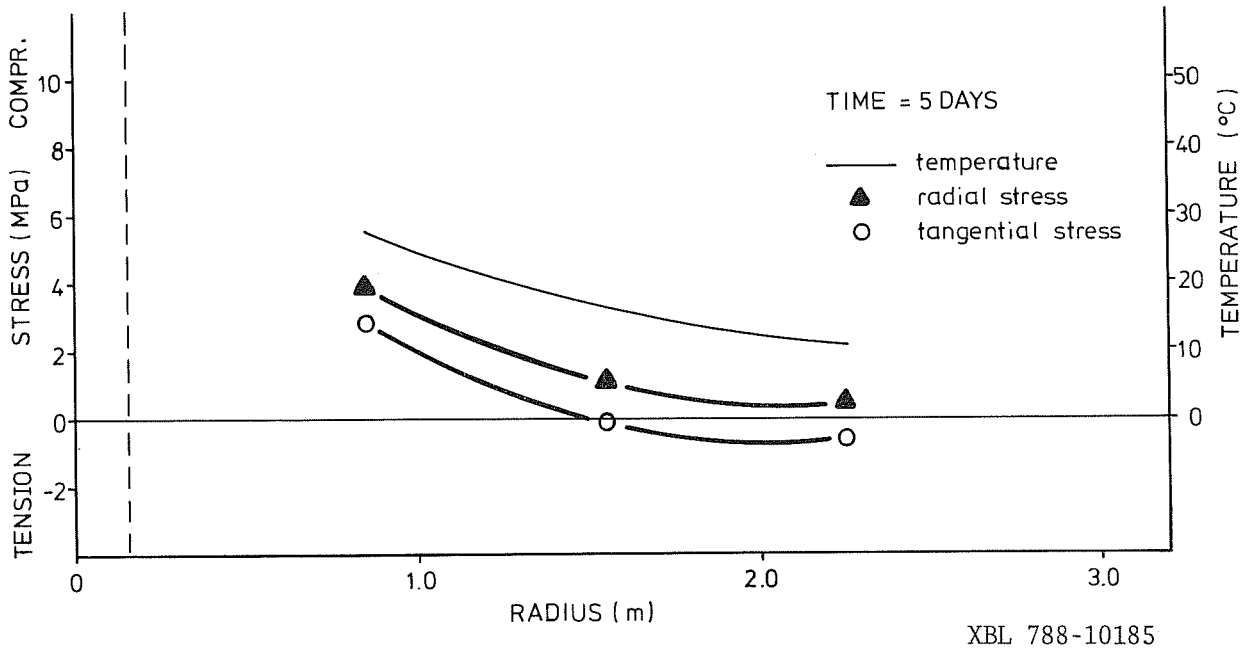


Fig 8.14 The thermally induced radial ( $\sigma_r$ ) and tangential ( $\sigma_\phi$ ) stresses as a function of radius from the 6 kW heater at 5 days (A-direction).

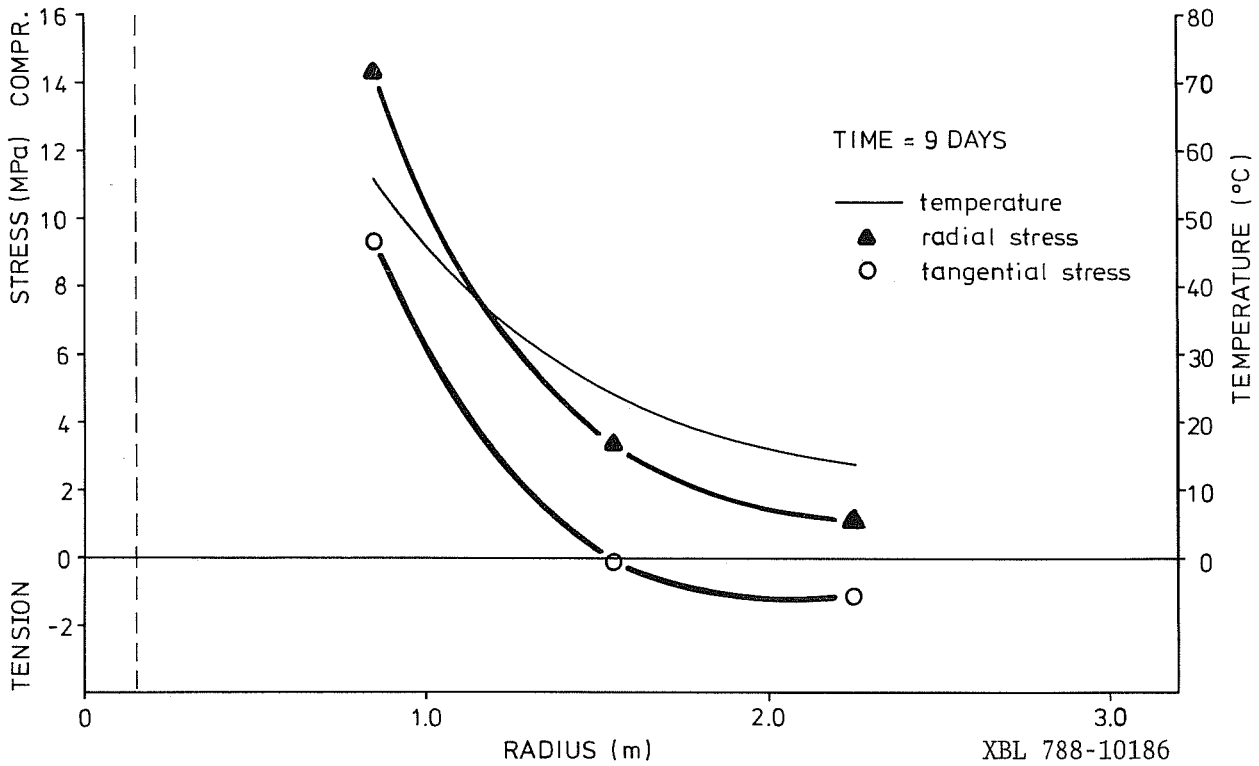
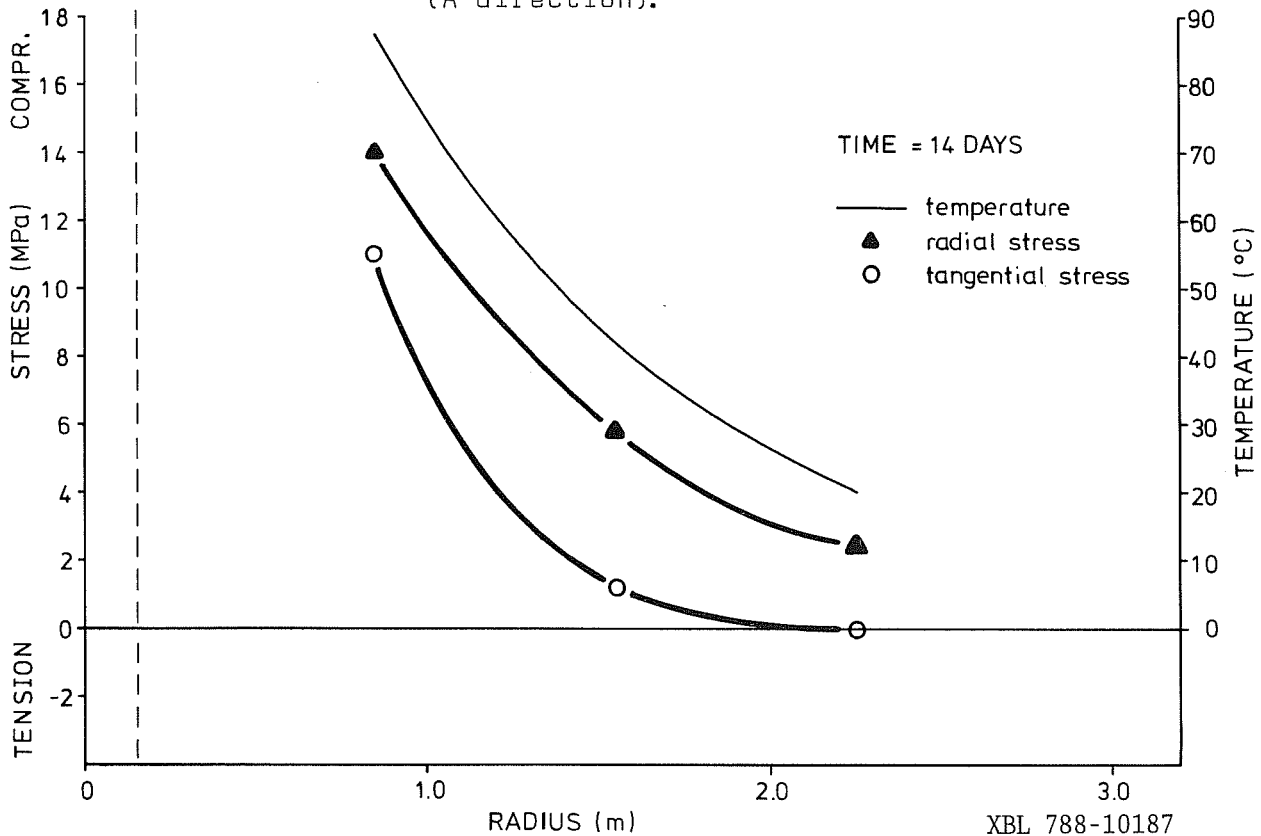


Fig 8.15 The thermally induced radial ( $\sigma_r$ ) and tangential ( $\sigma_\phi$ ) stresses as a function of radius from the 6 kW heater at 9 days (A-direction).



8.16 The thermally induced radial ( $\sigma_r$ ) and tangential ( $\sigma_\phi$ ) stresses as a function of radius from the 6 kW heater at 14 days (A-direction).

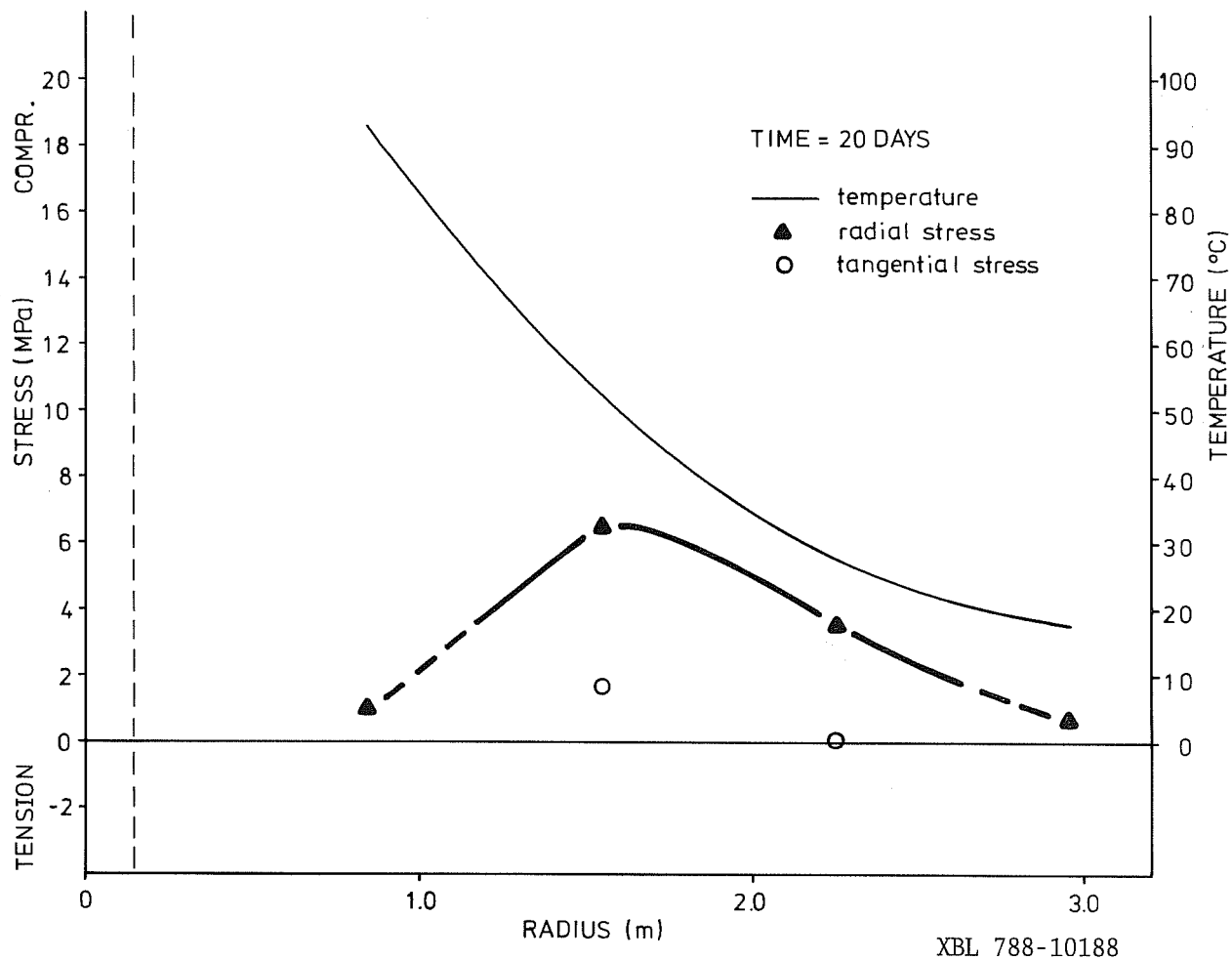


Fig 8.17 The thermally induced radial ( $\sigma_r$ ) and tangential ( $\sigma_\theta$ ) stresses as a function of radius from the 6 kW heater at 20 days (A-direction).

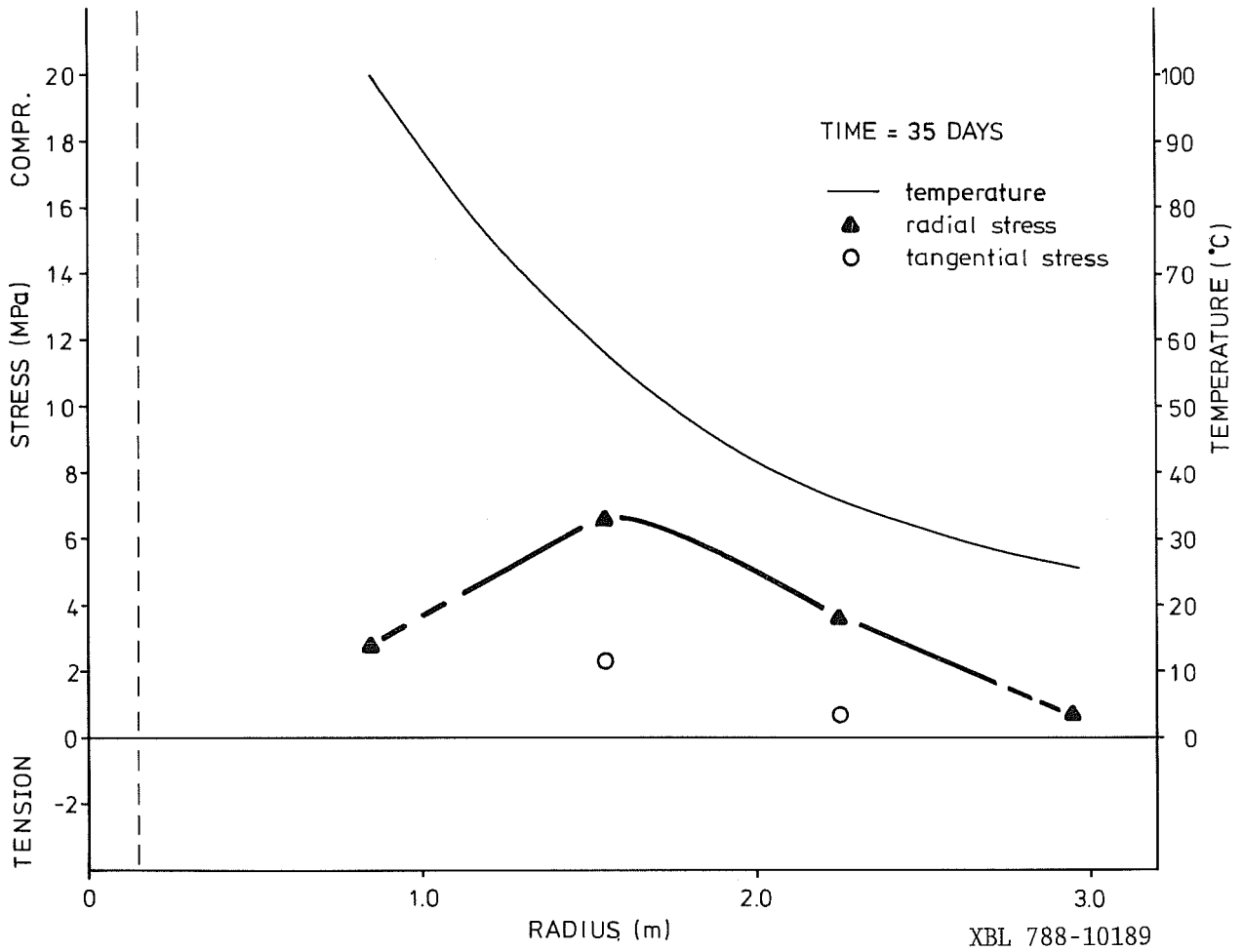
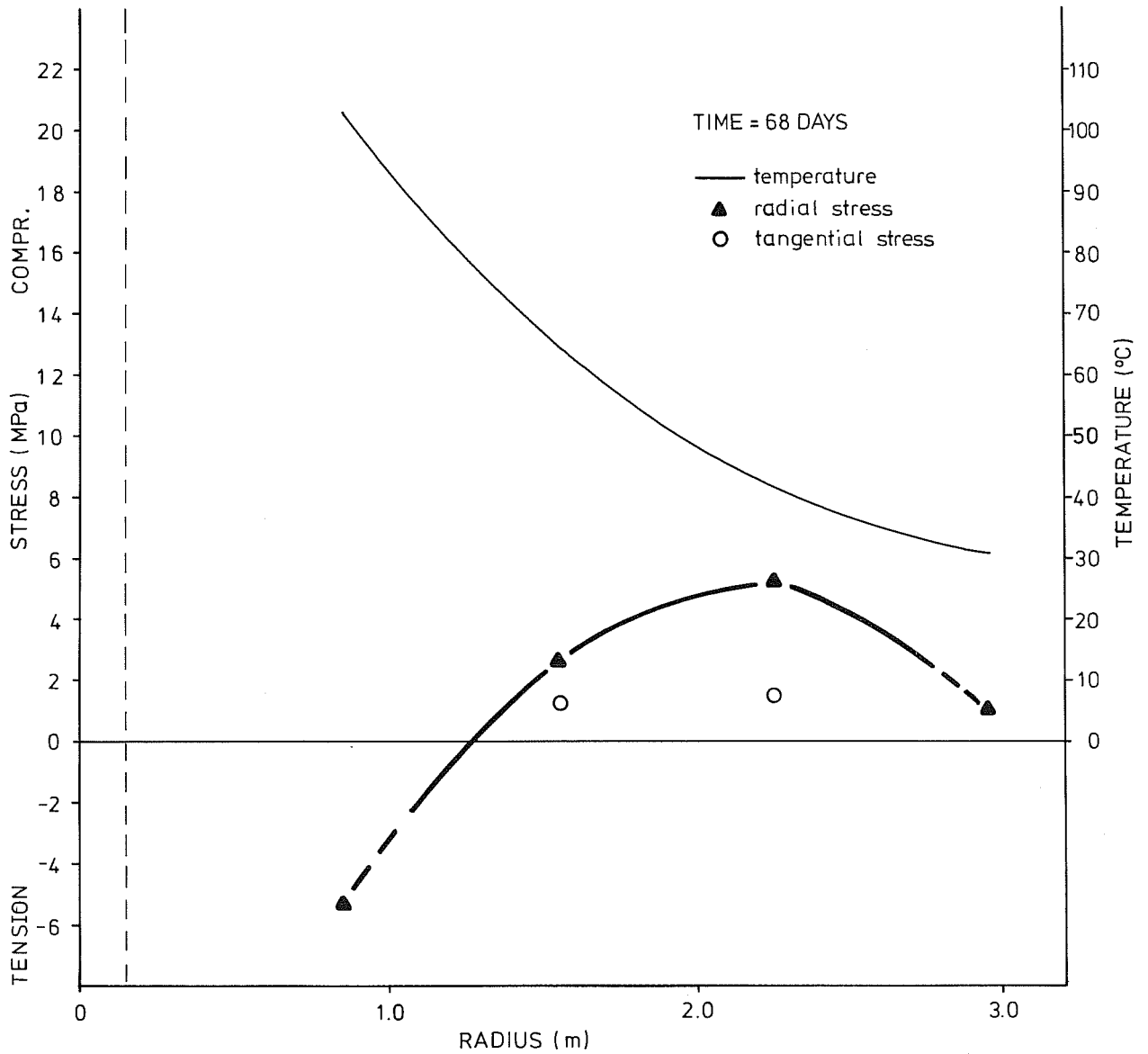


Fig 8.18 The thermally induced radial ( $\sigma_r$ ) and tangential ( $\sigma_\phi$ ) stresses as a function of radius from the 6 kW heater at 35 days (A-direction).

XBL 788-10189



XBL 788-10190

Fig 8.19 The thermally induced radial ( $\sigma_r$ ) and tangential ( $\sigma_\phi$ ) stresses as a function of radius from the 6 kW heater at 68 days (A-direction).

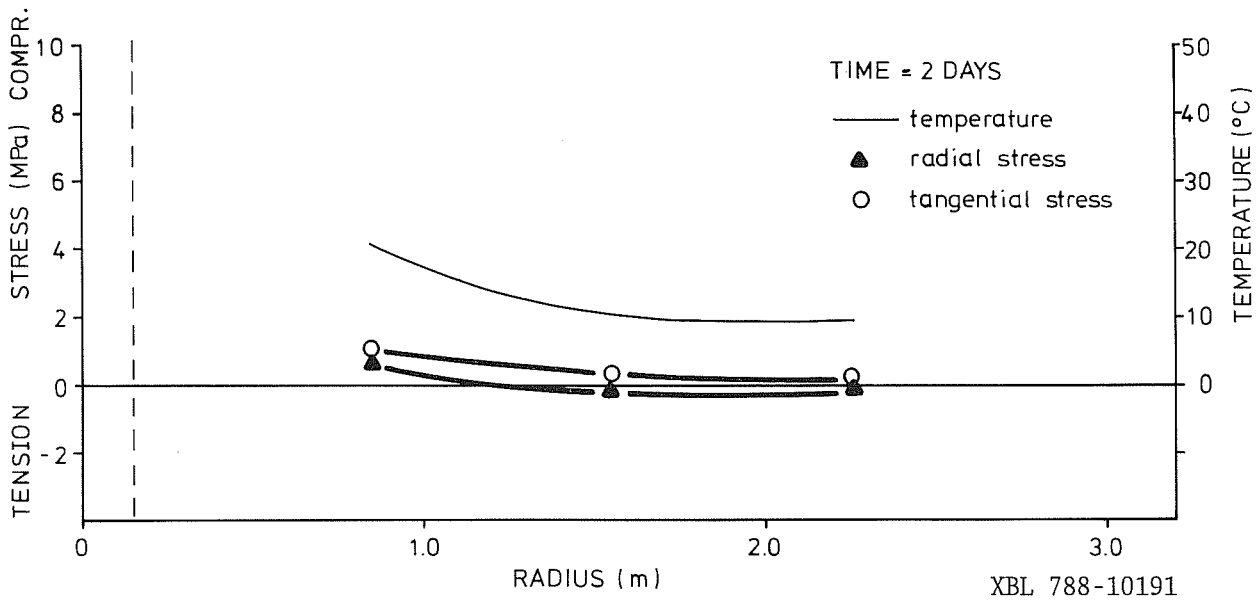


Fig 8.20 The thermally induced radial ( $\sigma_r$ ) and tangential ( $\sigma_\phi$ ) stresses as a function of radius from the 6 kW heater at 2 days (B-direction).

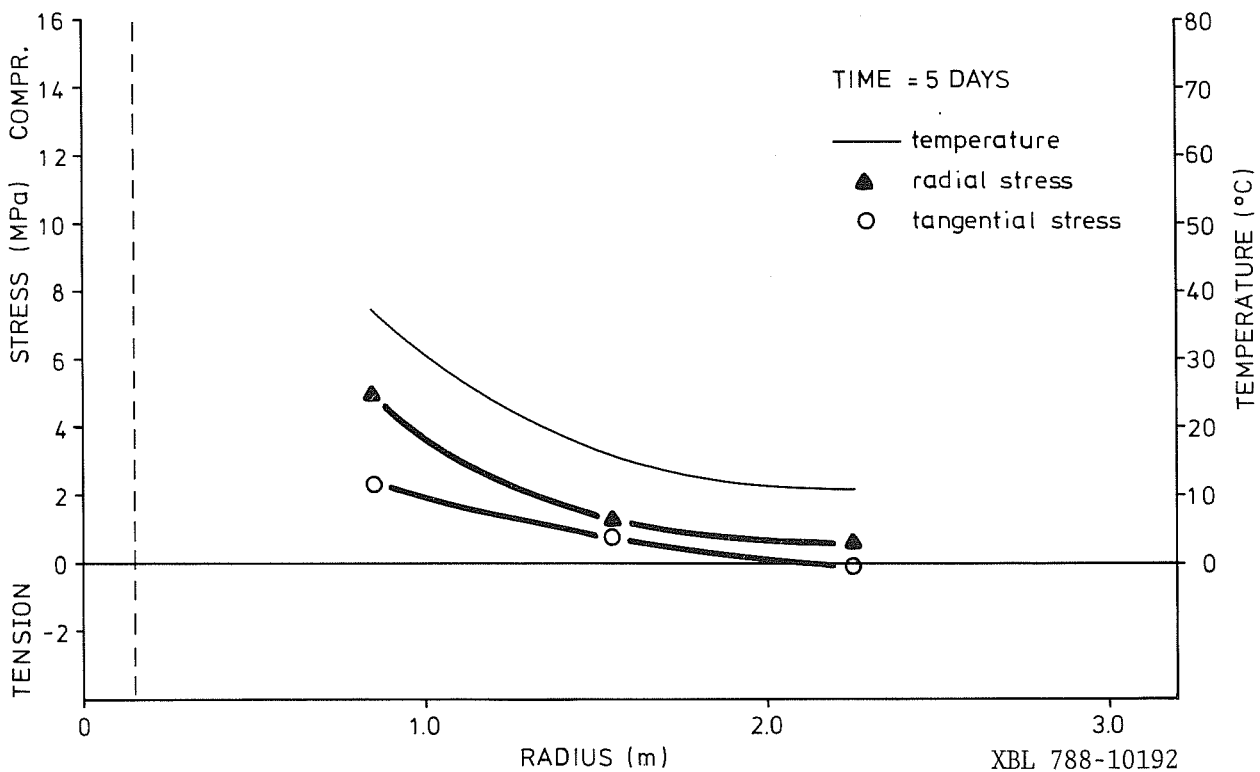


Fig 8.21 The thermally induced radial ( $\sigma_r$ ) and tangential ( $\sigma_\phi$ ) stresses as a function of radius from the 6 kW heater at 5 days (B-direction).

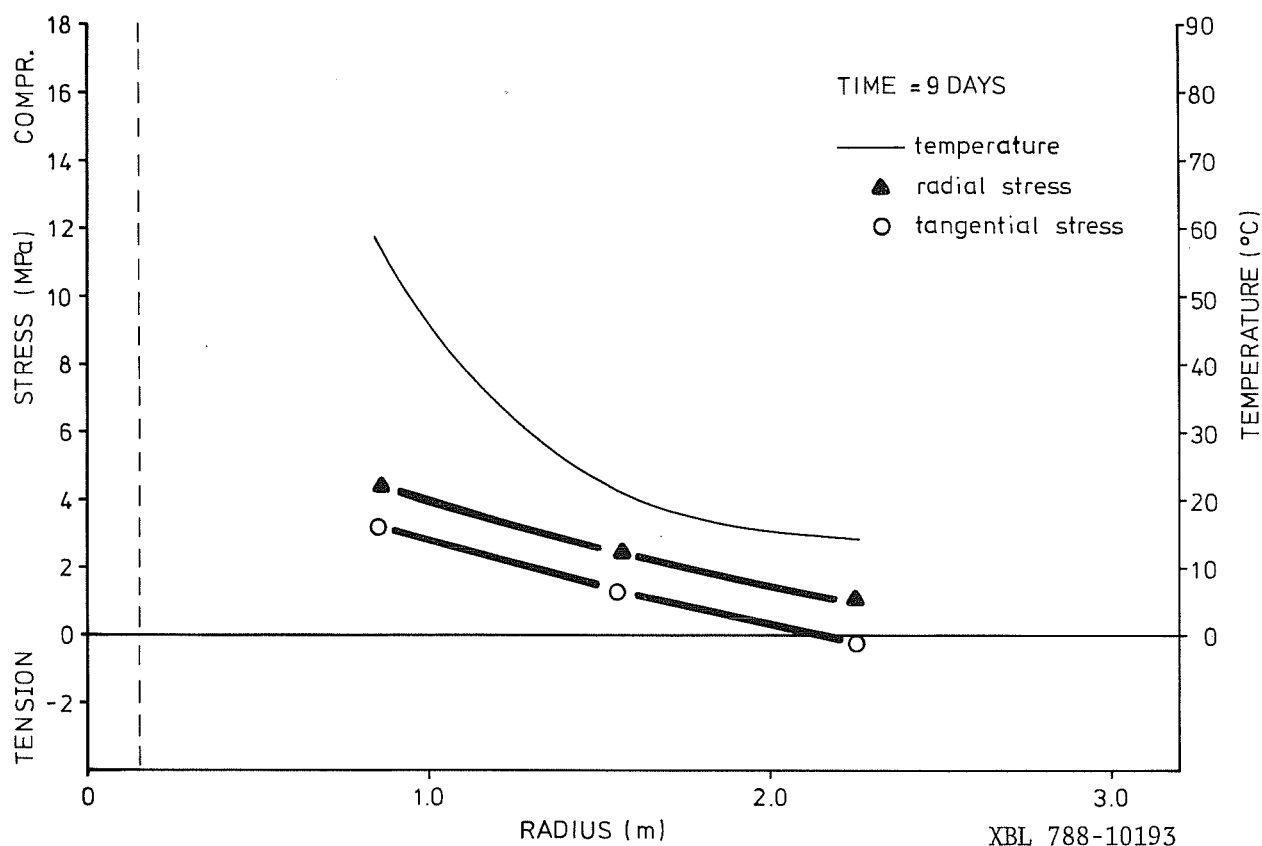


Fig 8.22 The thermally induced radial ( $\sigma_r$ ) and tangential ( $\sigma_\phi$ ) stresses as a function of radius from the 6 kW heater at 9 days (B-direction).

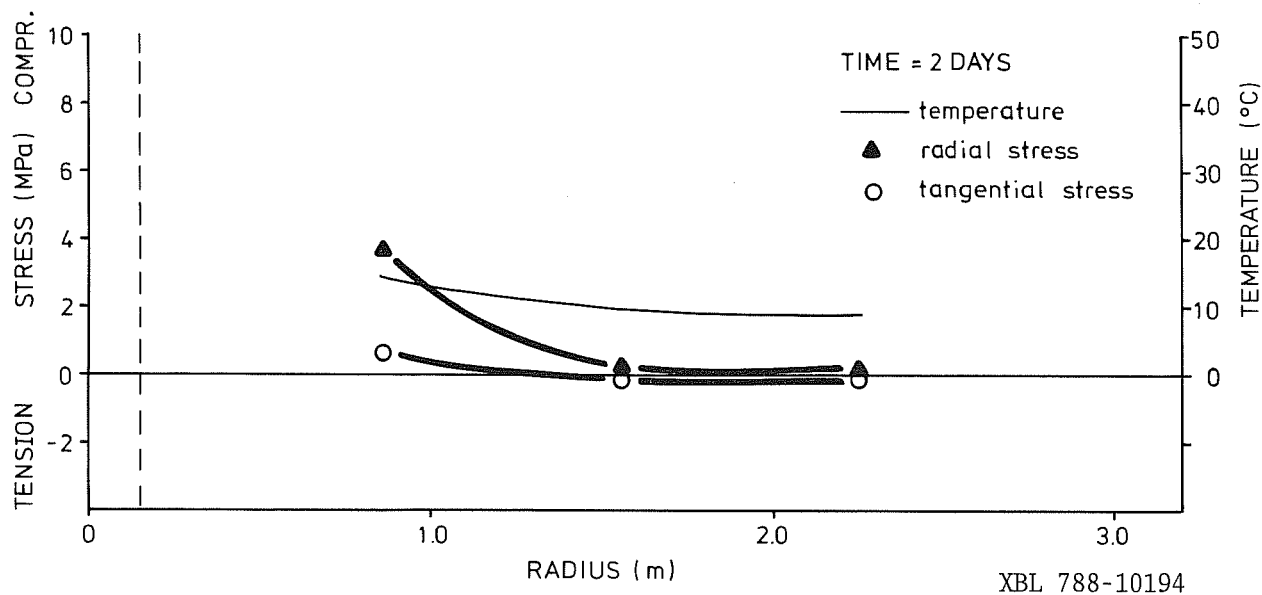


Fig 8.23 The thermally induced radial ( $\sigma_r$ ) and tangential ( $\sigma_\phi$ ) stresses as a function of radius from the 6 kW heater at 2 days (C-direction).

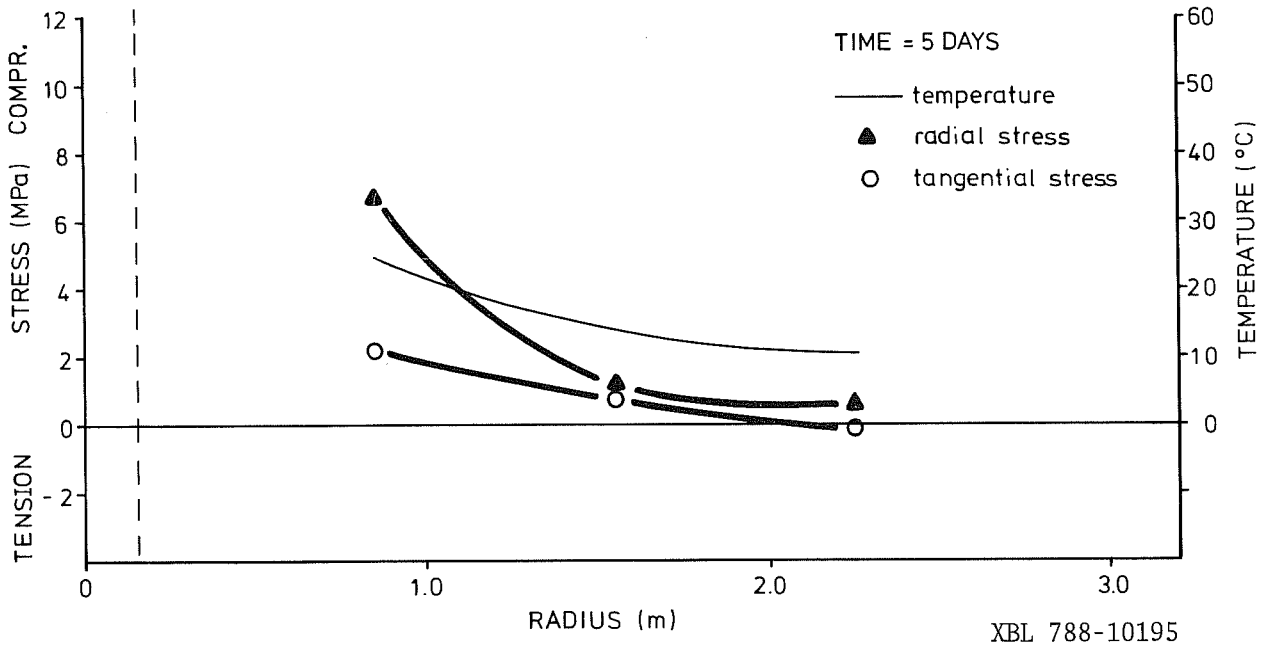


Fig 8.24 The thermally induced radial ( $\sigma_r$ ) and tangential ( $\sigma_\phi$ ) stresses as a function of radius from the 6 kW heater at 5 days (C-direction).

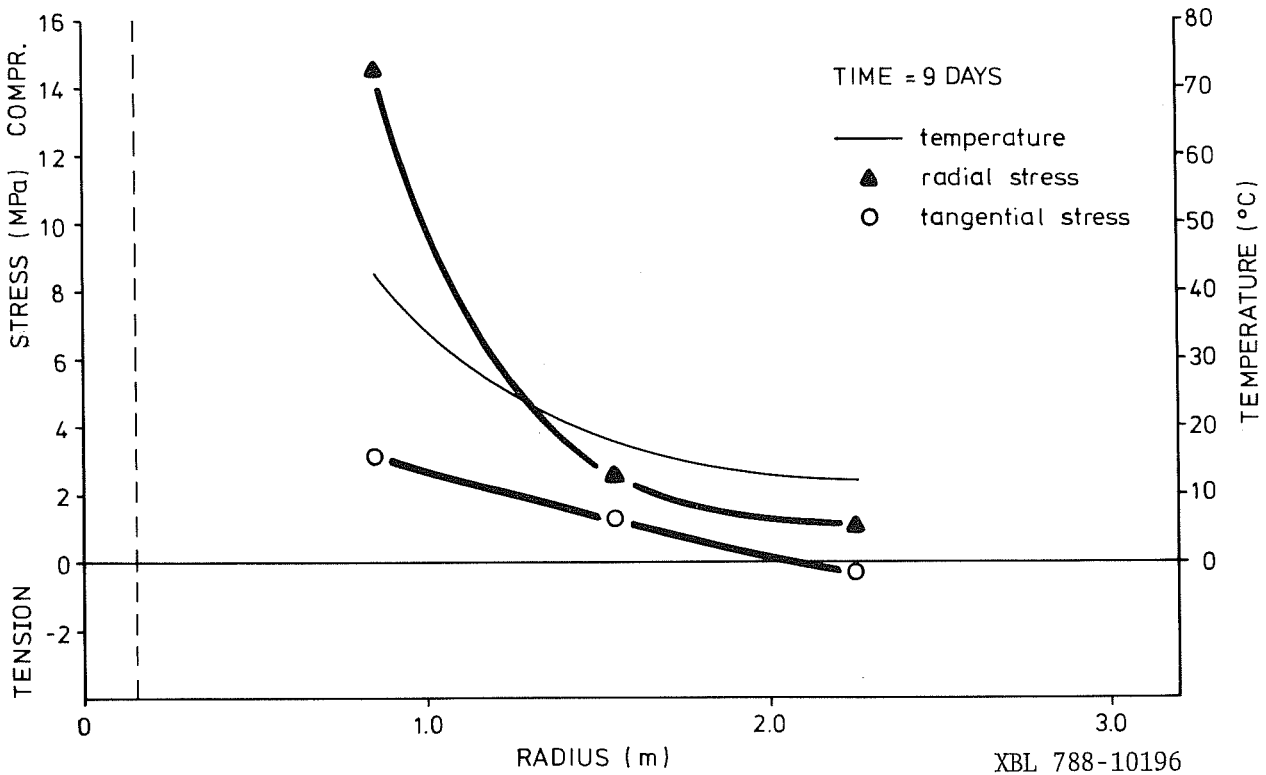


Fig 8.25 The thermally induced radial ( $\sigma_r$ ) and tangential ( $\sigma_\phi$ ) stresses as a function of radius from the 6 kW heater at 9 days (C-direction).

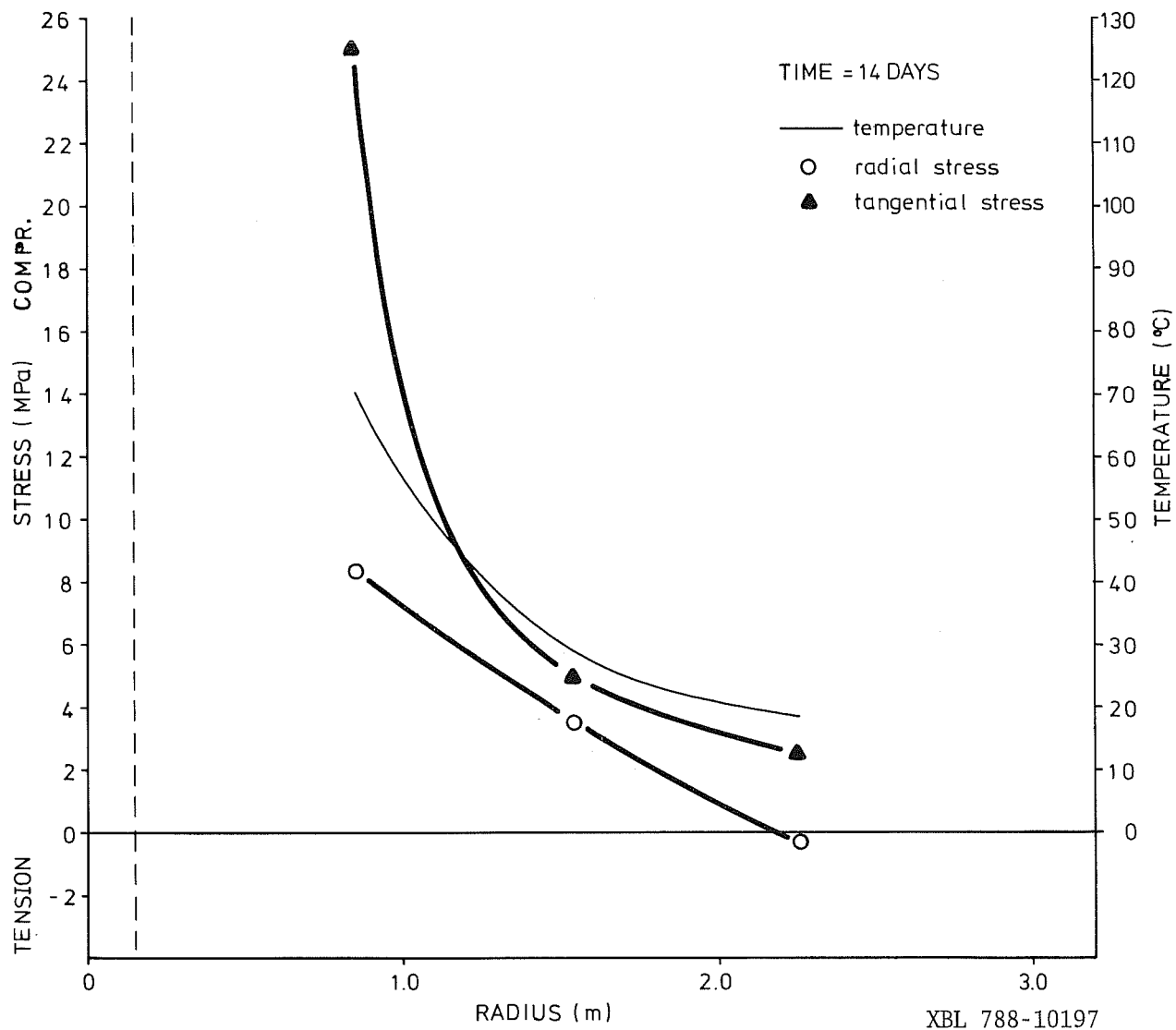


Fig 8.26 The thermally induced radial ( $\sigma_r$ ) and tangential ( $\sigma_\phi$ ) stresses as a function of radius from the 6 kW heater at 14 days (C-direction).

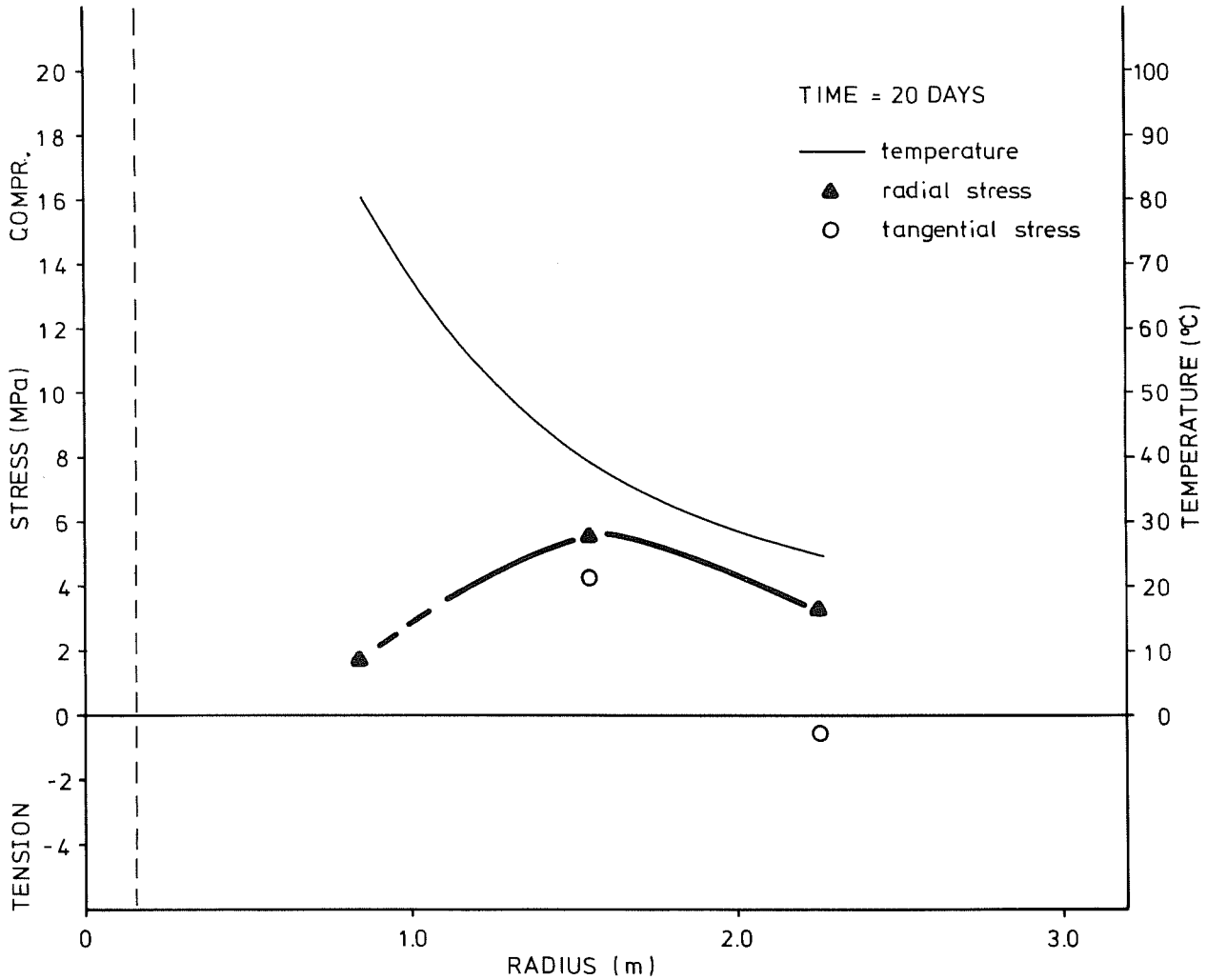
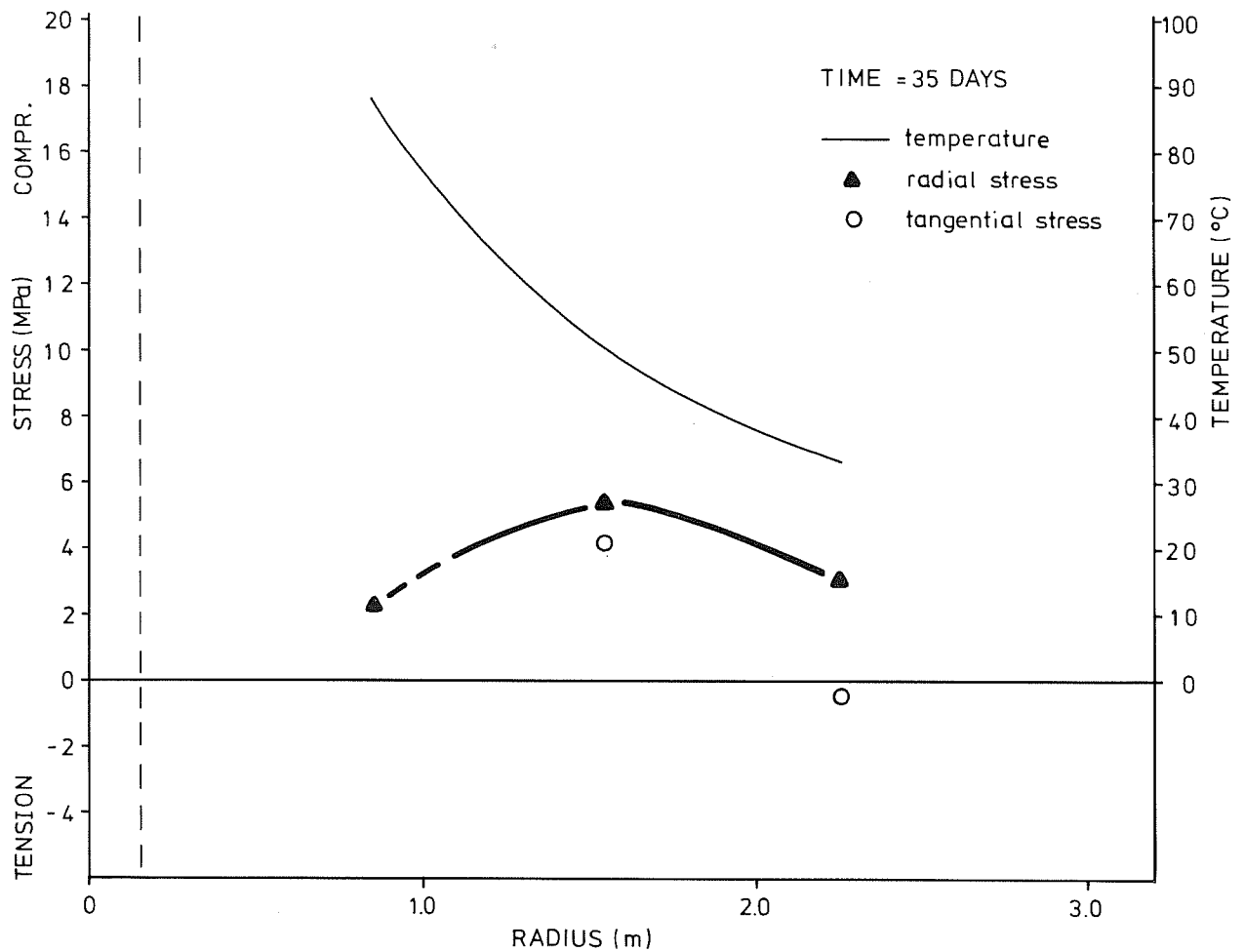


Fig 8.27 The thermally induced radial ( $\sigma_r$ ) and tangential ( $\sigma_\theta$ ) stresses as a function of radius from the 6 kW heater at 20 days (C-direction).



XBL 788-10199

Fig 8.28 The thermally induced radial ( $\sigma_r$ ) and tangential ( $\sigma_\phi$ ) stresses as a function of radius from the 6 kW heater at 35 days (C-direction).

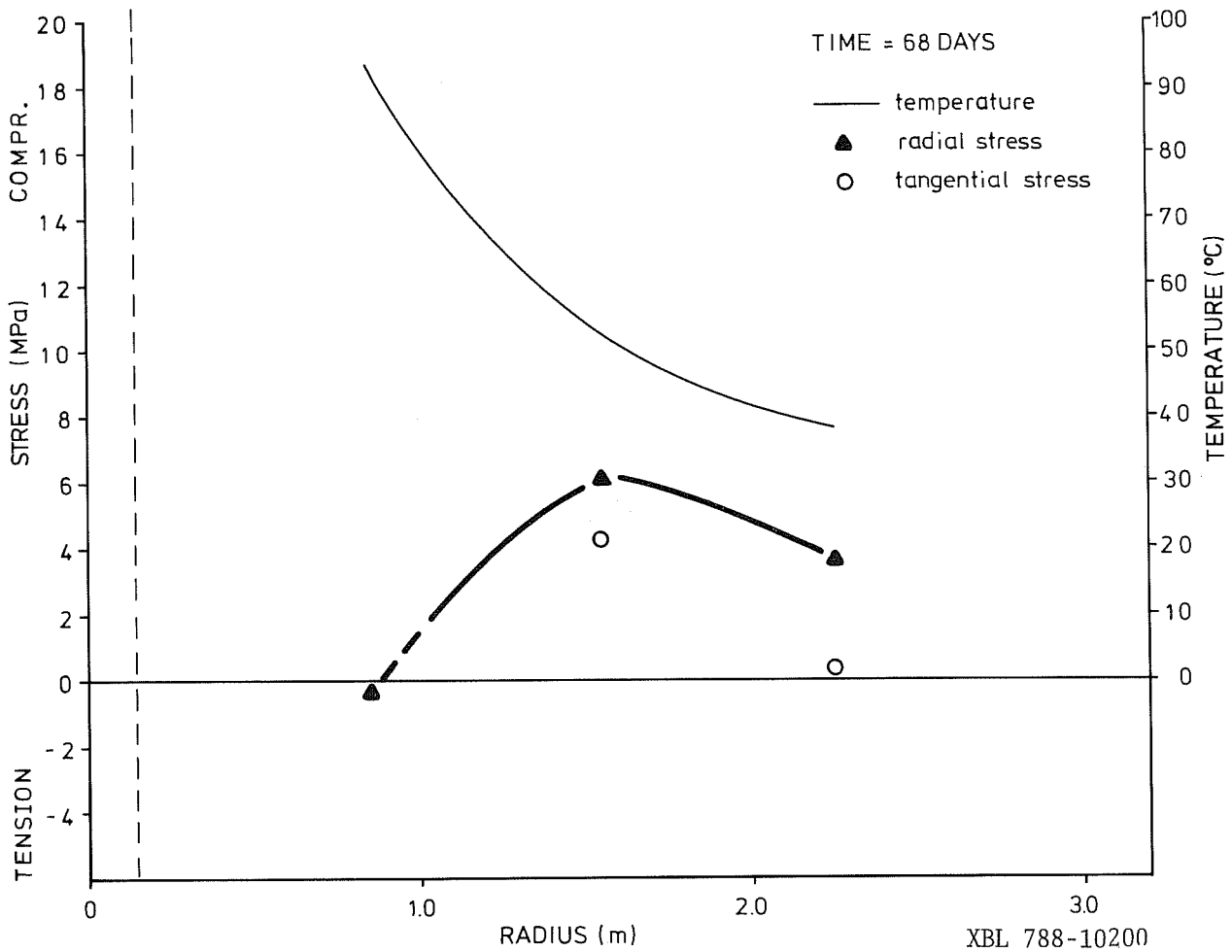


Fig 8.29 The thermally induced radial ( $\sigma_r$ ) and tangential ( $\sigma_\phi$ ) stresses as a function of radius from the 6 kW heater at 68 days (C-direction).

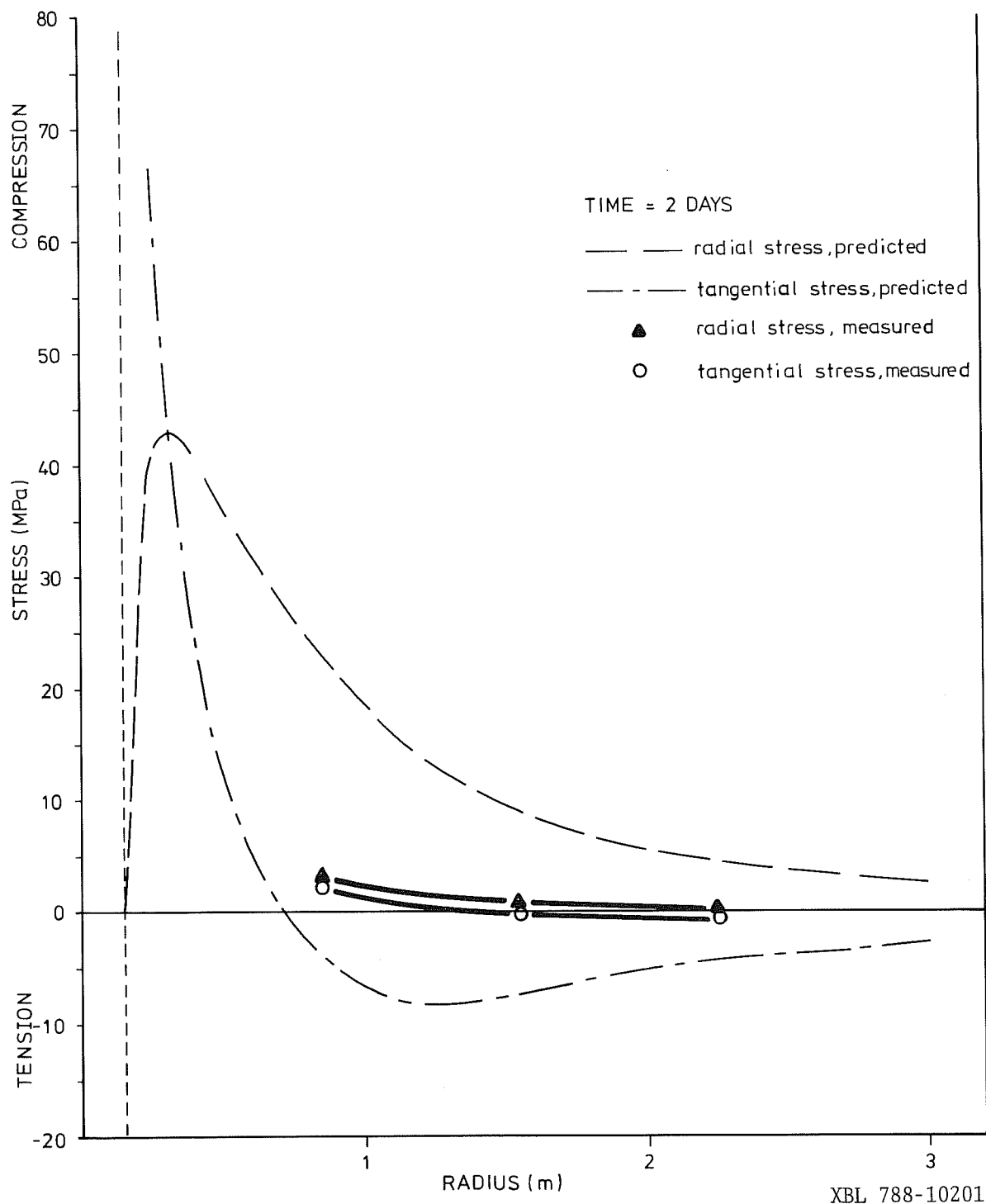
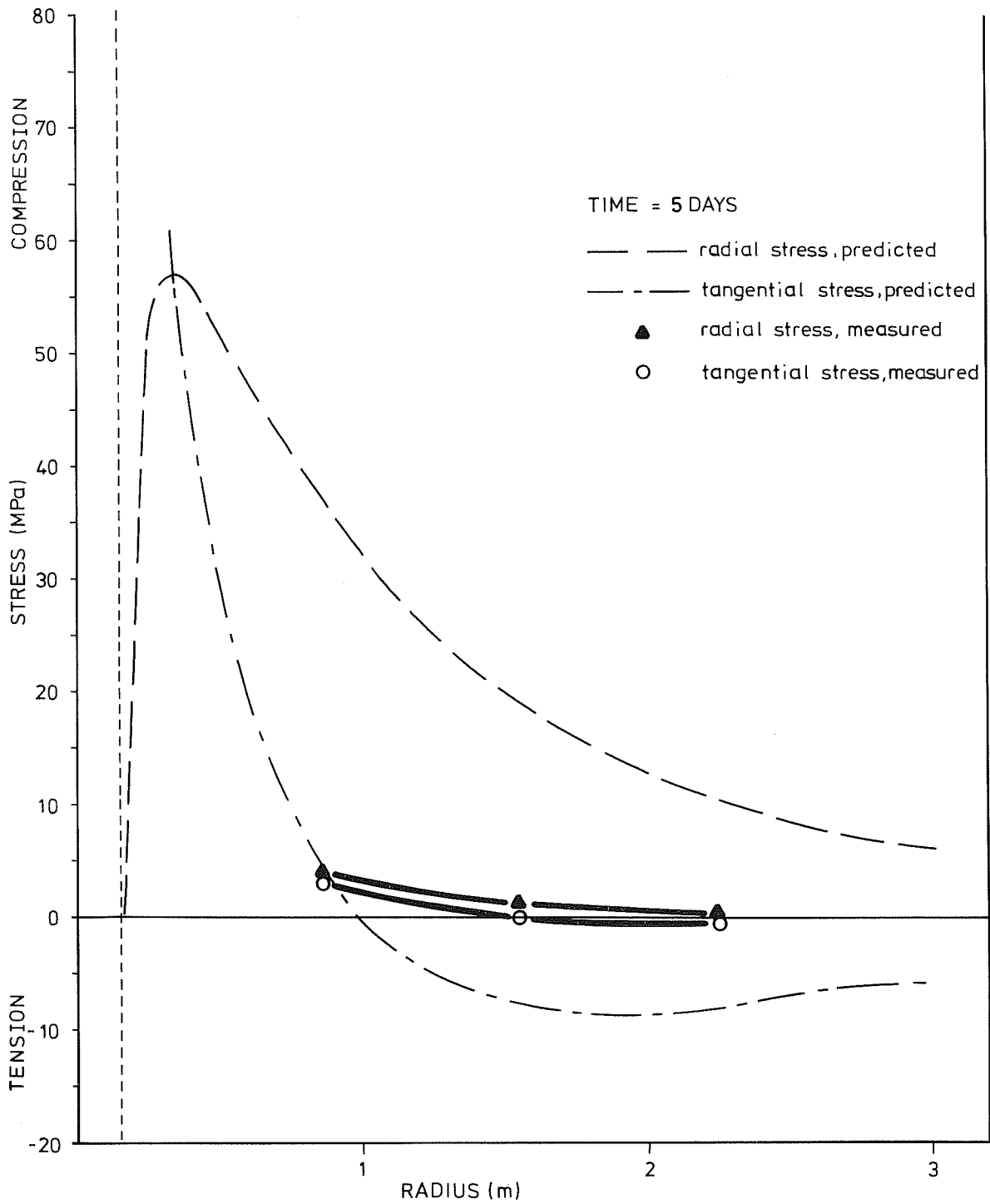
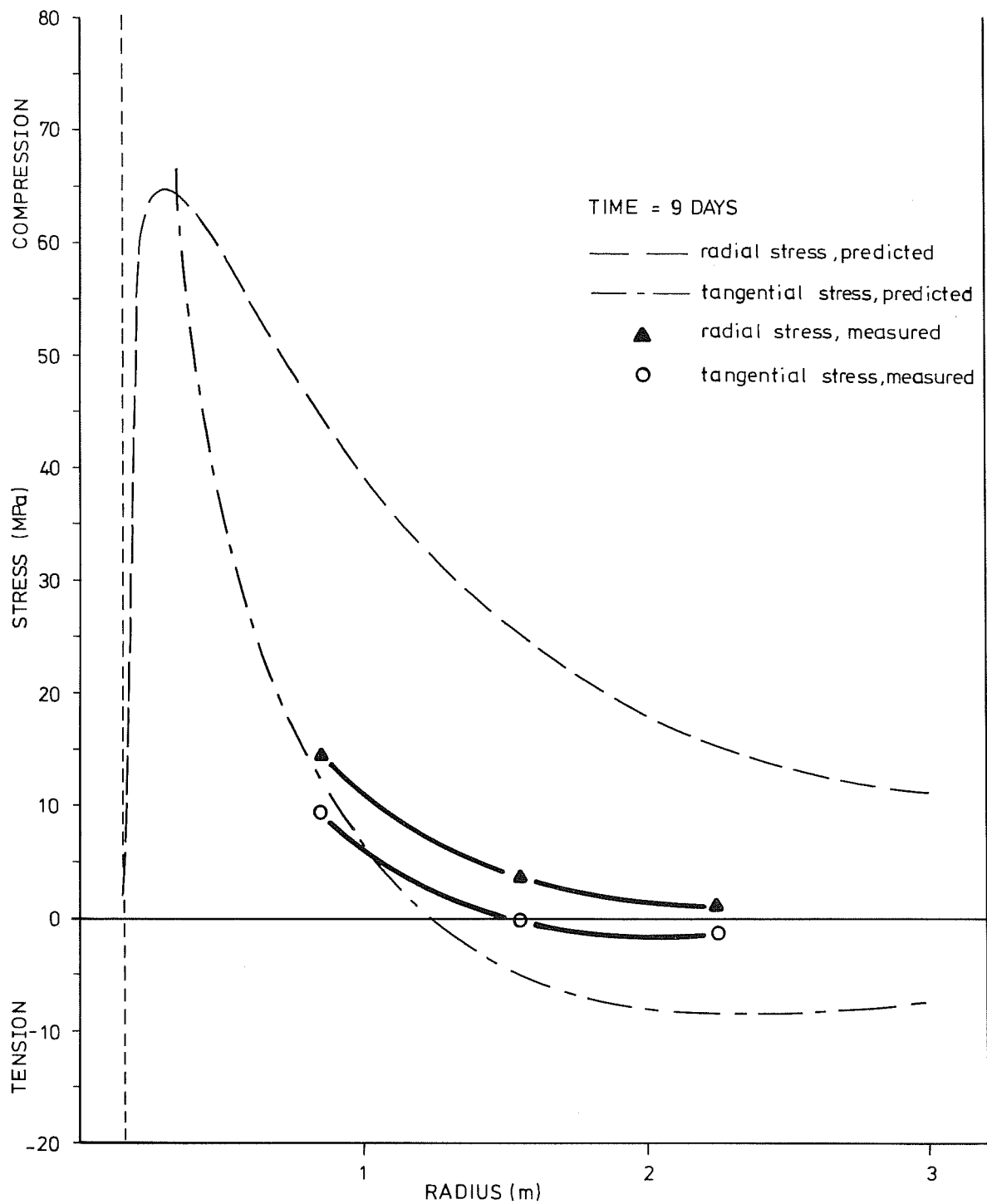


Fig 8.30 Measured (A-direction) and predicted stresses as a function of radius from the 6 kW heater at 2 days.



XBL 788-10202

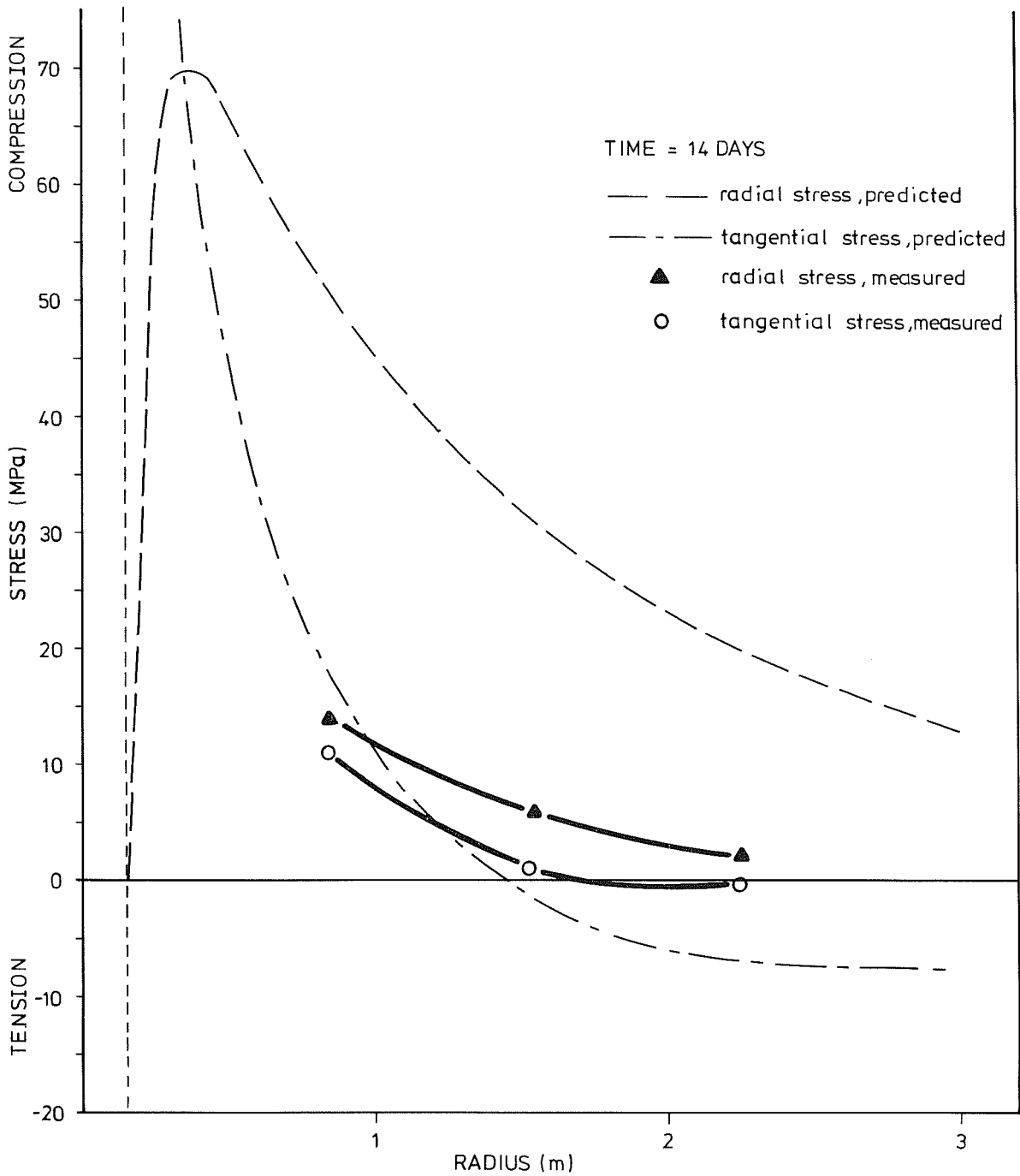
Fig 8.31 Measured (A-direction) and predicted stresses as a function of radius from the 6 kW heater at 5 days.



XBL 788-10203

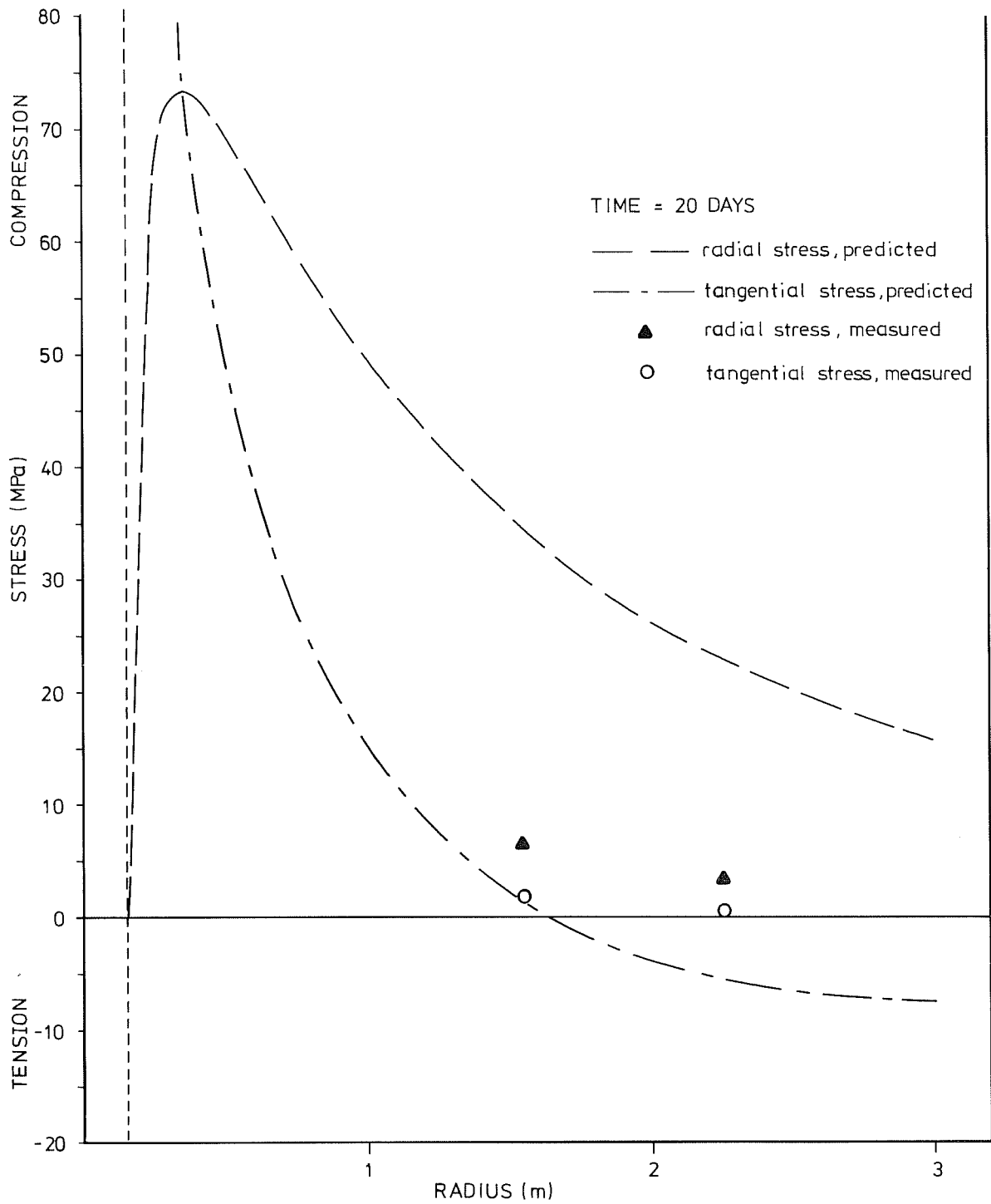
Fig 8.32

Measured (A-direction) and predicted stresses as a function of radius from the 6 kW heater at 9 days.



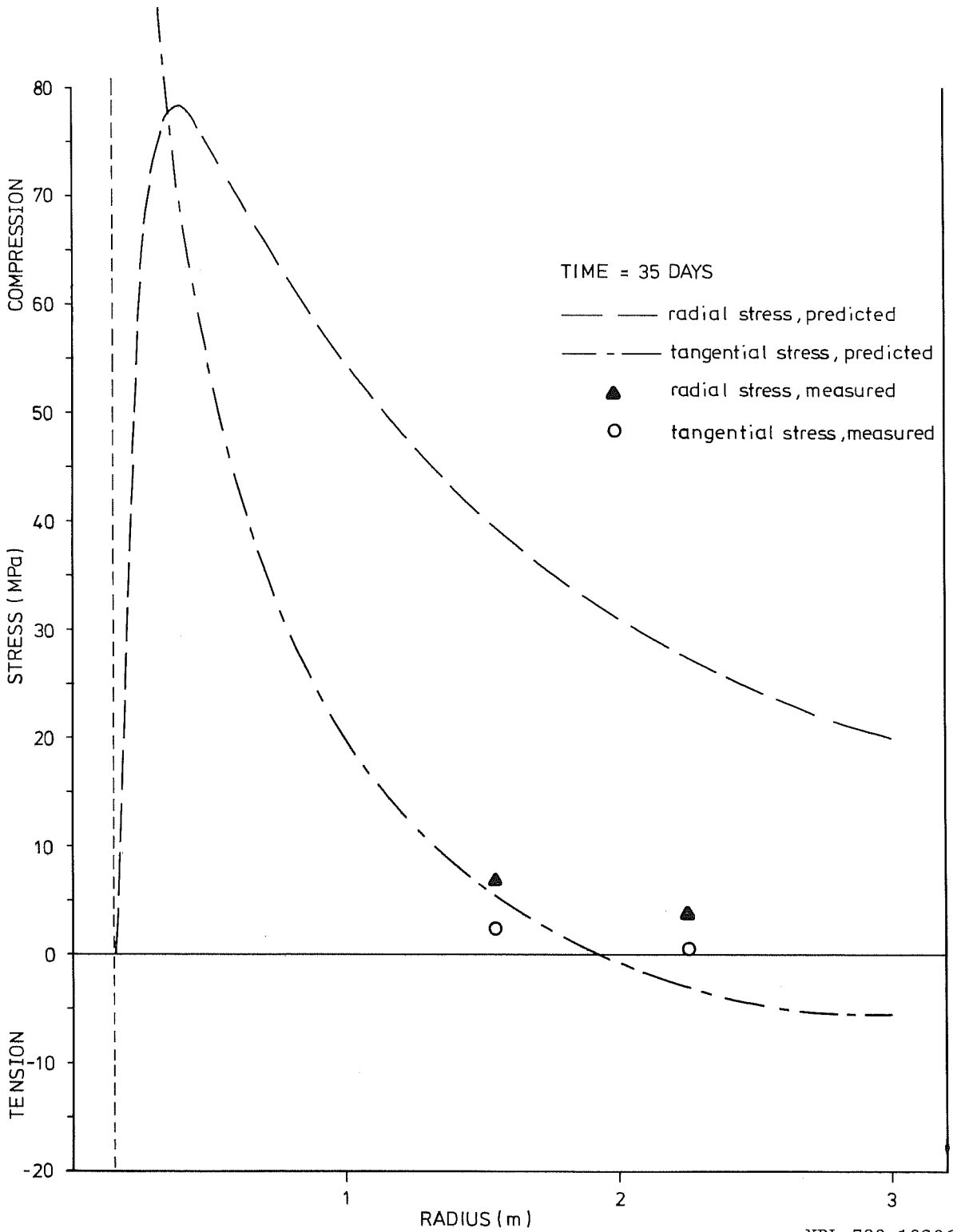
XBL 788-10204

Fig 8.33 Measured (A-direction) and predicted stresses as a function of radius from the 6 kW heater at 14 days.



XBL 788-10205

Fig 8.34 Measured (A-direction) and predicted stresses as a function of radius from the 6 kW heater at 20 days.



XBL 788-10206

Fig 8.35 Measured (A-direction) and predicted stresses as a function of radius from the 6 kW heater at 35 days.

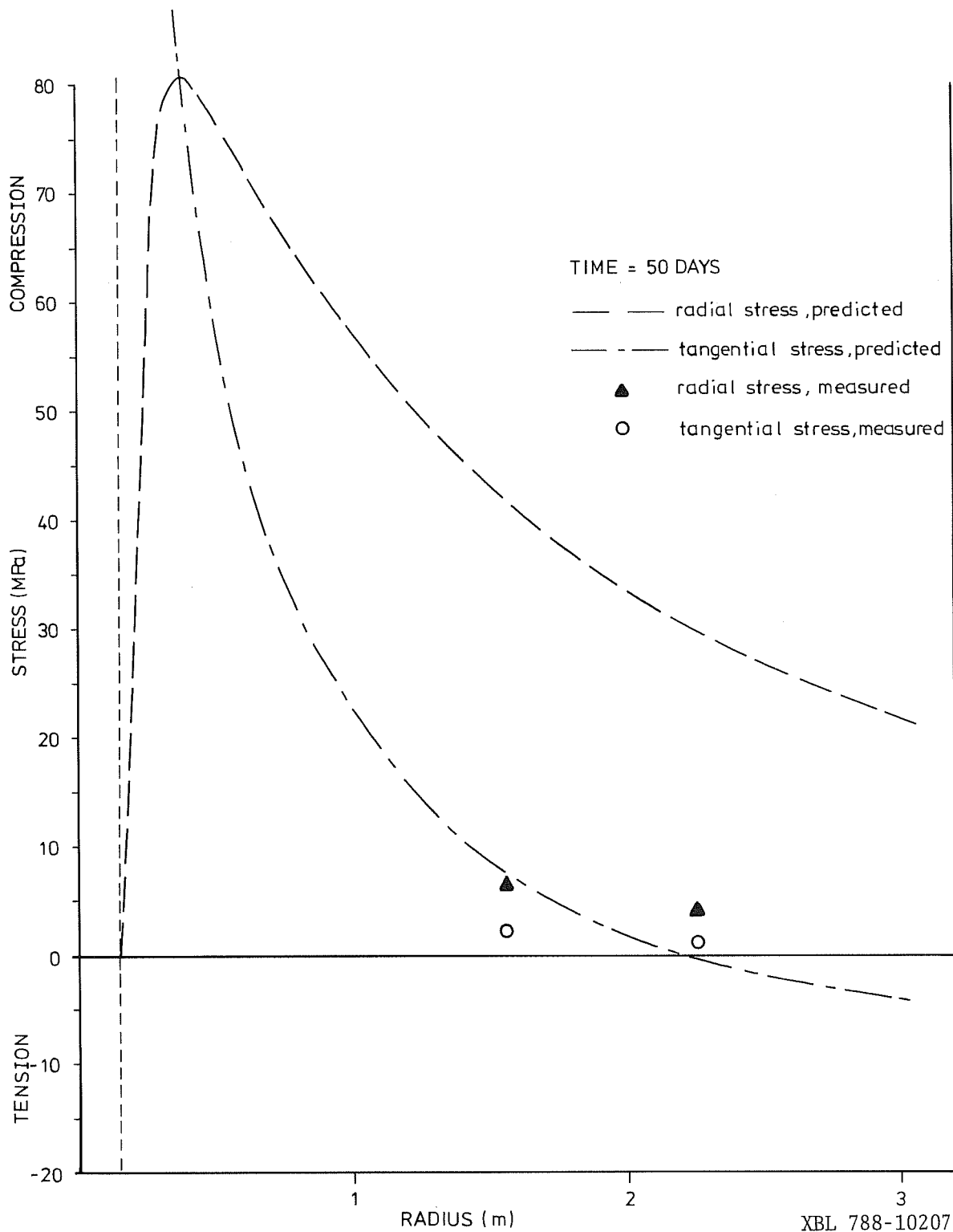
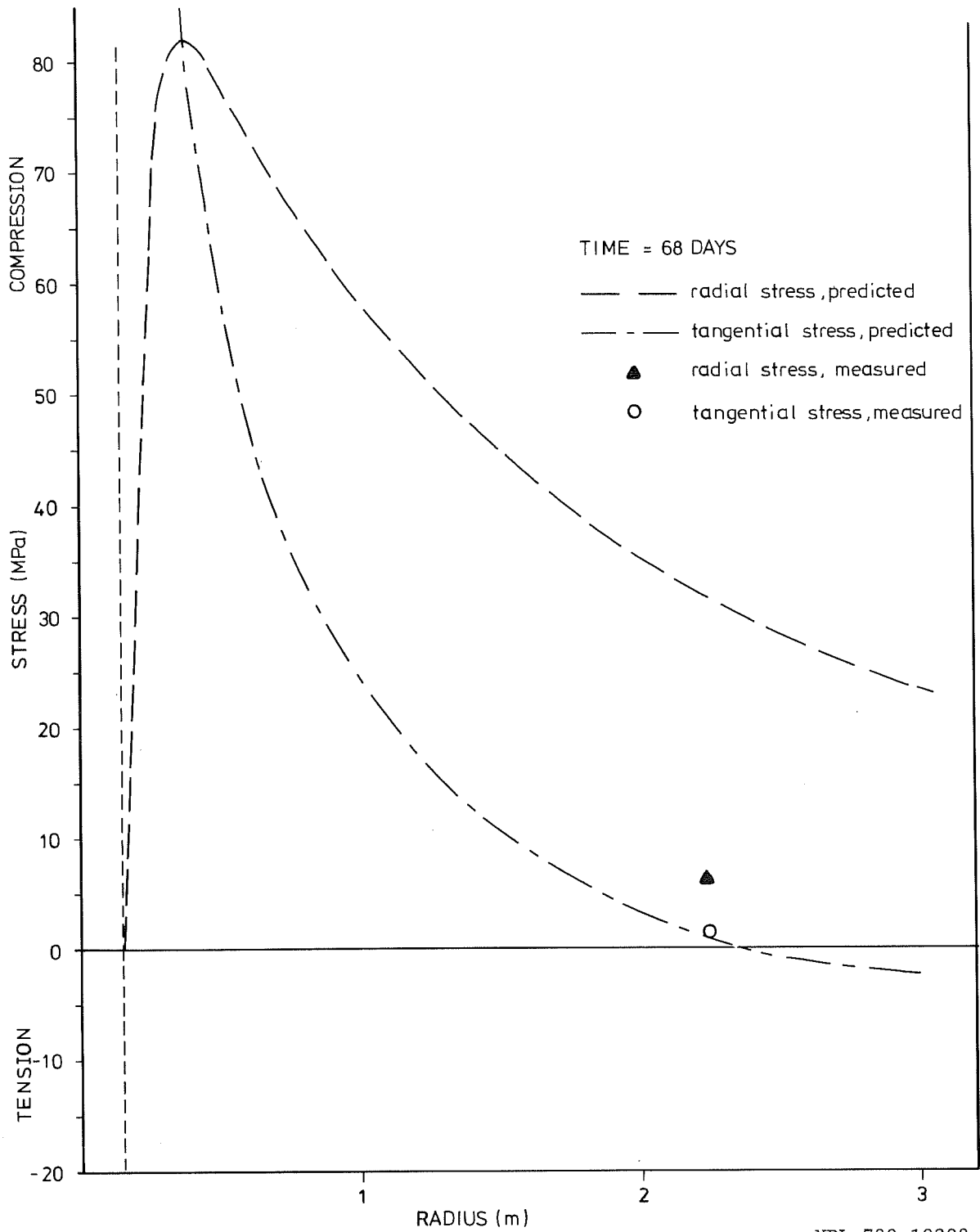
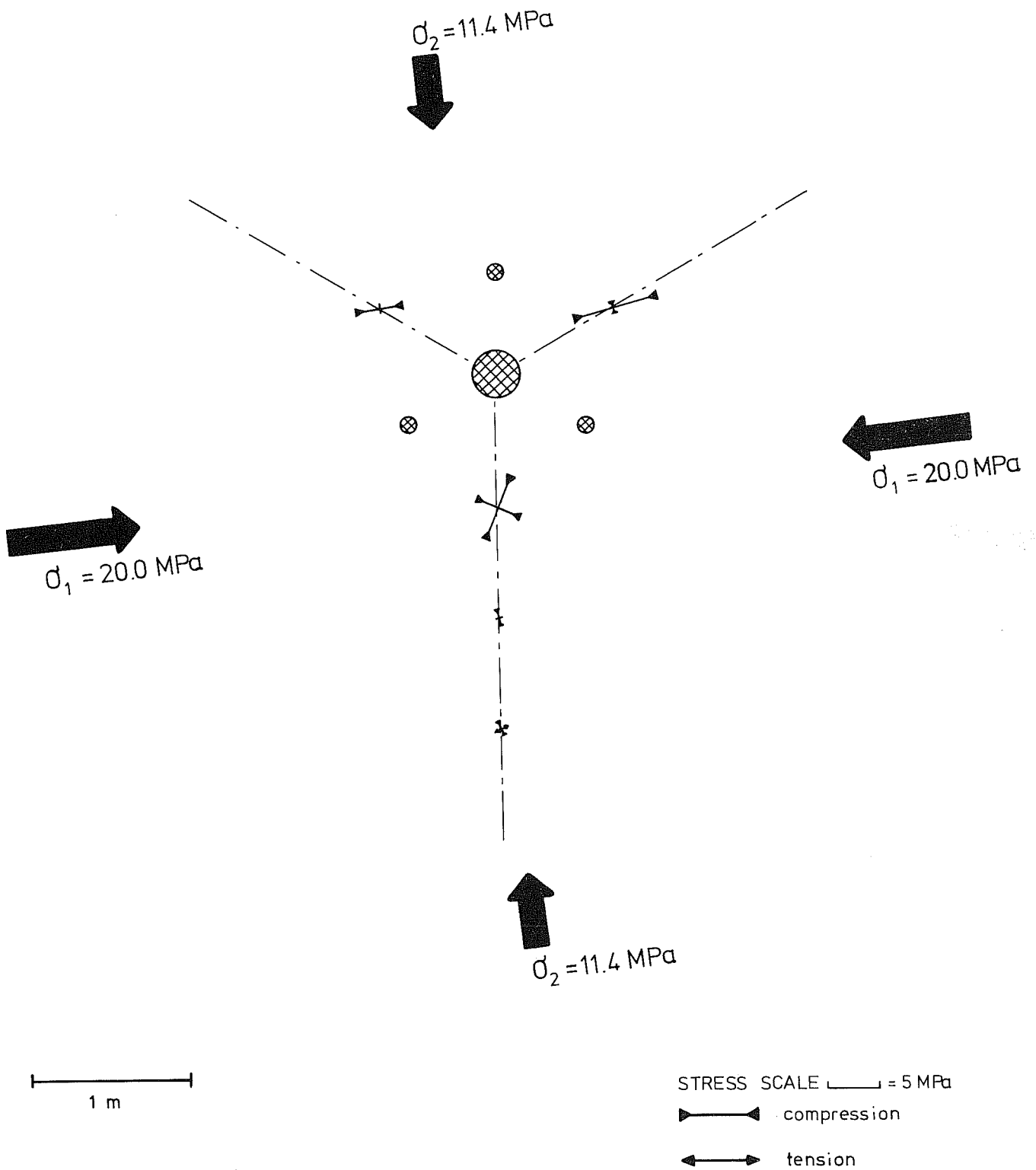


Fig 8.36 Measured (A-direction) and predicted stresses as a function of radius from the 6 kW heater at 50 days.



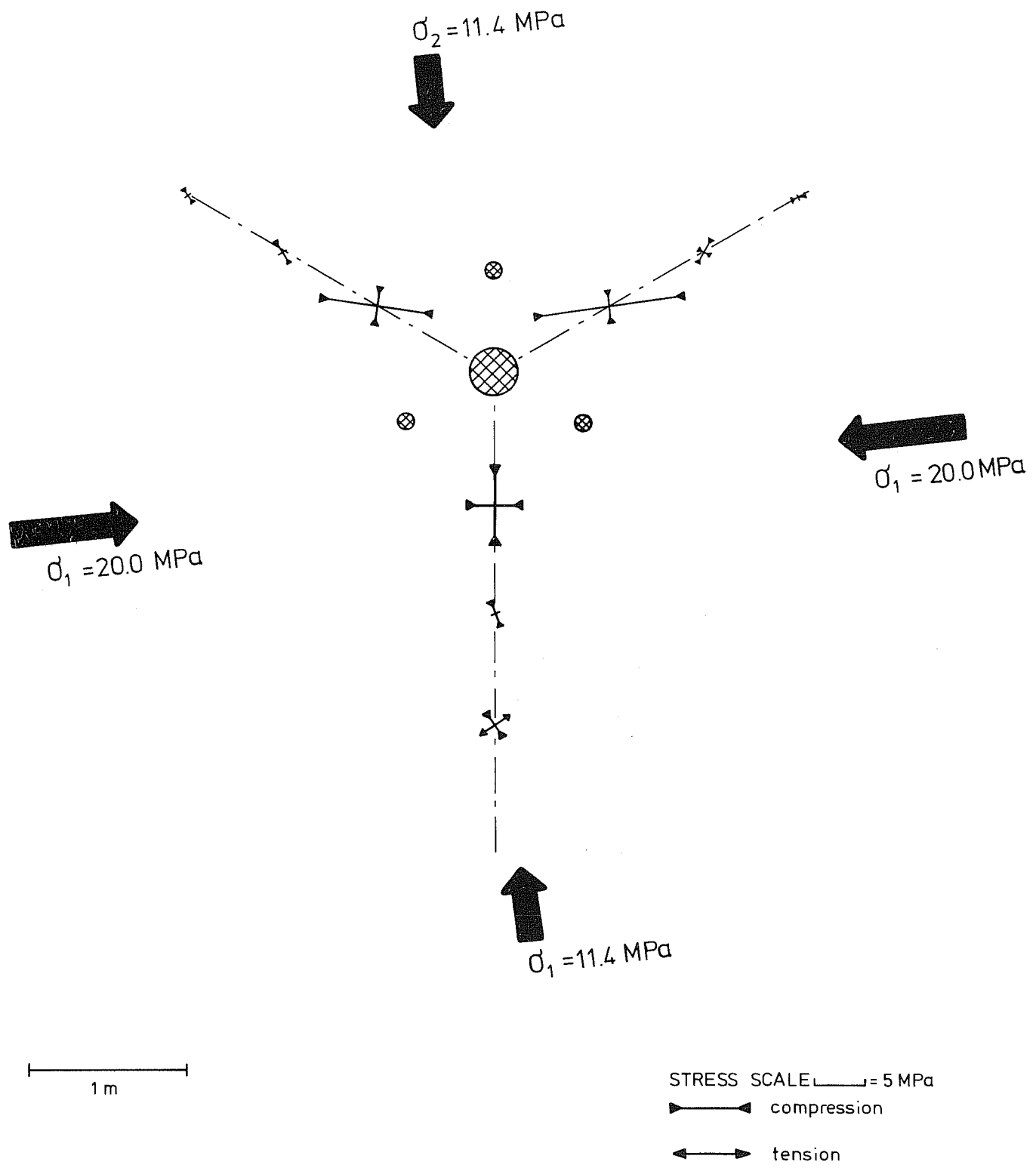
XBL 788-10208

Fig 8.37 Measured (A-direction) and predicted stresses as a function of radius from the 6 kW heater at 68 days.



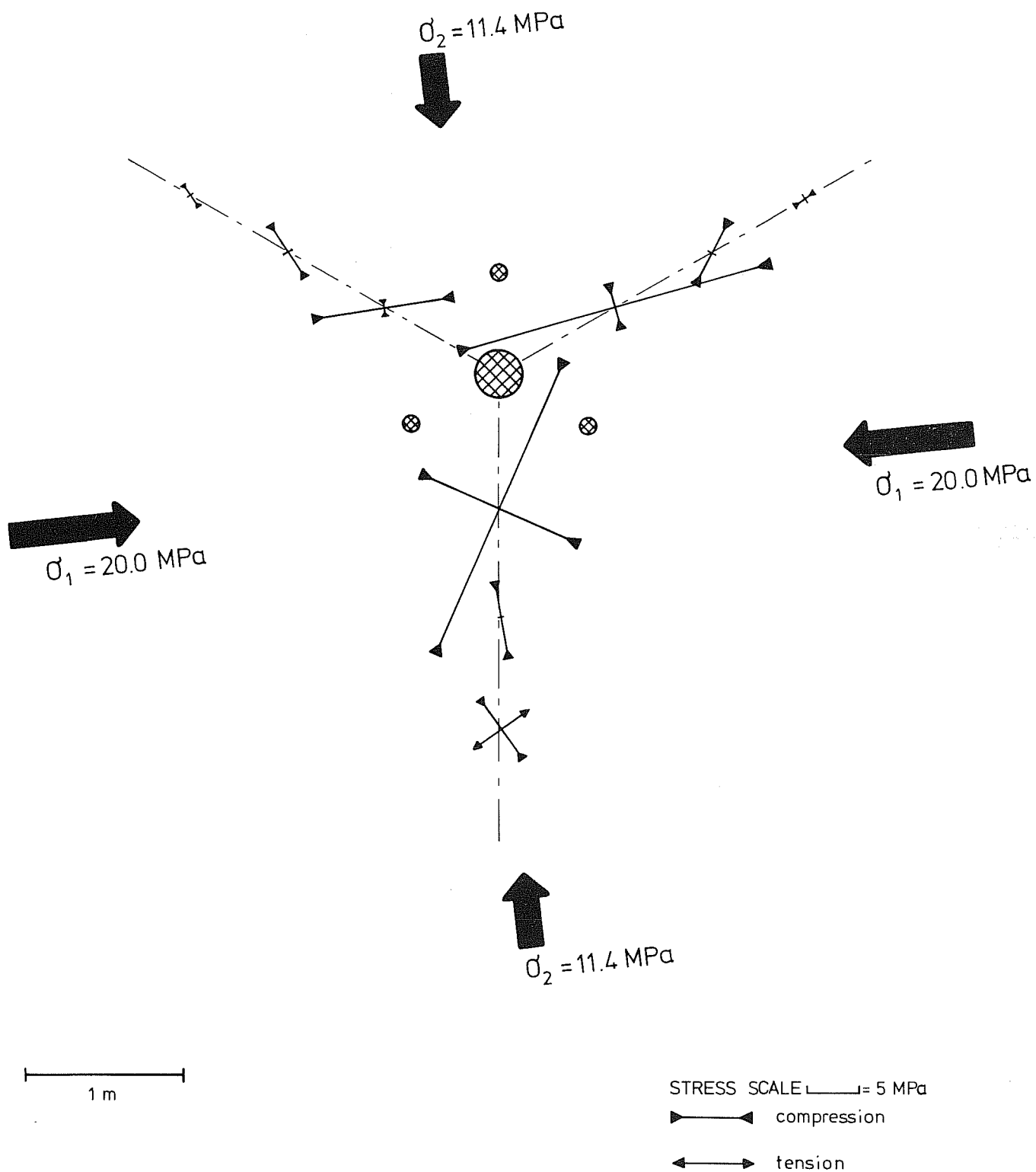
XBL 788-10209

Fig 8.38 Principal stresses calculated from the thermally induced stresses  $\Delta\sigma_r$ ,  $\Delta\sigma_{45}$  and  $\Delta\sigma_\phi$ : time = 2 days.



XBL 788-10210

Fig 8.39 Principal stresses calculated from the thermally induced stresses  $\Delta\sigma_r$ ,  $\Delta\sigma_{45}$  and  $\Delta\sigma_\phi$ : time = 5 days.



XBL 788-10211

Fig 8.40 Principal stresses calculated from the thermally induced stresses  $\Delta\sigma_r$ ,  $\Delta\sigma_{45}$  and  $\Delta\sigma_\phi$ : time = 9 days.

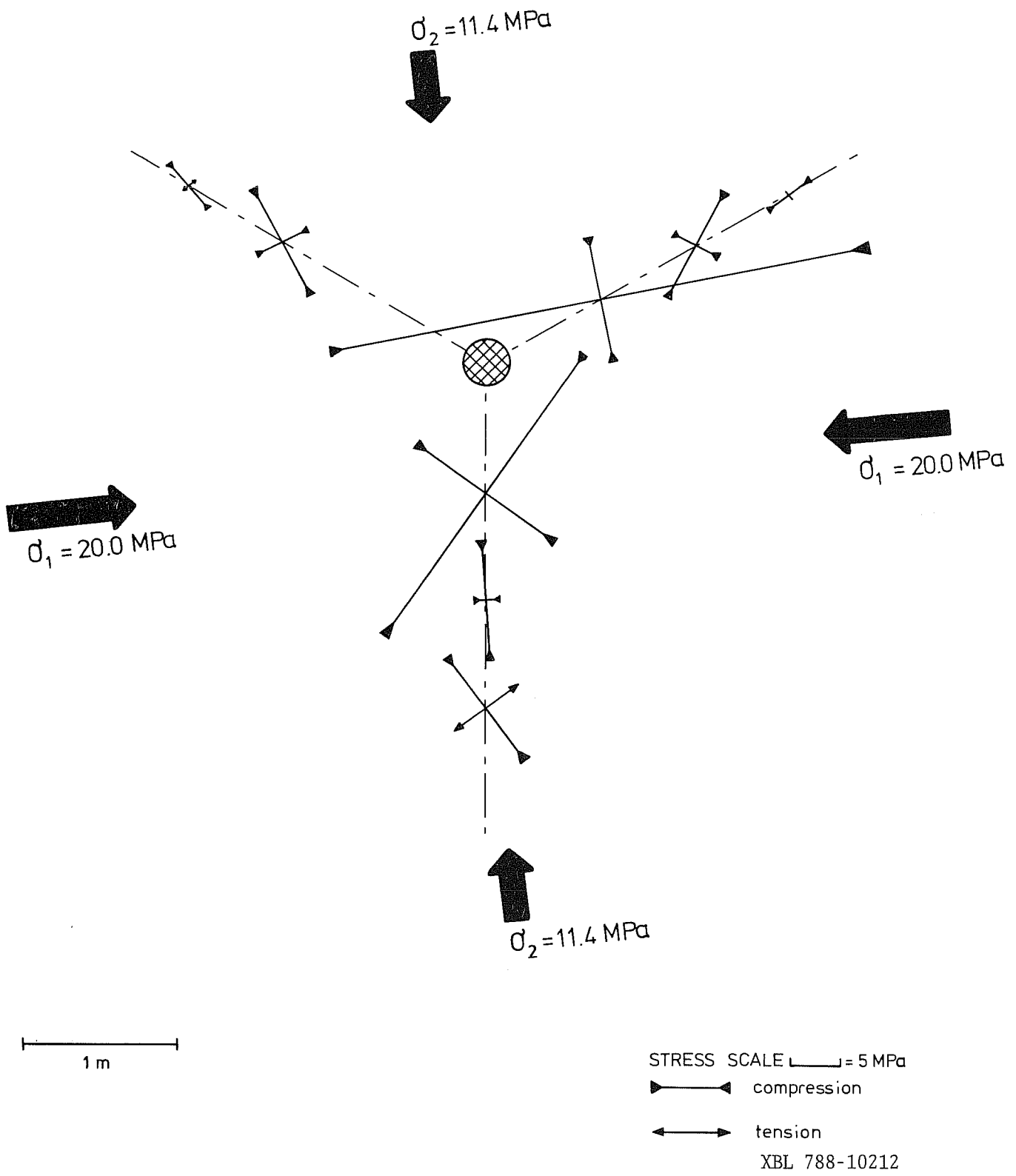
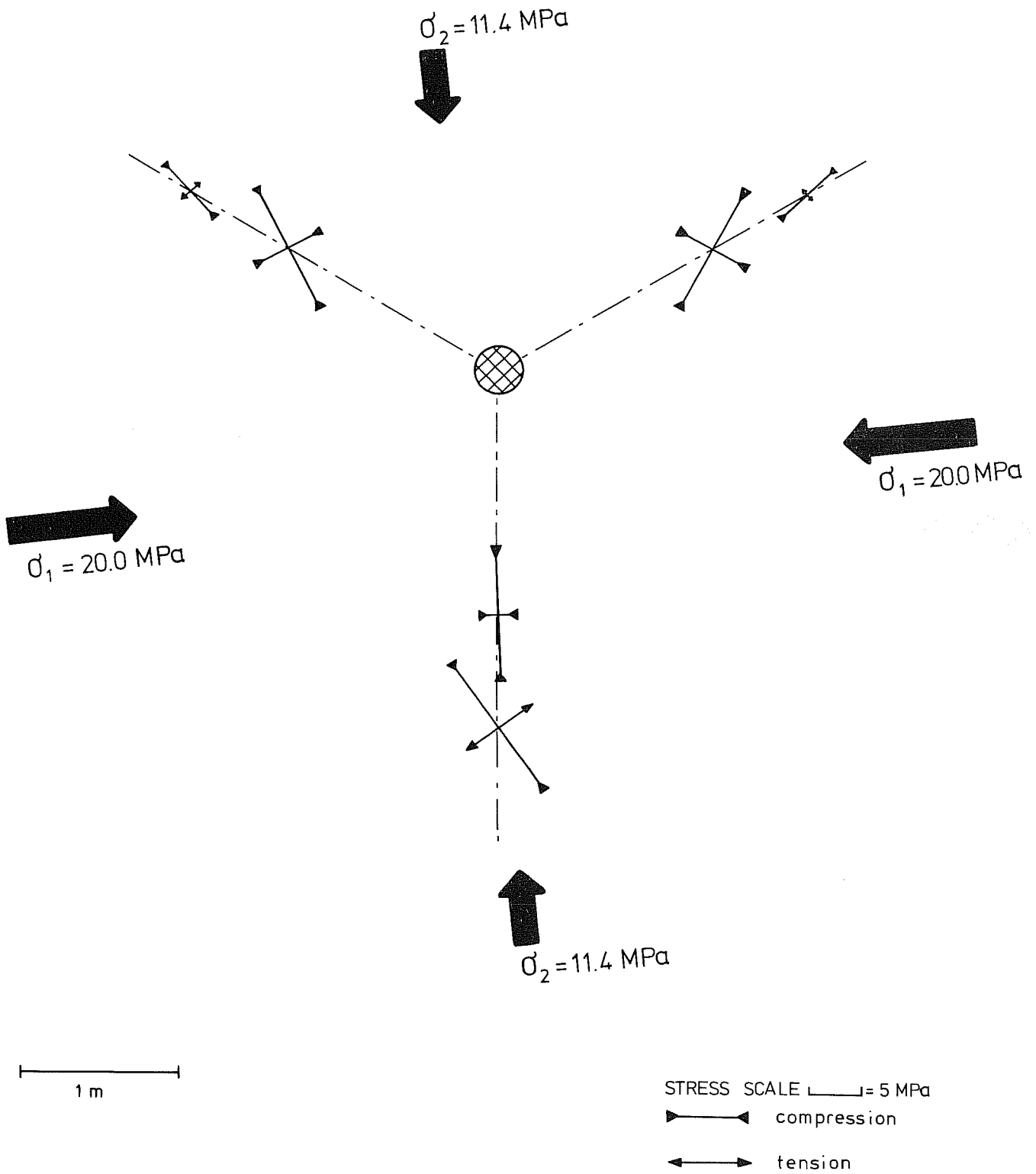


Fig 8.41 Principal stresses calculated from the thermally induced stresses  $\Delta\sigma_r$ ,  $\Delta\sigma_{45}$  and  $\Delta\sigma_\phi$ : time = 14 days.



XBL 788-10213

Fig 8.42 Principal stresses calculated from the thermally induced stresses  $\Delta\sigma_r$ ,  $\Delta\sigma_{45}$  and  $\Delta\sigma_\phi$ : time = 20 days.

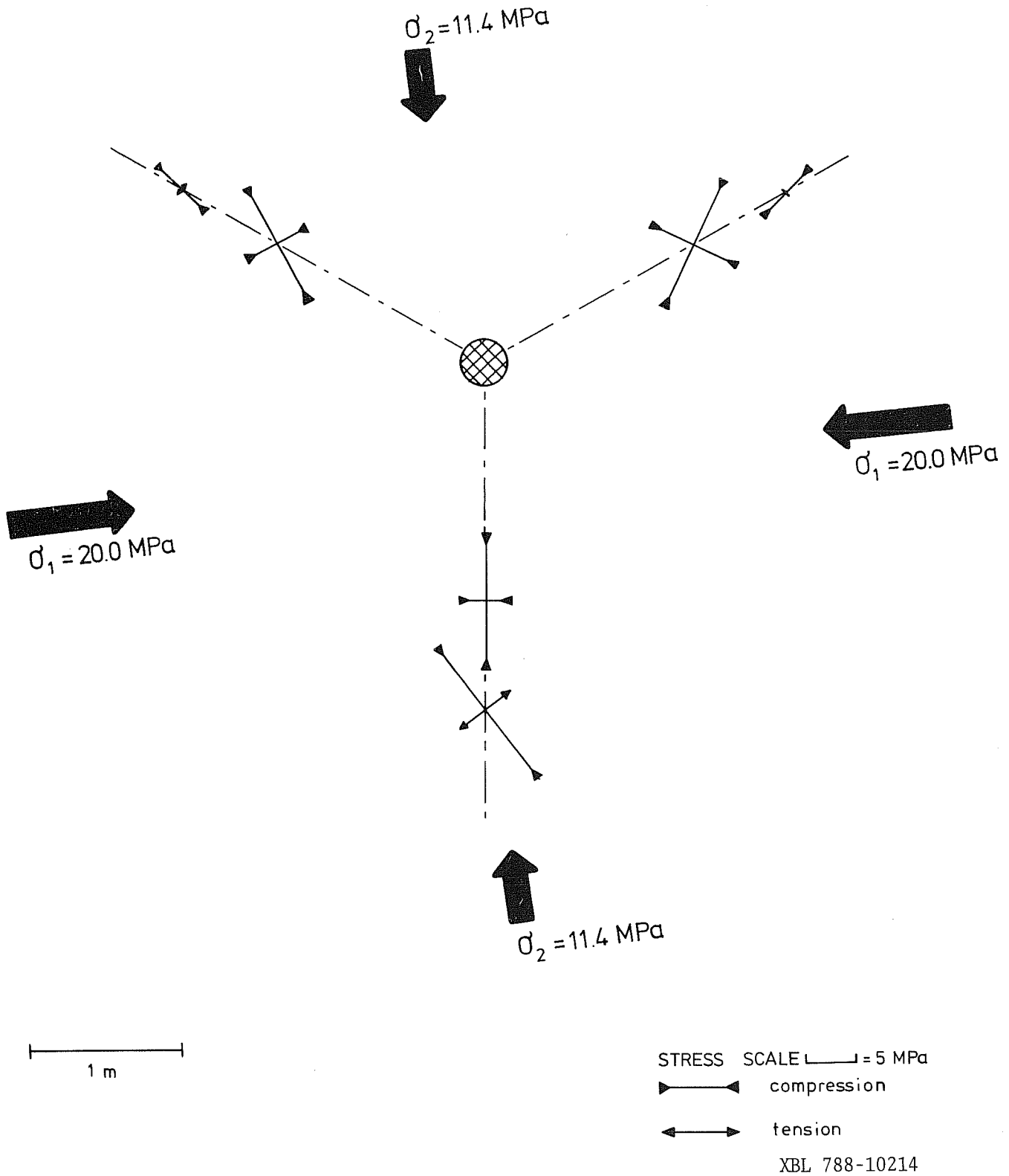
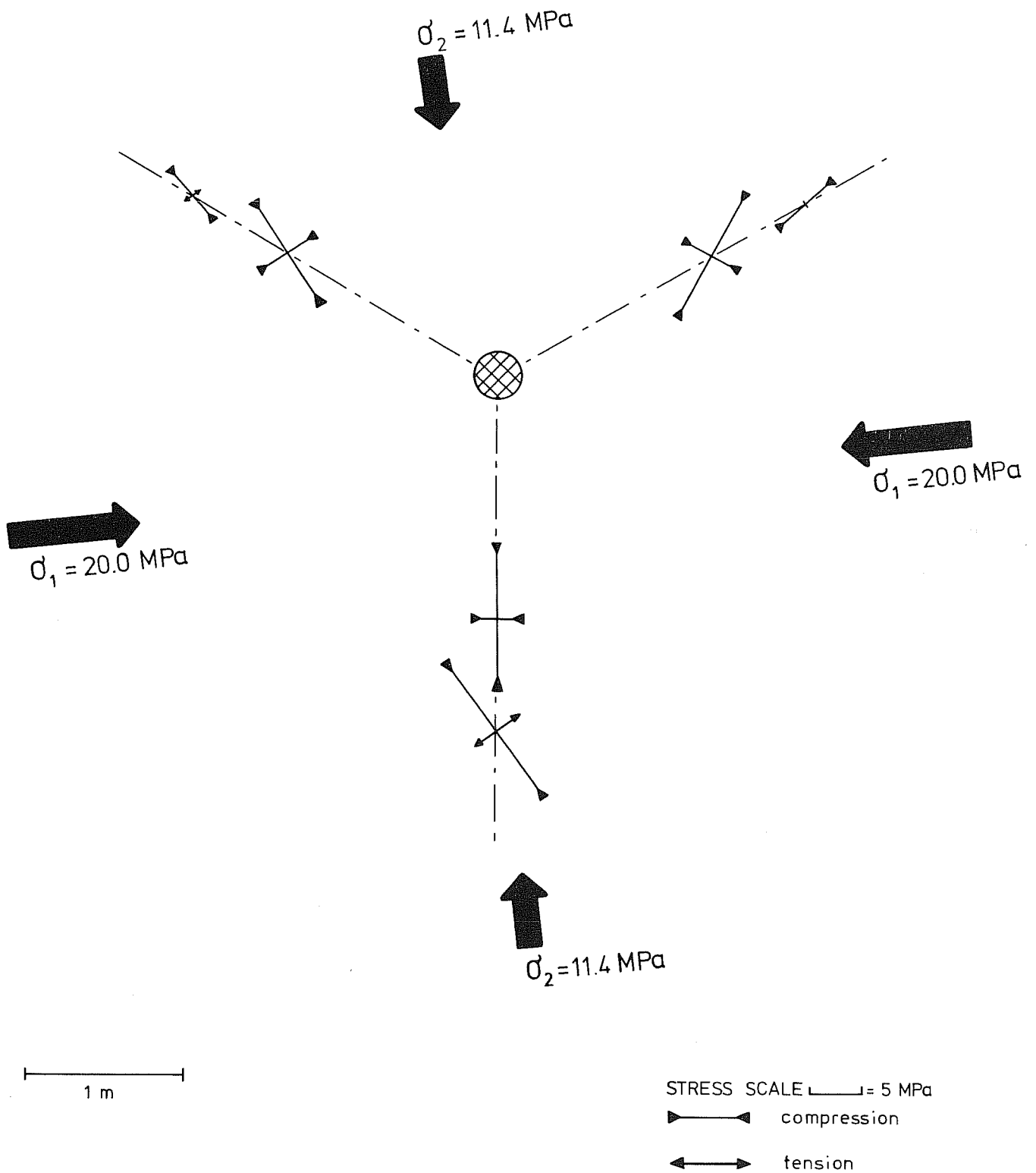
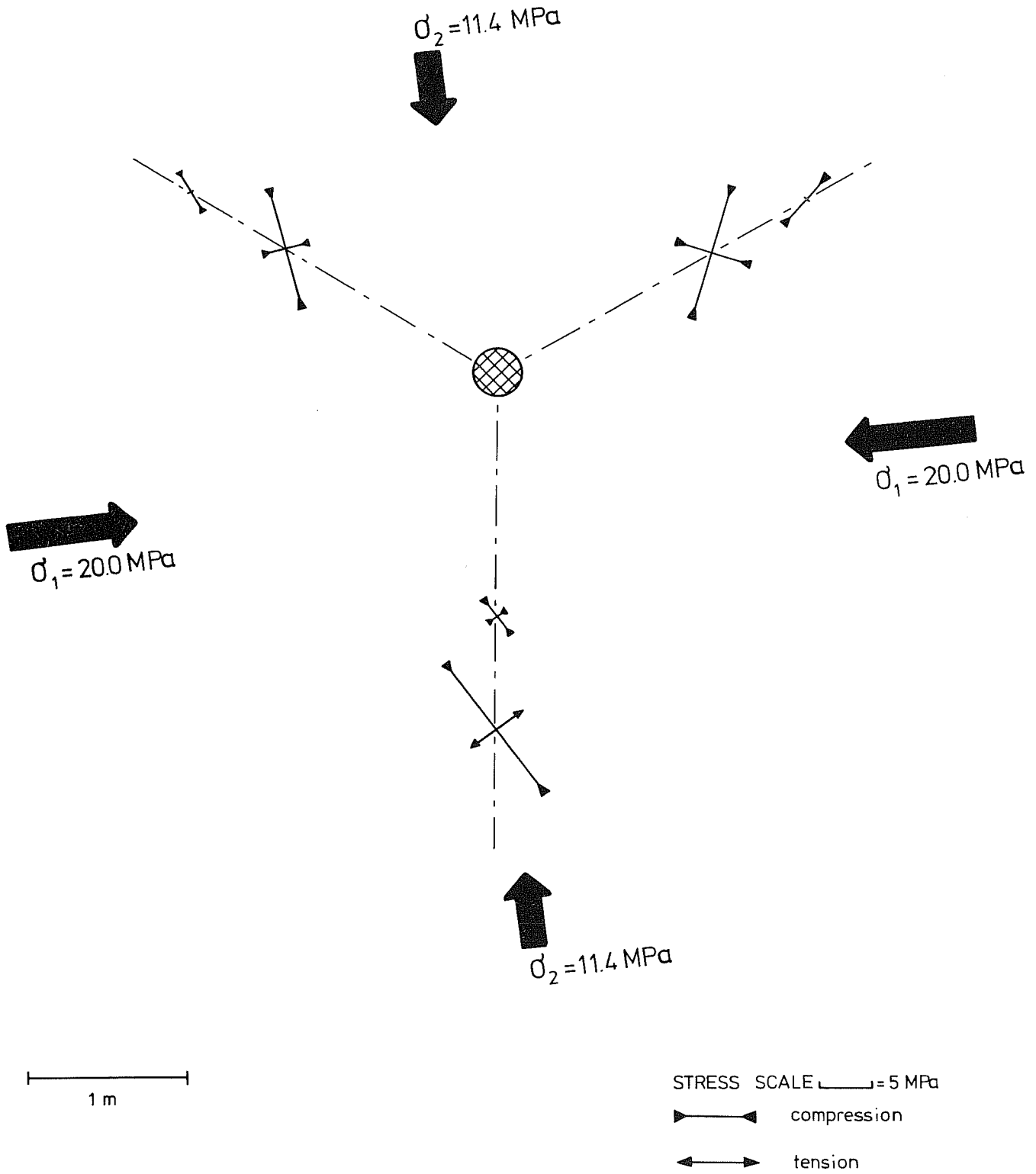


Fig 8.43 Principal stresses calculated from the thermally induced stresses  $\Delta\sigma_r$ ,  $\Delta\sigma_{45}$  and  $\Delta\sigma_\phi$ : time = 40 days.



XBL 788-10215

Fig 8.44 Principal stresses calculated from the thermally induced stresses  $\Delta\sigma_r$ ,  $\Delta\sigma_{45}$  and  $\Delta\sigma_\phi$ : time = 60 days.



XBL 788-10216

Fig 8.45 Principal stresses calculated from the thermally induced stresses  $\Delta\sigma_r$ ,  $\Delta\sigma_{45}$  and  $\Delta\sigma_\phi$ : time = 70 days or 1 after the heater was turned off.

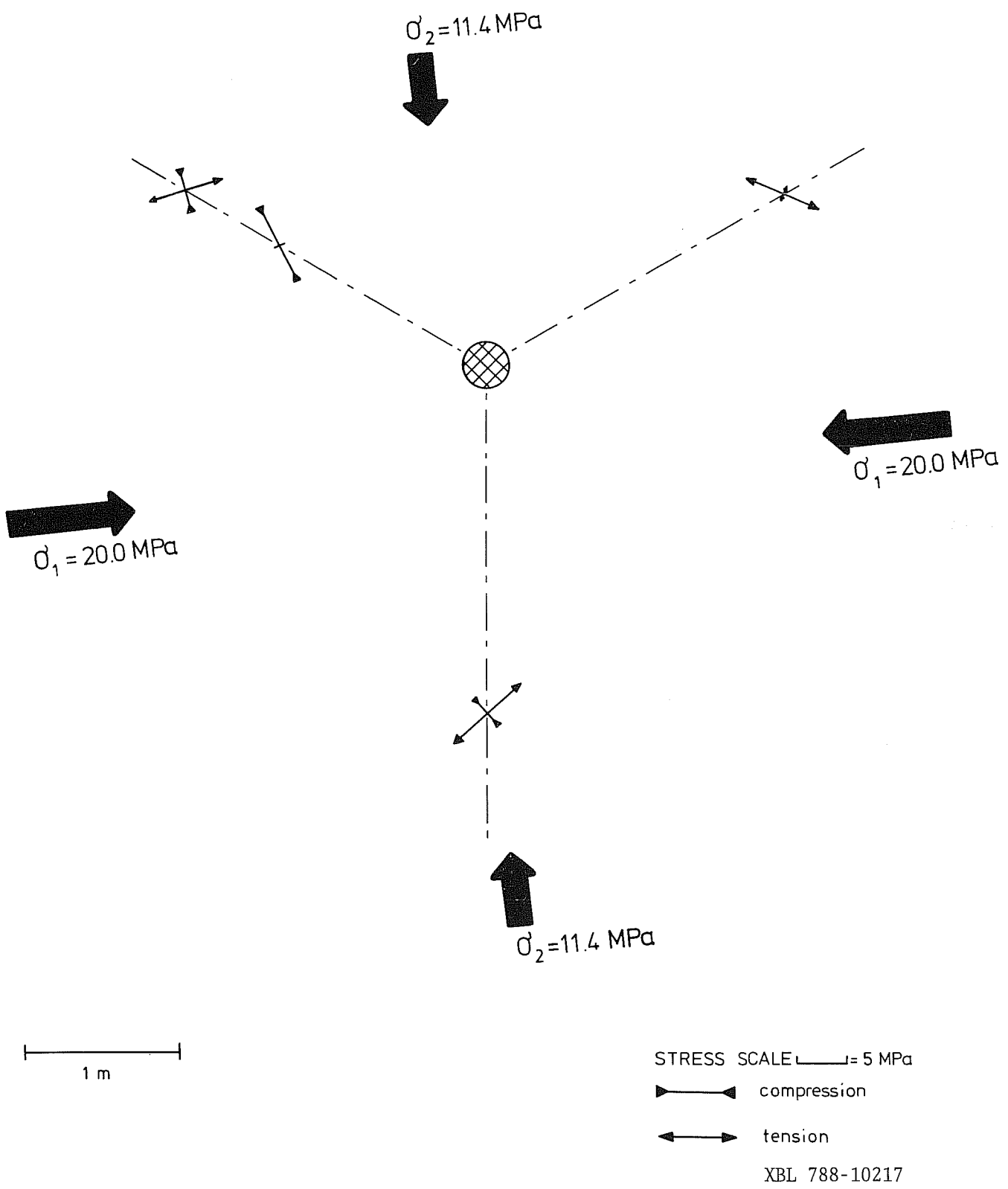


Fig 8.46 Principal stresses calculated from the thermally induced stresses  $\Delta\sigma_r$ ,  $\Delta\sigma_{45}$  and  $\Delta\sigma_\phi$ : time = 90 days or 21 days after the heater was turned off.

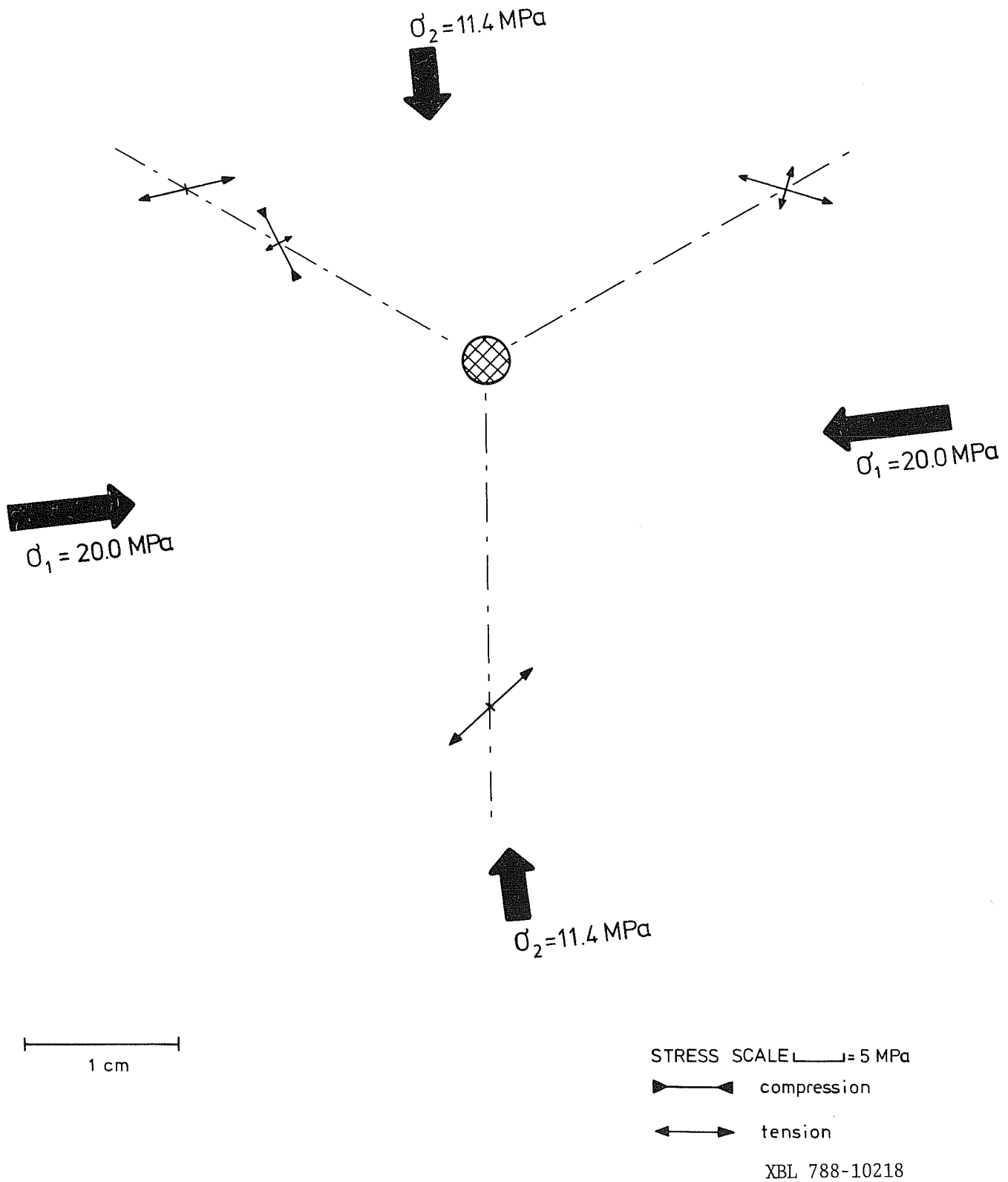
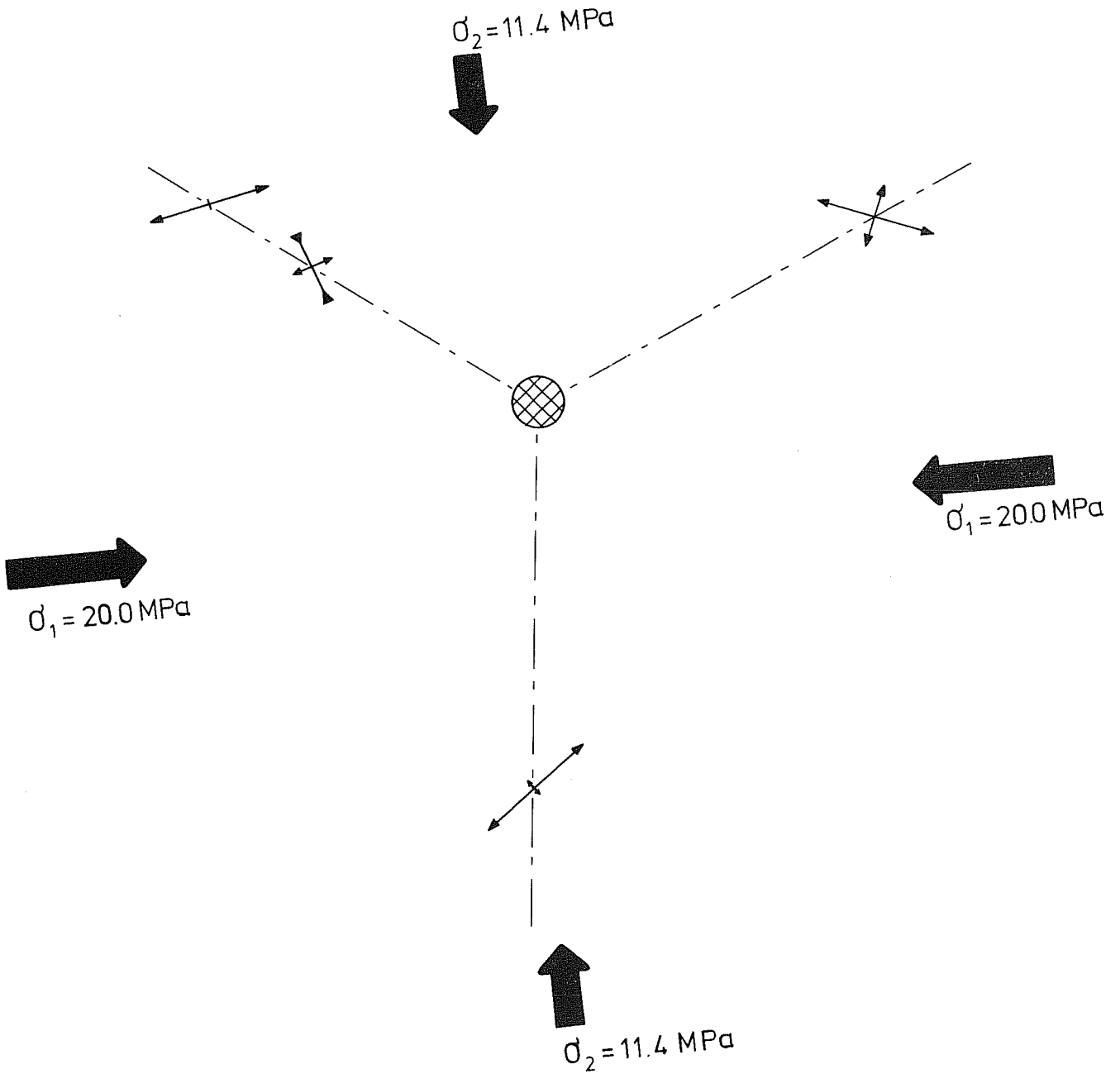


Fig 8.47

Principal stresses calculated from the thermally induced stresses  $\Delta\sigma_r$ ,  $\Delta\sigma_{45}$  and  $\Delta\sigma_\phi$ : time = 110 days or 41 days after the heater was turned off.



STRESS SCALE  $\text{—} = 5 \text{ MPa}$

$\blacktriangleleft \blacktriangleright$  compression

$\blacktriangleleft \blacktriangleright$  tension

XBL 788-10219

Fig 8.48

Principal stresses calculated from the thermally induced stresses  $\Delta\sigma_r$ ,  $\Delta\sigma_{45}$  and  $\Delta\sigma_\phi$ : time = 155 days or 86 days after the heater was turned off.

## 8.5 Comments on measured data

As can be observed in Figures 8.10 - 8.15 and 8.31-8.37, the predicted magnitudes and directions of the thermally induced stresses do not correspond with the measured data. The predicted stresses are based upon the assumption that the rock is homogeneous, linear elastic and isotropic. In a fractured rock, and especially in the Stripa granite, where a large number of the fractures are filled with minerals such as chlorite and calcite, the magnitude of the induced stresses was measured to have much lower values [6].

As shown in Figures 8.49 - 8.50, the induced stresses in a structure with a high frequency of fractures will be much lower than the stresses in a structure with few major fractures deformed under the influence of the same total strain. In this way, the rock mass in the test site could be regarded as a number of blocks limited by chlorite filled fractures. The individual blocks are not constrained and hence they are free to expand, which results in low and irregular induced stresses.

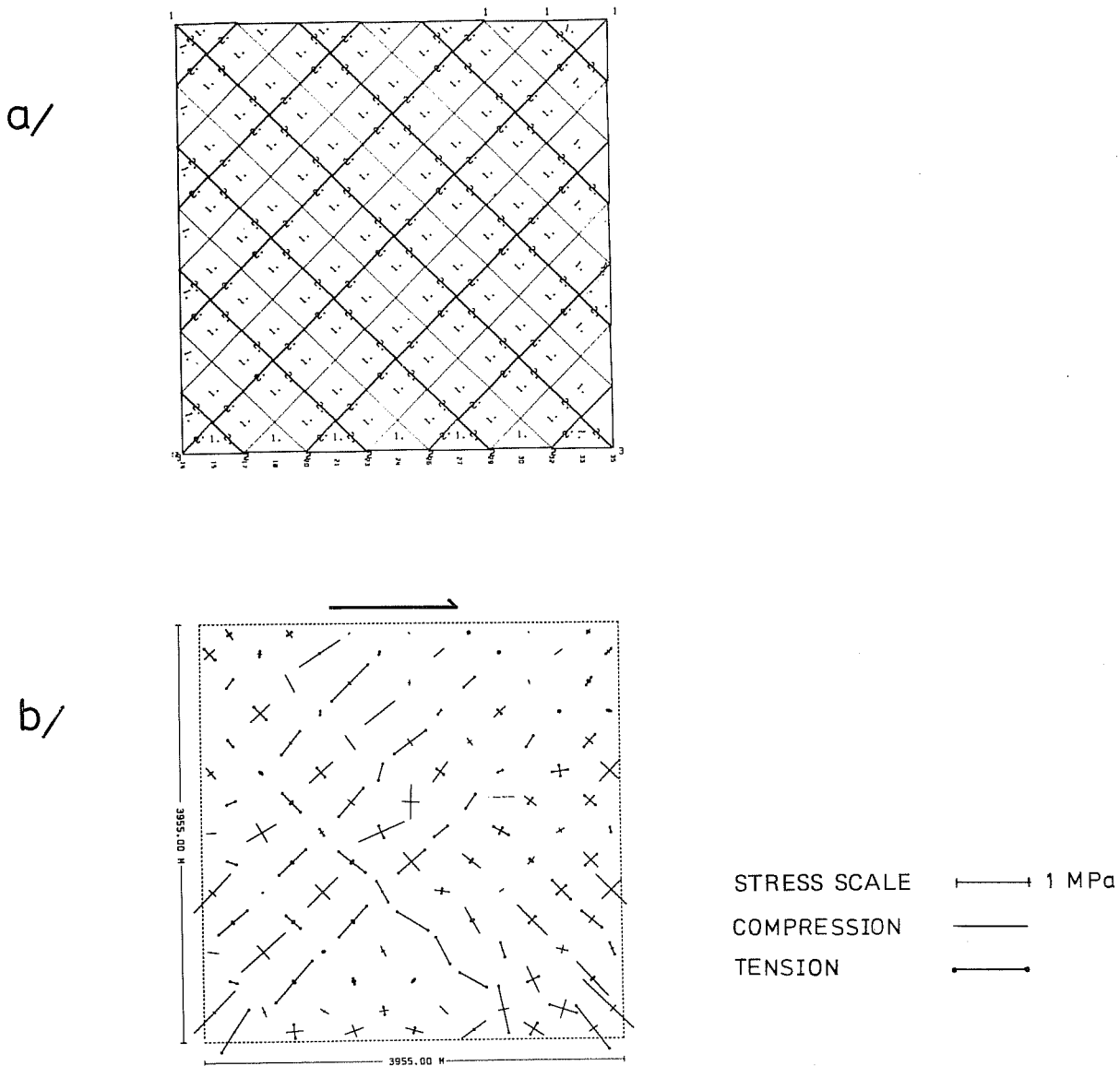
The predicted stresses have been computed for a Young's Modulus of 69.4 GPa, as determined from measurements of in situ stresses in the Stripa granite. This value is valid for the unfractured rock sample but is not representative for the rock mass.

In order to check the in situ modulus of the rock mass at the test site, a pressure cell developed at the Colorado School of Mines has been used [11]. The cell operates by pressurizing a cylindrical membrane against the sides of an EX (38 mm) borehole. Data produced are in the form of a linear pressure-volume curve from which the stress-strain relationship of the rock may be determined. The measurements have been carried out in borehole number 5 at 0.85 m distance from the main heater

and in borehole 8 at a 2.95 m distance from the main heater (see Fig 4.4). In each case, the Young's Modulus has been determined at several places along the borehole. The results are plotted in Fig 8.51. As can be observed, the Young's Modulus of the rock mass has a magnitude of roughly half of that measured for the core samples in the laboratory. This implies that the predicted thermally induced stresses will be reduced by a factor of two. Nevertheless the calculated stresses are still much higher than the measured stresses.

The measurements have been carried out after the duration of the heater test. As shown in Fig 8.51, there is no significant difference between the determinations in the hole close to the heater (0.85 m) compared to the determinations at 2.95 m distance to the main heater. Further determinations, carried out by Terra Tek in non-heated Stripa granite gives a modulus of approximately the same value (personal communication, T. Schrauf).

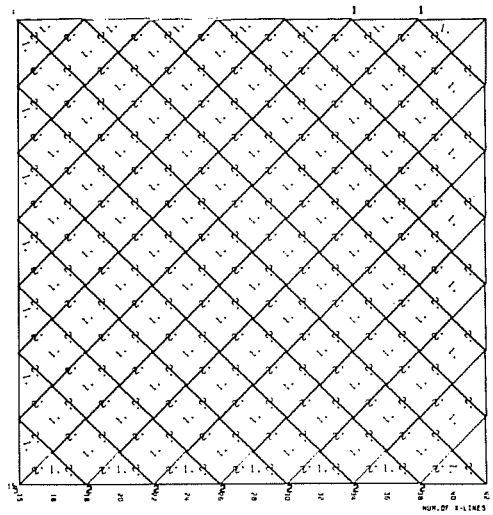
As can be observed in figures 8.2 - 8.9, the compressive stresses normally turn into tensile when the heater is turned off. So far, there is no adequate explanation for this behaviour.



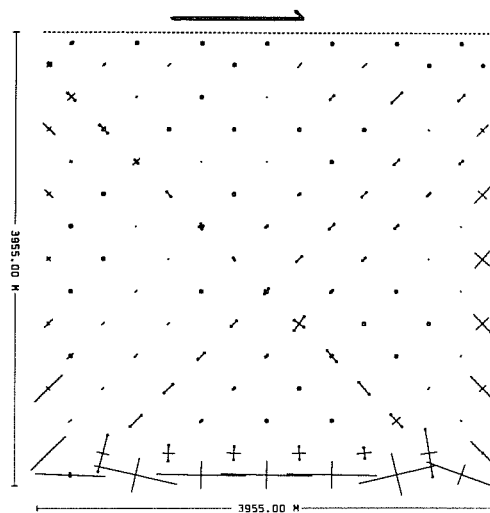
XBL 788-10220

Fig 8.49 a) Undeformed structure: fracture distance 0.8 km;  
 b) induced principal stresses due to deformation  
 (after Stephansson, 1977).

a/



b/



STRESS SCALE     $\longleftrightarrow$  1 MPa  
 COMPRESSION     $\text{———}$   
 TENSION          $\text{———}$

XBL 788-10221

Fig 8.50 a) Undeformed structure: fracture distance 0.4 km;  
 b) induced principal stresses due to deformation  
 (after Stephansson, 1977).

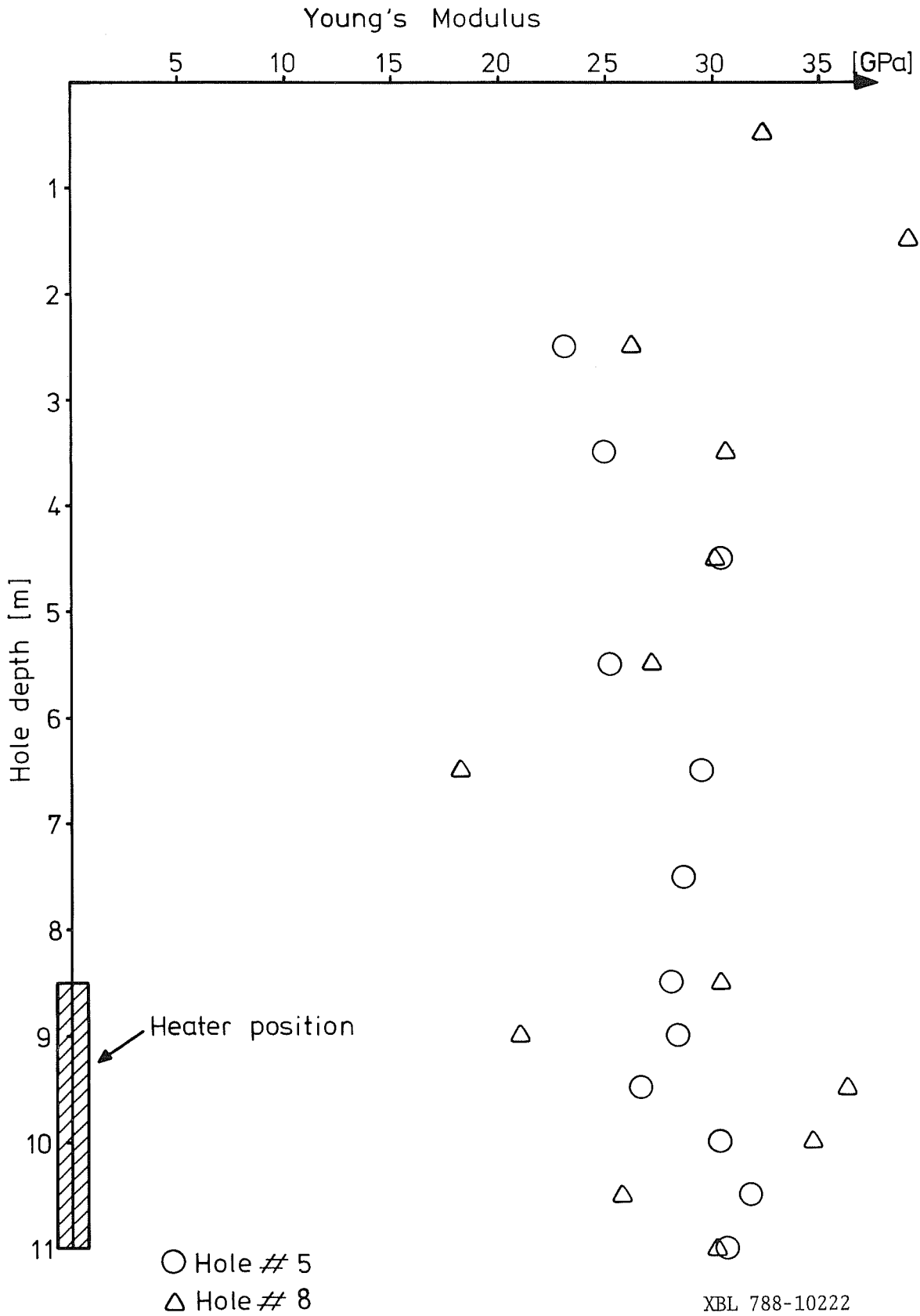


Fig 8.51 Variation of the in situ modulus of deformation with depth in hole 5 and hole 8; data from pressure cell test.

## 9 MEASURED DISPLACEMENTS OF MAJOR FRACTURES

### 9.1 General comments

Measurements of displacements of major fractures, as described in chapter 4.7, were carried out at five different places on the floor of the test site. The arrangement of the gages is shown in Fig 9.1.

### 9.2 Displacements as a function of time

Figures 9.2 and 9.3 show the displacements as a function of time. A positive sign is equal to contraction of the fracture and a negative sign is equal to dilatation.

### 9.3 Comments on measured data

As shown in Figs. 9.2 and 9.3, the measured displacements are extremely small. The maximum value measured is a dilatation of  $13.5 \cdot 10^{-6}m$ . Furthermore, no contraction of fractures has been observed.

Although the measured displacements are very small, a similar appearance of the curves from all gages can be observed. This is especially true for gage 2, 4 and 5. As can also be observed, the apertures of some of the fractures do not close to the same width as they were in the original state.

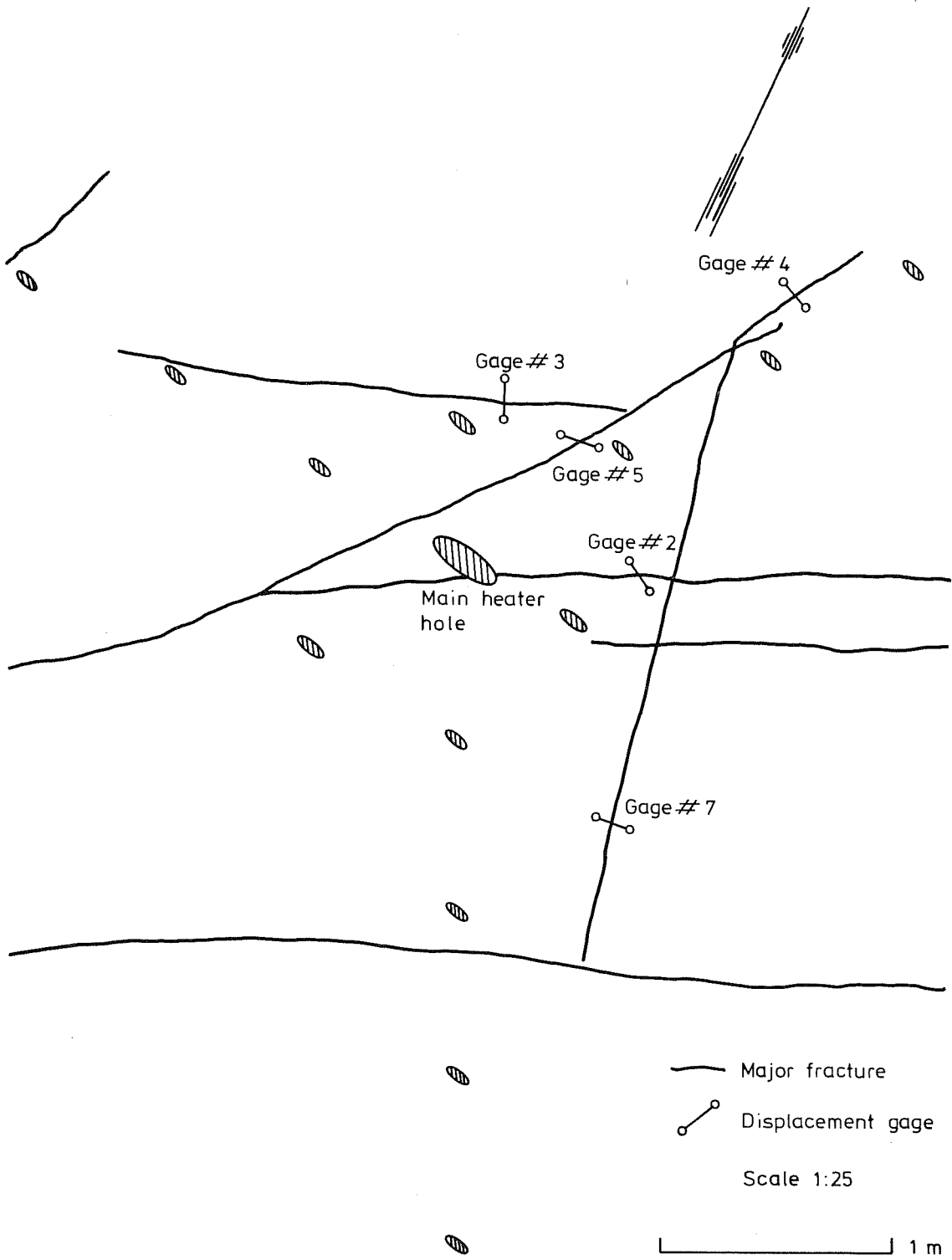
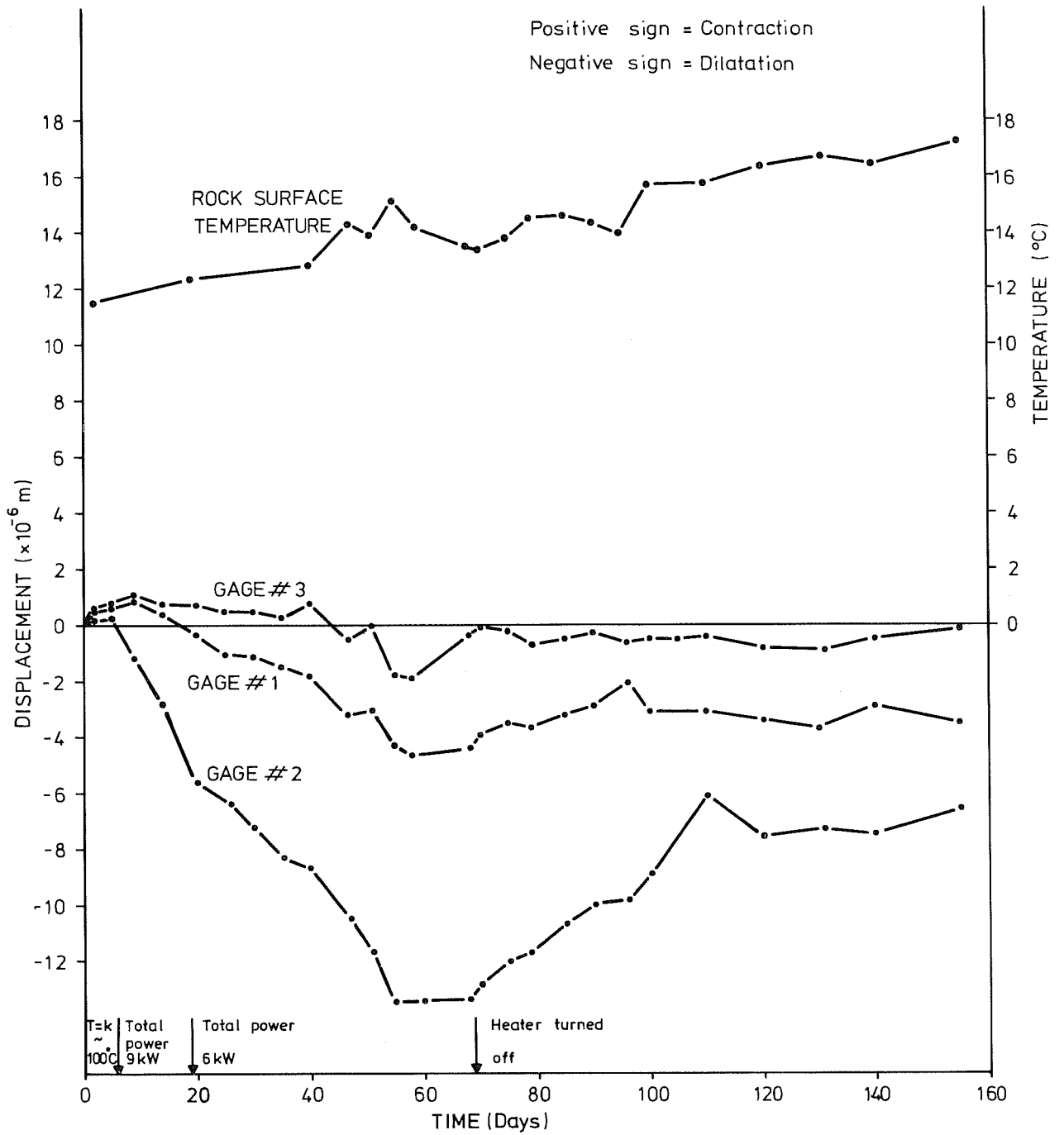


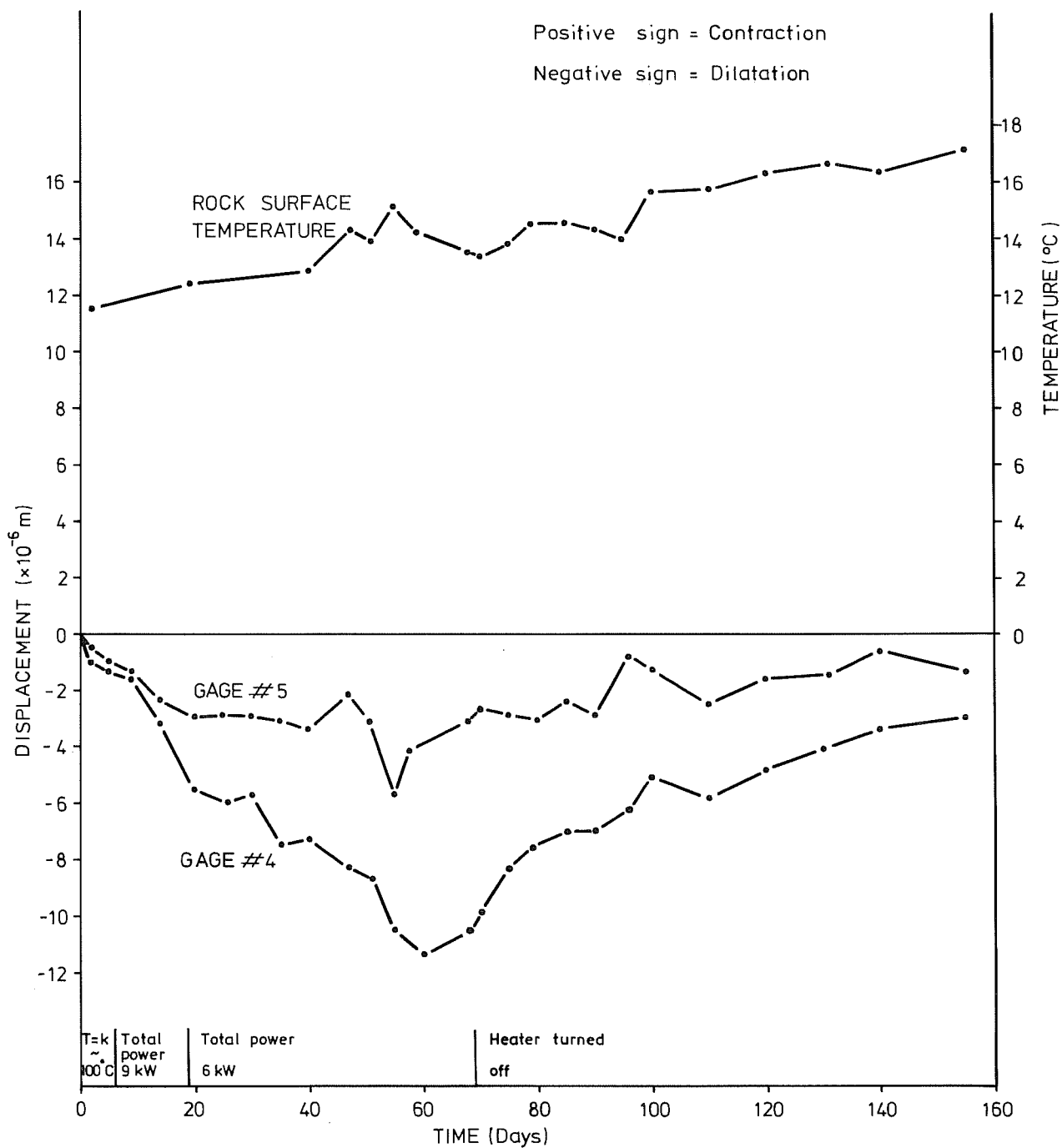
Fig 9.1 Arrangement of displacement gages on the floor of the test site.

XBL 788-10223



XBL 788-10224

Fig 9.2 Contraction and dilatation of major fractures on the floor as a function of time; for gage arrangement, see Fig. 9.1.



XBL 788-10225

Fig 9.3 Contraction and dilatation of major fractures on the floor as a function of time; for gage arrangement, see Fig. 9.1.

## 10 MEASURED WATER INFLOW IN THE PERIPHERAL HEATER HOLES

### 10.1 General comments

As mentioned in chapter 5 the three peripheral heater holes were used for measuring the water inflow to the test site. The measurements started 19 days after the heaters were turned on and continued throughout the duration of the test.

The measurements were carried out so that when one of the holes became filled with water to the collar, all holes were blown dry and the measurements restarted.

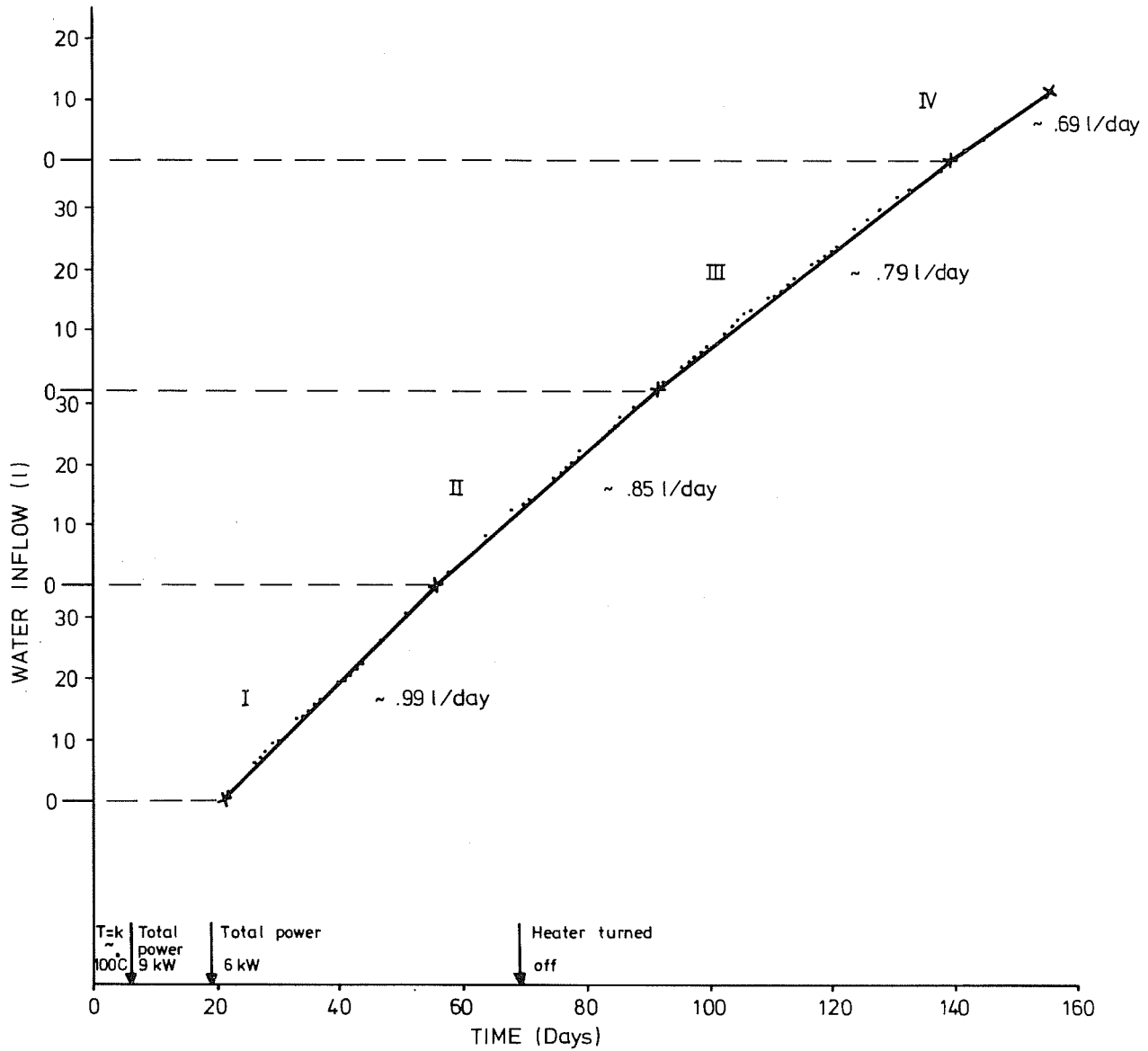
### 10.2 Water inflow as a function of time

In Fig 10.1 the water inflow in hole number 2 is shown as a function of time, (Fig 4.4). The radial distance to the main heater is 0.65 m. As can be observed in the figure the first set of measurements gives an inflow of 0.99 l/day. The water inflow is then reduced successively to 0.69 l/day as calculated from measurements between day no 140 and 155.

### 10.3 Comments on measured data

The data presented in Fig 10.1 refers to borehold no. 2. The data from the peripheral heater holes nos. 2 and 3 give the same appearance of the curves although the magnitude of the water inflow is lower.

The lower inflow of water as a function of time implies that the fractures are closing during the test. After the heater was turned off the same appearance is observed. The explanation for this is somewhat unclear. A possible explanation is that the rock behaves in a visco-elastic manner, i.e., the closure of the apertures is time dependent.



XBL 788-10226

Fig 10.1 Water inflow as a function of time in hole No. 2; the location of the borehole is given in Fig. 4.4.

## 11 ACKNOWLEDGMENTS

The author would like to express his grateful thanks for assistance in the project to Prof Ove Stephansson, Drs. Ove Alm and Graham Swan, and research engineers Göran Bäckblom and Bengt Leijon, all at the Department of Rock Mechanics, University of Luleå.

Prof. W. Hustrulid, Drs. H. Pratt and R. Simonson, and Mr. T. Schrauf, all of Terra Tek, Salt Lake City, Utah, offered assistance and valuable discussions concerning the results of the heater test.

I am grateful to the Lawrence Berkeley Laboratory and their staff at the Stripa test site for assistance in the field work.

Ms. Monica Lövgren made the drawings and Ms. Gunilla Törnqvist typed the manuscript. Both are gratefully acknowledged.

This project was initiated and financed by the Swedish Nuclear Fuel Safety Program operated for the Swedish Nuclear Power Utility Industry.

## 12 REFERENCES

- [1] Carlsson, H. Bergspänningsmätningar i Stripa Gruva, University of Luleå. KBS Technical report no. 49, Stockholm, 1977. (Reprinted by LBL as Stress Measurements in the Stripa Granite. LBL-7078, SAC-04).
- [2] Lundberg, J. Tv- och kikargranskning av borrhål i ÖV<sub>1</sub>, Stripa Gruva. Hagconsult. Stockholm, 1977.
- [3] Lundström, L., Stille, H. Permeabilitetsprovning av graniten i Stripa Gruva - Rapport. Hagconsult, Stockholm, 1977. (Reprinted by LBL as Large Scale Permeability Test of the Granite in the Stripa Mine and Thermal Conductivity Test. LBL-7052, SAC-02).
- [4] Olkiewicz, A., Hansson, K., Almén, K-E., Gidlund, G. Geologisk och hydrogeologisk grunddokumentation av Stripa försöksstation. SGU. KBS Technical report no. 63, Stockholm 1978.
- [5] Pratt, H.R., Schrauf, T.W., Hustrulid, W.A. Thermal and Mechanical Properties of Granite, Stripa, Sweden. Terra Tek, Salt Lake City, Utah, 1977.
- [6] Stephansson, O. Deformationer i sprickigt berg, University of Luleå. KSB Technical report no. 29, Stockholm, 1977.

- [7] Swan, G. The mechanical properties of the rocks in Stripa, Kråkemåla, Finnsjön and Blekinge, University of Luleå. KBS Technical report no. 48, Stockholm, 1977. (Reprinted by LBL. LBL-7074, SAC-03).
- [8] Witherspoon, P.A., Cook, N.G.W., Gale, J.E. Cooperative work program with Swedish Nuclear Fuel Supply Company on radioactive waste storage in mined caverns. Internal report. KBS, Stockholm, 1977.
- [9] IRAD GAGE, Vibrating wire stressmeter instruction manual, 1977, 33 pp.
- [10] Carslaw, H.S. and Jaeger, J.C., 1959. Conduction of heat in solids, 2nd ed. Oxford University Press, Oxford, 510 pp.
- [11] Hustrulid, A. and Hustrulid, W.B. Development of a Borehole Device to Determine the Modulus of Rigidity of Coal Measure Rocks. Colorado School of Mines, 1972.

THE TRANSIENT HEAT DISTRIBUTION FROM A CYLINDRICAL  
HEATER IN ROCK

Göran Bäckblom

## 1 INTRODUCTION

The aim of this work has been to theoretically calculate the temperature distribution in rock with respect to KBS' heater test at the Stripa mine.

A complete calculation which takes into account all factors that arise is extremely difficult. Hence to deal effectively with the problem some assumptions and approximations have been stated. If it is necessary to adopt more complicated assumptions than those of the present analysis, a wholly numerical method is preferable. Associate Prof. Torbjörn Hedberg, University of Luleå, is acknowledged for his participation in the theoretical development.

## 2 CALCULATION OF TEMPERATURES

2.1 Assumptions

In the present analysis the cylinder is approximated by a finite line source. The approximation is very good at large distances from the heater.

Hodgkinson [1] has studied a cylinder with exponential decaying heat generation. In order to evaluate the discrepancy between a line source and a cylinder, accurate temperatures with respect to a cylinder geometry from the calculations of Hodgkinson [1] were obtained.

The input data used are given in Table I and the actual differences in temperature between a cylinder and a finite line source are presented in Table II. From Table II it becomes evident that the geometrical simplifications affect the results only to a slight extent.

Table I Input to temperature calculations  
(after Hodgkinson [1])

Radius of cylinder	0.25	m
Length	2.0	m
Initial heat generation	1000	W
Decay constant	30	yrs
Thermal capacity	879	J/kg, °C
Thermal conductivity	2.51	W/m, °C
Density	2600	kg/m <sup>3</sup>

The relevant physical properties of the Stripa rock has been supplied by Terra Tek [3]. The thermal conductivity is, according to experimental studies

$$\lambda = -3.745 \cdot 10^{-2} \cdot T + 3.60$$

where

$\lambda$  = thermal conductivity W/m, °C

T = temperature °C

Table II Differences in temperature between a cylinder and a finite line source

Time yrs	Differences in temperature °C				
	Distance from center of heater [m]				
	0.25	0.50	1.0	2.0	4.0
0.01	0.410	0.336	0.169	0.017	-
0.1	0.229	0.182	0.093	0.027	0.005
0.2	0.224	0.177	0.090	0.024	0.005
0.5	0.220	0.175	0.087	0.023	0.004
1.0	0.218	0.171	0.085	0.022	0.004

Table III presents the assigned values of the other necessary parameters.

Table III Input calculation of temperature by means of theory for a finite line source

L	Length of the line source	3	m
c	Thermal capacity	824.8	J/kg, °C
p	Density	2600	kg/m <sup>3</sup>
q	Heat generation	6000	W
T <sub>0</sub>	Initial temperature	9.12	°C

The present analysis assumes that the thermal conductivity is independent of temperature. The calculation has been restricted to estimate the temperature field for some different values of the conductivity.

Further assumptions made are:

- The heater is in perfect contact with the rock

- There is no groundwater flow.
- The surrounding rock is homogeneous and isotropic.

## 2.2 Theory

A continuous point source [2] gives the temperature distribution:

$$T = \frac{q}{4\pi \lambda r} \operatorname{erfc} \left( \frac{r}{\sqrt{4\kappa t}} \right) \quad (1)$$

where

$T$  = temperature  $^{\circ}\text{C}$   
 $r$  = distance from point source m  
 $\lambda$  = thermal conductivity W/m,  $^{\circ}\text{C}$   
 $\kappa$  = thermal diffusivity =  $\lambda/\rho c$   $\text{m}^2/\text{s}$   
 $q$  = heat generation W

The function  $\operatorname{erfc}(x)$  is the complementary error function

$$\operatorname{erfc}(x) = 1 - \operatorname{erf}(x) = \frac{2}{\sqrt{\pi}} \int_x^{\infty} e^{-u^2} du \quad (2)$$

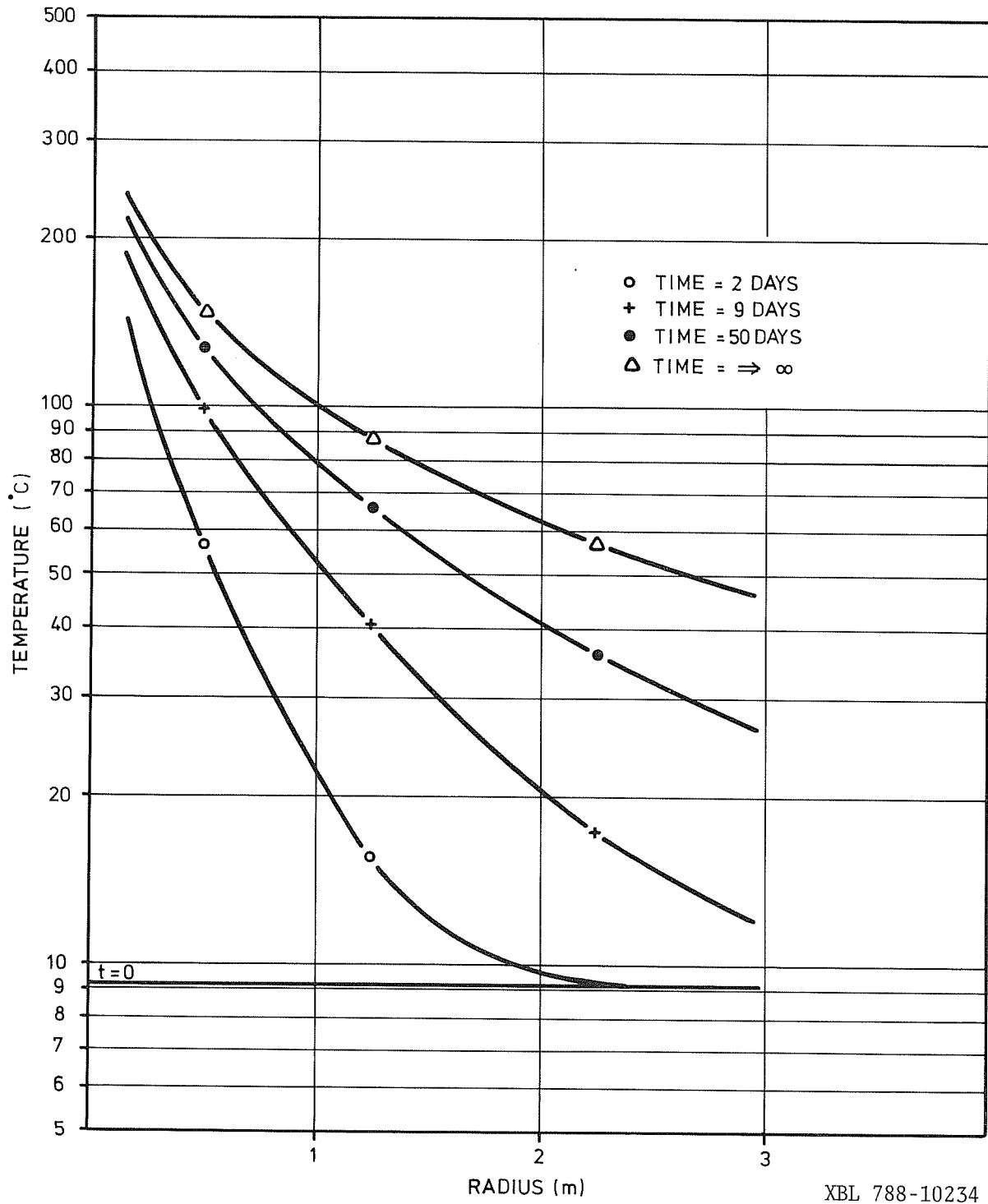
If the equation (1) is integrated over the length  $2l$ , the temperature  $T$  can be obtained in the equatorial plane of the line source as:

$$T = \frac{2 q_l}{4\pi \lambda} \int_0^l \frac{\operatorname{erfc} \left( \frac{x^2+r^2}{\sqrt{4\kappa t}} \right) dx}{\sqrt{x^2+r^2}} \quad (3)$$

where

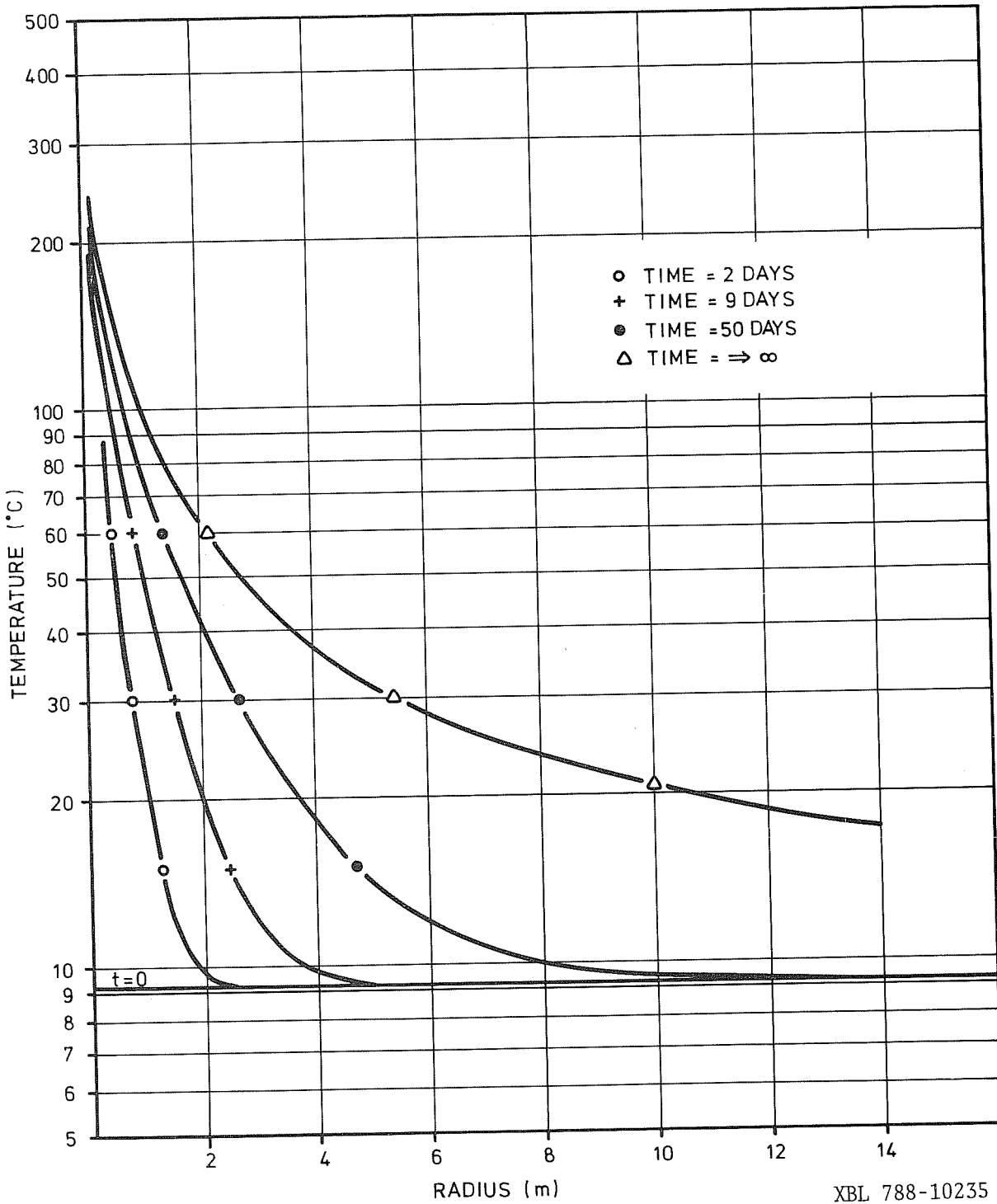
$x$  = variable of integration m  
 $l$  = half the length of the source m  
 $q_l$  = effect per unit of length W/m

Equation (3) is solved by means of numerical quadrature.



XBL 788-10234

Fig A.I.6a Temperature plot vs radial distance to main heater:  $\lambda = 4.12 \text{ W/m}^\circ\text{C}$ .



XBL 788-10235

Fig A.I.6b Temperature plot vs radial distance to main heater:  $\lambda = 4.12 \text{ W/m}^\circ\text{C}$ .

## 3 REFERENCES

- [1] Hodgkinson, D.P. Deep rock disposal of high radioactive waste: transient heat conduction from dispersed blocks AERE-R 8763. Harwell, Oxfordshire, June 1977
- [2] Carslaw, H.S. & Jaeger, J.C. Conduction of heat in solids, 2 nd ed. Oxford University Press. Oxford 1959, 510 pp
- [3] Pratt, H.R. et al. Thermal and Mechanical Properties of Granite, Stripa, Sweden. Terra Tek, Salt Lake City, USA, 1977.

PREDICTED ROCK STRESSES FOR THE PILOT HEATER  
AT THE STRIPA MINE

Bengt Leijon

## GENERAL

In order to predict the stresses caused by increased temperature in the rock mass surrounding the heater, two theoretical analyses have been carried out:

1. An analytical calculation based on the theory of elasticity.
2. A two-dimensional, finite-element calculation.

In both cases, the following basic assumptions were made:

1. The rock mass is a linear elastic, homogeneous and isotropic medium
2. The rock properties are constant and not temperature dependent
3. The following rock properties were chosen:

Young's Modulus	$E = 69.4 \text{ GPa}$
Poisson's Ratio	$\nu = 0.21$
Thermal expansion	$\alpha = 11.1 \cdot 10^{-6} / ^\circ\text{C}$
Thermal conductivity	$\lambda = 3.4 \text{ W/m}^\circ\text{C}$

4. Temperature distributions were calculated according to Appendix I

Since all temperature and stress measurements were carried out in the midplane of the heater, the stress analyses also refer to this plane. The strains, perpendicular to this plane, i.e., parallel to the long axis of the heater, should by symmetry be zero. Thus, the plane strain condition has been assumed.

The two analyses will be presented in two separate sections together with some results.

## A. ANALYTICAL CALCULATION

Consider a plane, thin, circular plate with infinite outer radius and with a central hole of radius  $r_0$  (peripheral heater holes and measuring holes are not taken into account). The plate is loaded by the temperature load  $T(r, t)$ , where  $r$  and  $t$  denote radius from center, and time respectively. With symbols according to Fig A.2.1, the radial and tangential stresses - and also principal stresses - are given by the equations

$$\sigma_r = A - \frac{B}{r^2} - \frac{E\alpha}{(1-\nu)} \cdot \frac{1}{r^2} \int_{r_0}^r r \cdot T(r) \cdot dr$$

$$\sigma_\varphi = A + \frac{B}{r^2} + \frac{E\alpha}{(1-\nu)} \left[ \frac{1}{r^2} \int_{r_0}^r r \cdot T(r) \cdot dr - T(r) \right]$$

where  $A$  and  $B$  are constants determined from the boundary conditions. Utilizing the boundary conditions:

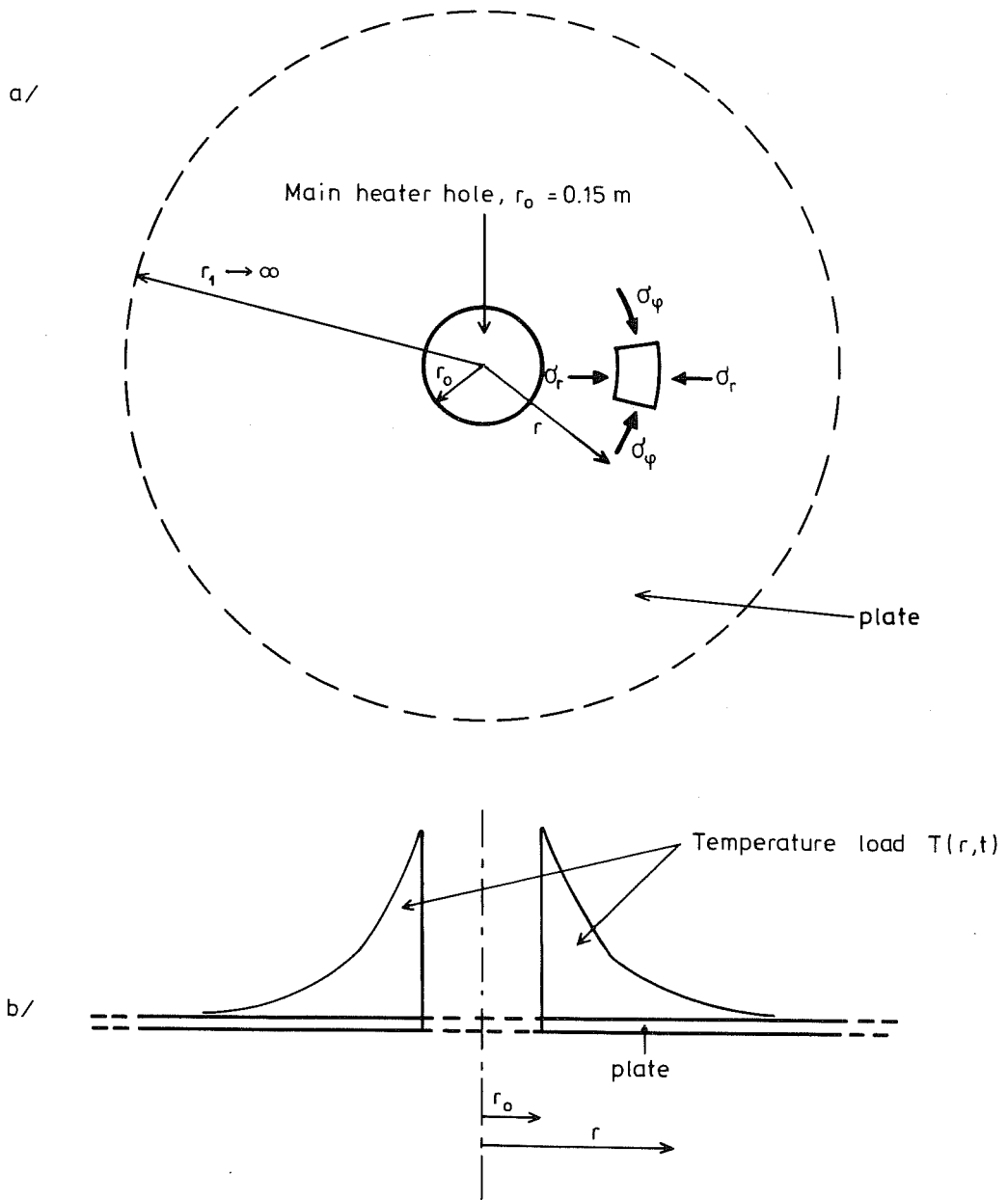
$$\sigma_r = 0 \quad \text{for} \quad r = r_0 \quad \text{and}$$

$$\sigma_r, \sigma_\varphi \rightarrow 0 \quad \text{for} \quad r \rightarrow \infty \quad \text{we get}$$

$$\sigma_r = \frac{E\alpha}{(1-\nu)} \cdot \frac{1}{r^2} \cdot \int_{r_0}^r r \cdot T(r) \cdot dr \quad (1)$$

$$\sigma_\varphi = - \frac{E\alpha}{(1-\nu)} \left[ \frac{1}{r^2} \cdot \int_{r_0}^r r \cdot T(r) \cdot dr - T(r) \right] \quad (2)$$

At the time  $t_0$ , with a specific temperature load  $T(r, t_0)$ , the state of stress in the plate is a function of radius



XBL 788-10236

Fig A.2.1 Theoretical model of thermal stress distribution in the plane perpendicular to the heater: a) Viewed along the heater axis; b) Viewed perpendicular to the heater axis.

and material properties only. Notice that it is not the total state of stress that is calculated, since the in situ stresses are not considered. The absolute stresses could easily be determined by superposition of thermal stresses and in situ stresses.

Since the temperature is known only for discrete arbitrarily chosen points, the integral in equation (1) and (2) had to be calculated numerically. This was carried out using a fourth order method and a radial steplength, small enough to prevent the influence of numerical truncation errors.

### Results

Stresses have been calculated using predicted temperatures after 2, 5, 9, 14, 20, 35, 50 and 68 days of heating. The results are presented in chapter 8 of the main report, together with measured stresses, and will not be repeated here.

## B. FINITE ELEMENT CALCULATION

The finite element analyses were performed using the computer program system FEMFAB III, developed at Chalmers Institute of Technology by Kenneth Axelsson and Mats Fröier. The program is intended for stress analyses of homogeneous, elastic, two- or three-dimensional structures loaded with temperature loads, volume forces and boundary forces.

The structure used for these analyses (shown in Fig A.2.2) has the shape of a semicircular plate loaded with temperature loads and boundary forces. It is assumed to be a model of the heater's midplane. The temperature loads are applied as temperatures in the nodal points. The polar geometry is chosen to facilitate the temperature loading. Boundary forces are provided by the in situ measured stresses  $\sigma_1 = 20.0$  MPa and  $\sigma_2 = 11.4$  MPa in the test site of the Stripa mine. The stresses are converted into equivalent forces attacking in the nodal points along the boundaries.

Due to symmetry, it is possible to reduce the structure to a semicircular plate with all tangential displacements along the symmetry line prescribed to zero (see Fig A.2.2). The structure was made very large (radius 15 m) in order to prevent disturbance from boundary loads into its inner, temperature-loaded parts.

### Results

Two main load cases were considered:

- |              |  |
|--------------|--|
| Load case 1: | Temperature loads and boundary loads in form of <u>in situ</u> stresses $\sigma_1$ and $\sigma_2$ are applied to the structure |
| Load case 2: | Only temperature loads are applied   |

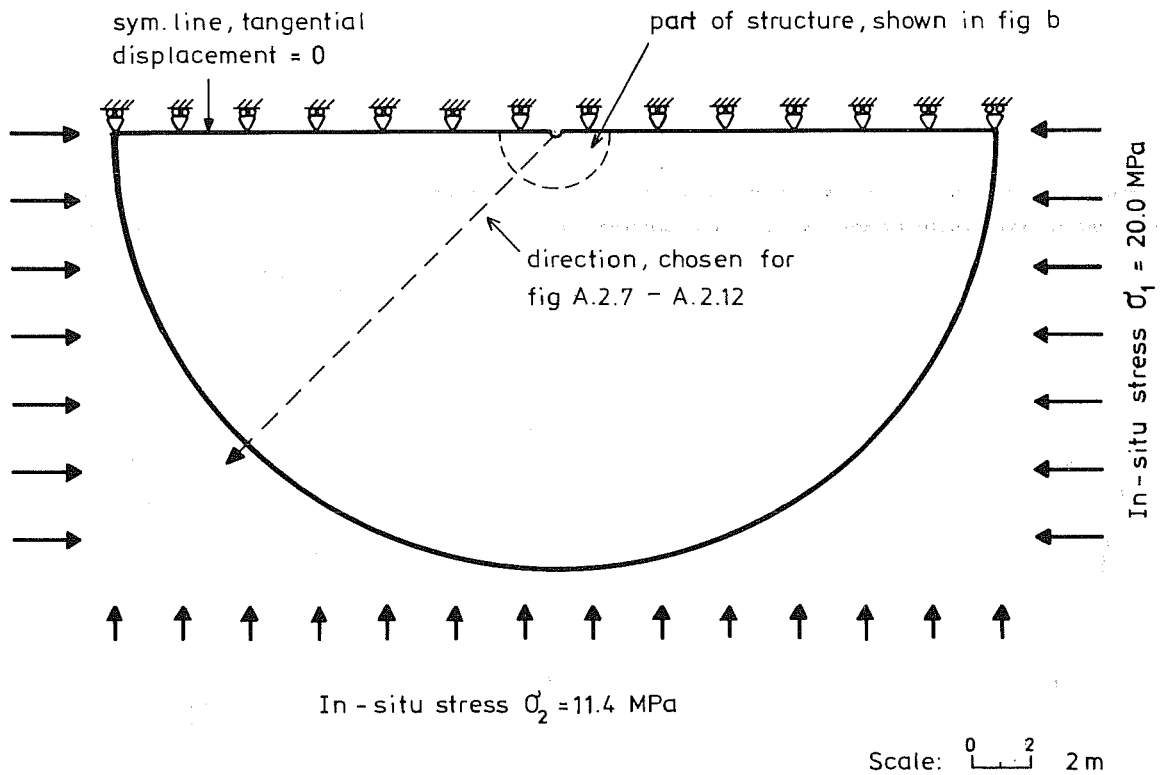
Load case 1

Figures A.2.3 - A2.6 show the principal stresses  $\sigma_1$  and  $\sigma_2$  for some points on the central part of the left half of the structure; the stress pattern on the right half is symmetrical. It can easily be seen that the stress distribution is a result of radial and tangential thermal stresses, in cooperation with the in situ stresses. Figures A.2.7 - A.2.10 show the principal stresses  $\sigma_1$ ,  $\sigma_2$  and  $\sigma_3$  as a function of radius for a chosen direction (see Fig A.2.2).

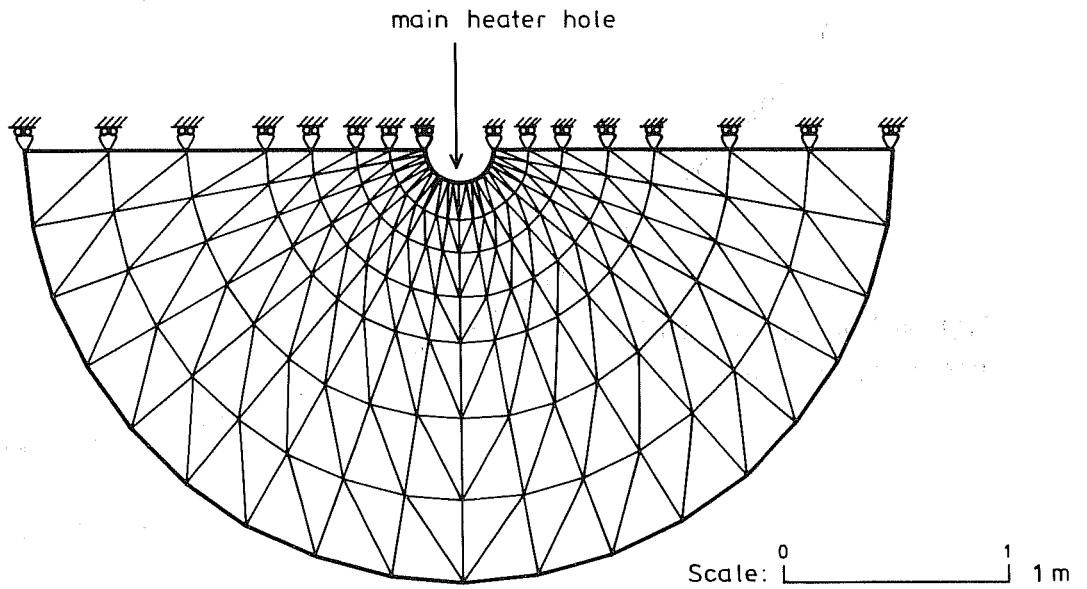
Load case 2

The principal stresses after 2 and 35 days are shown in Fig A.2.11 and A.2.12 respectively. The orientation of the two principal stresses parallel to the midplane of the heater is close to radial and tangential. These stresses are the thermally induced stresses, comparable with the analytically determined stresses in section A. Hence, the stresses from section A have been drawn in the same plots for comparison. As can be seen in the figures, the agreement is very close, as would be expected.

a/

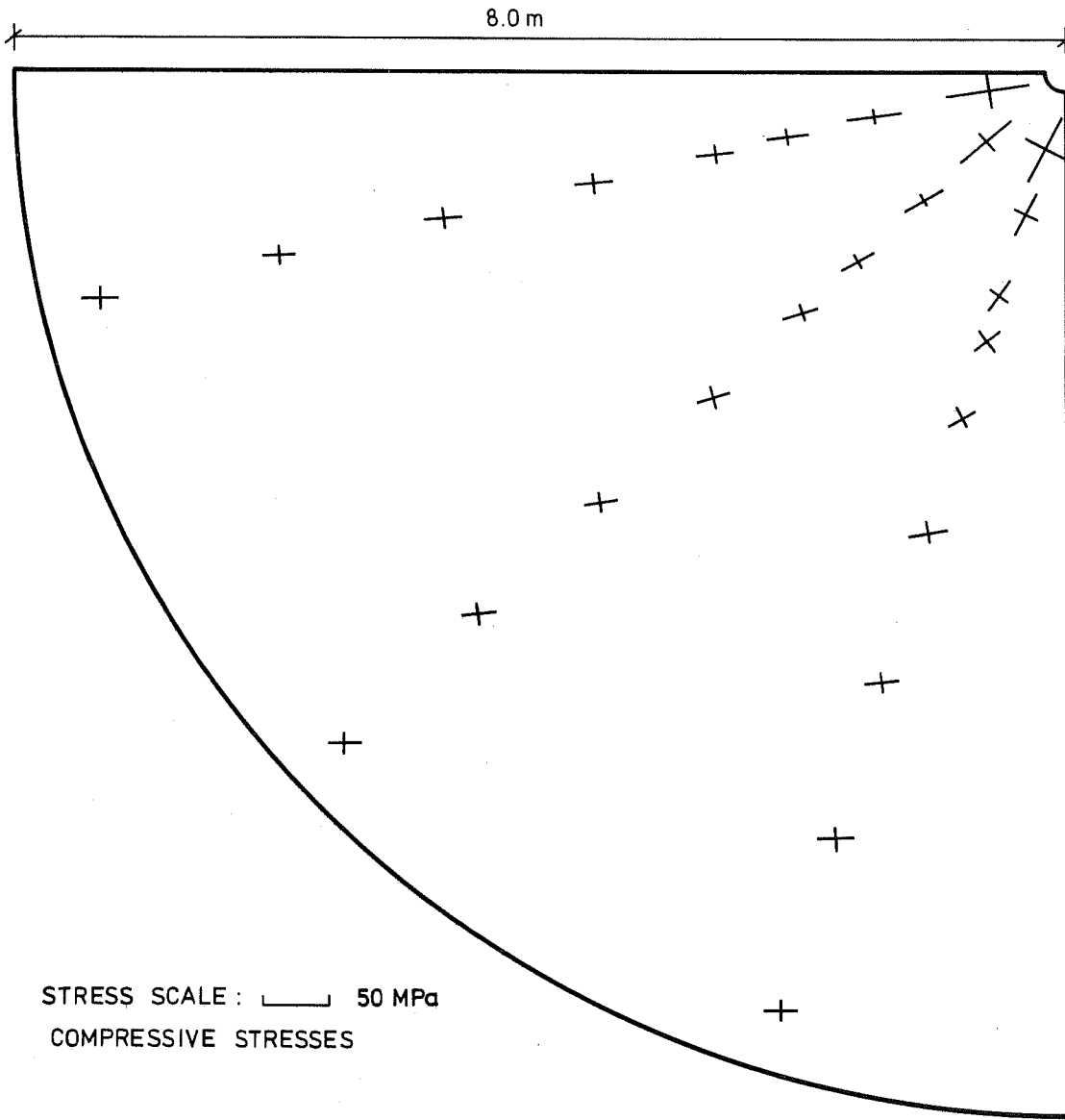


b/



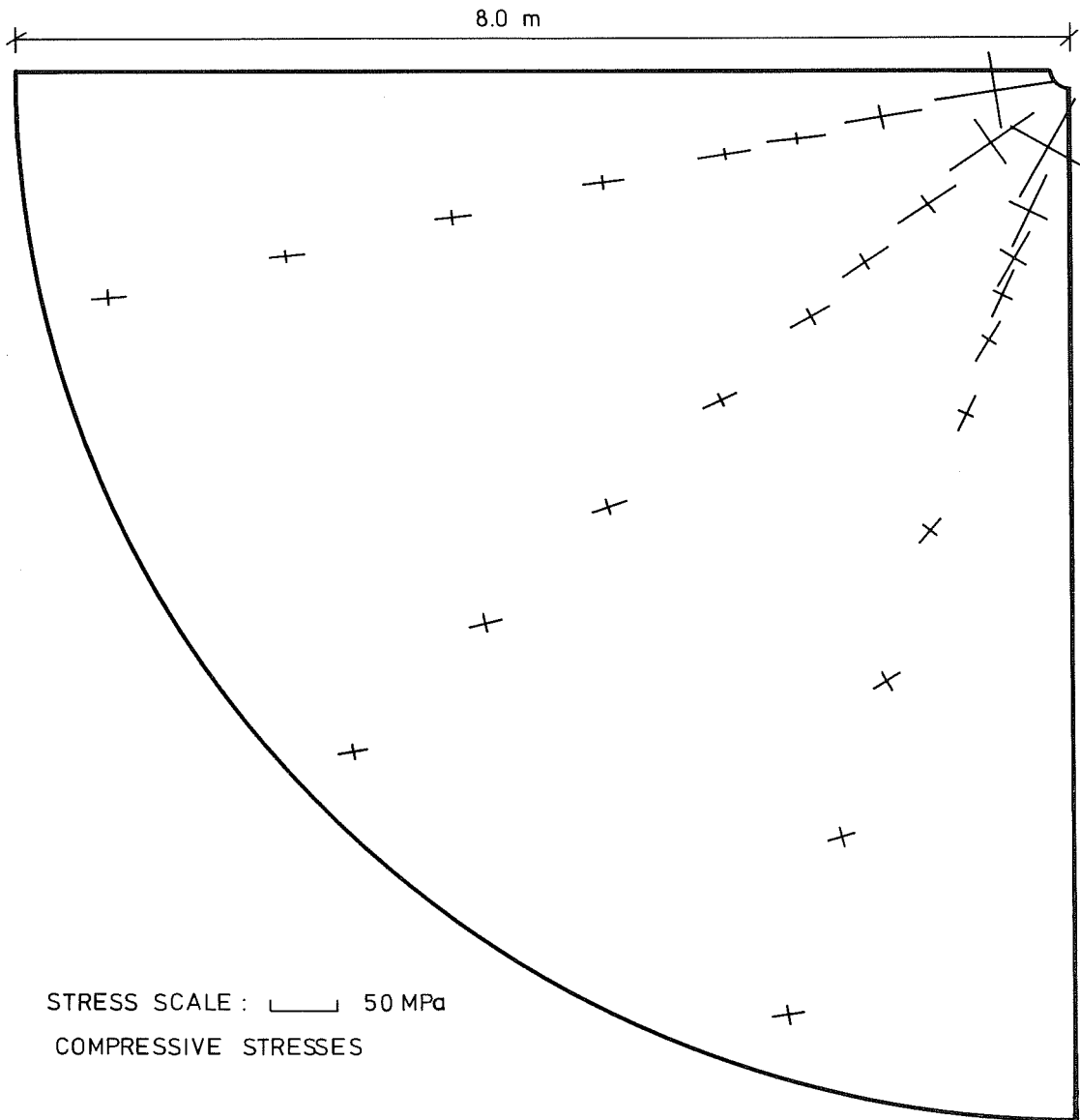
XBL 788-10237

Fig A.2.2 Structure for FEM-analysis: a) Complete structure with boundary loads; b) Central part of structure with mesh.



XBL 788-10238

Fig A.2.3 Principal absolute stresses perpendicular to the heater after 2 days heating.



XBL 788-10239

Fig A.2.4 Principal, absolute stresses perpendicular to the heater after 9 days heating.

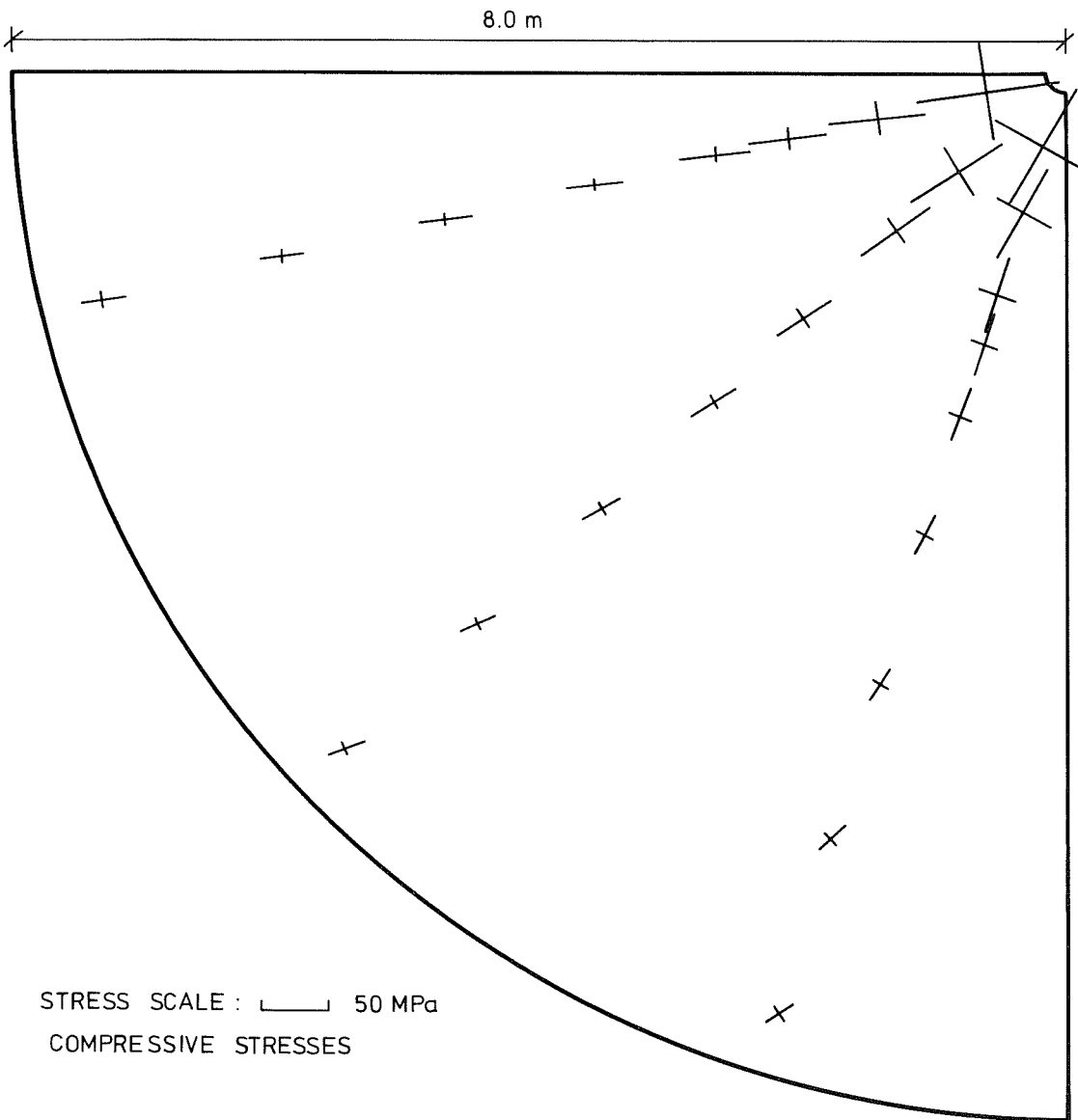
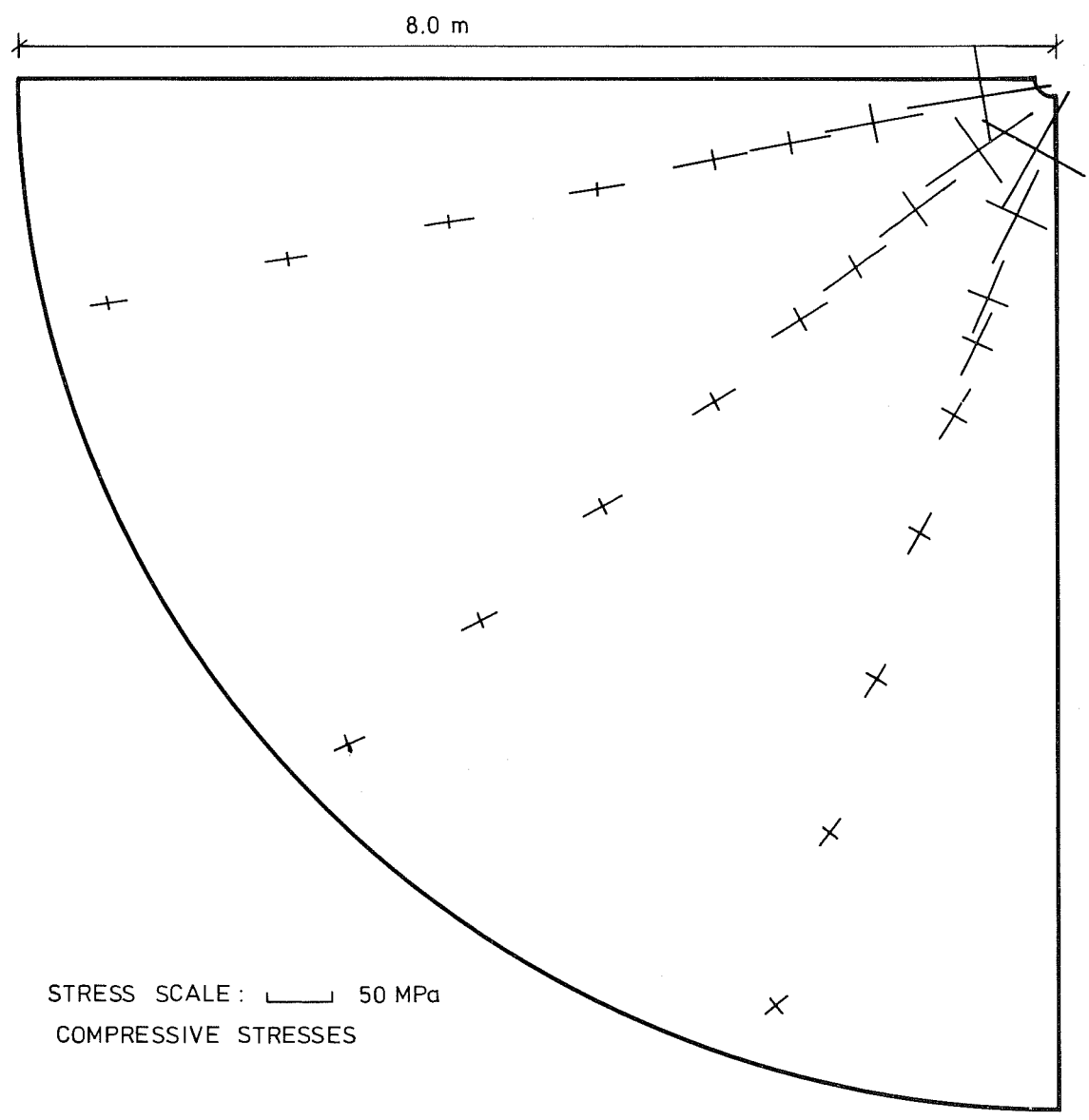
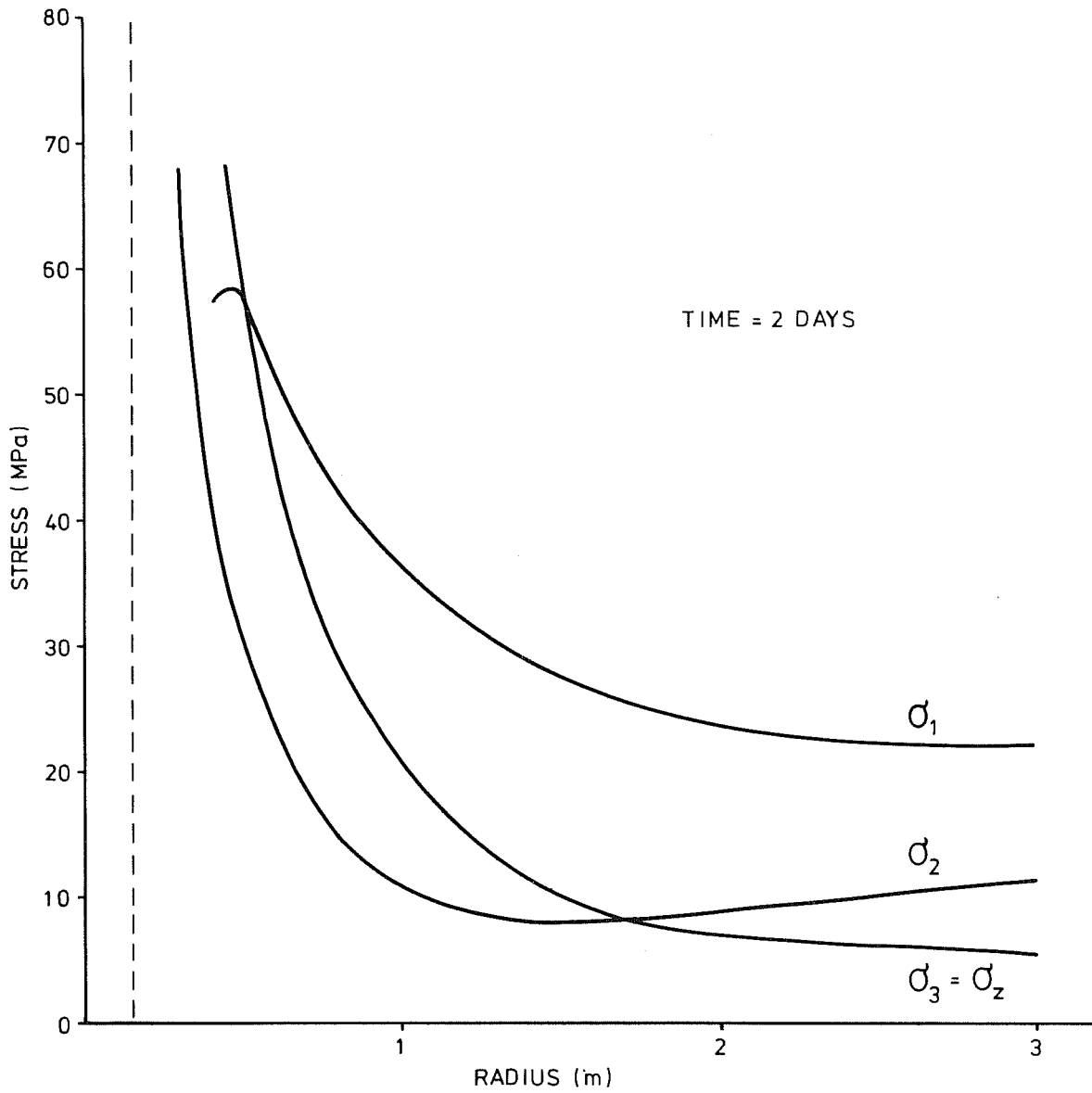


Fig A.2.5 Principal, absolute stresses perpendicular to the heater after 35 days heating.



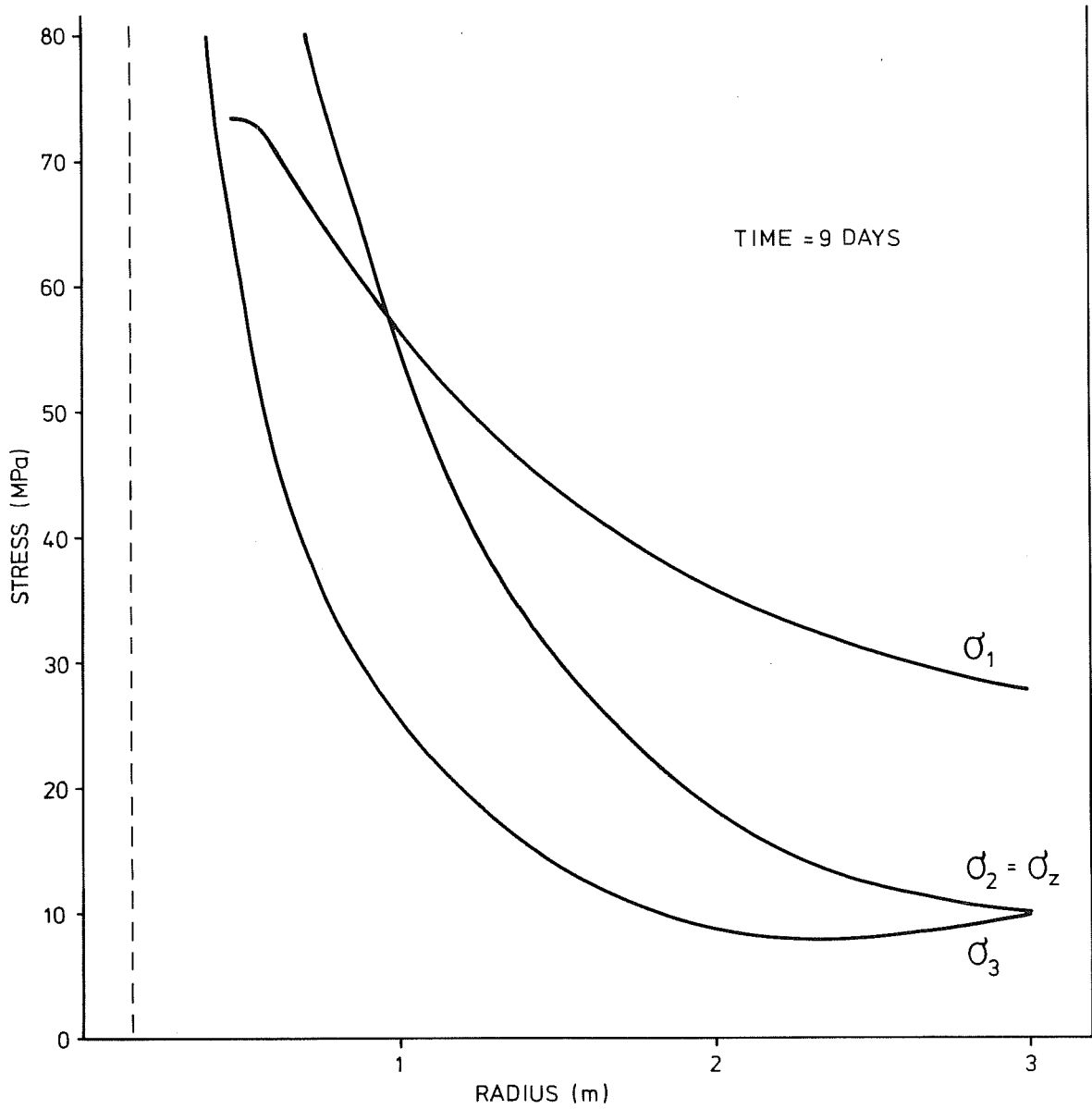
XBL 788-10241

Fig A.2.6 Principal, absolute stresses perpendicular to the heater after 50 days heating.



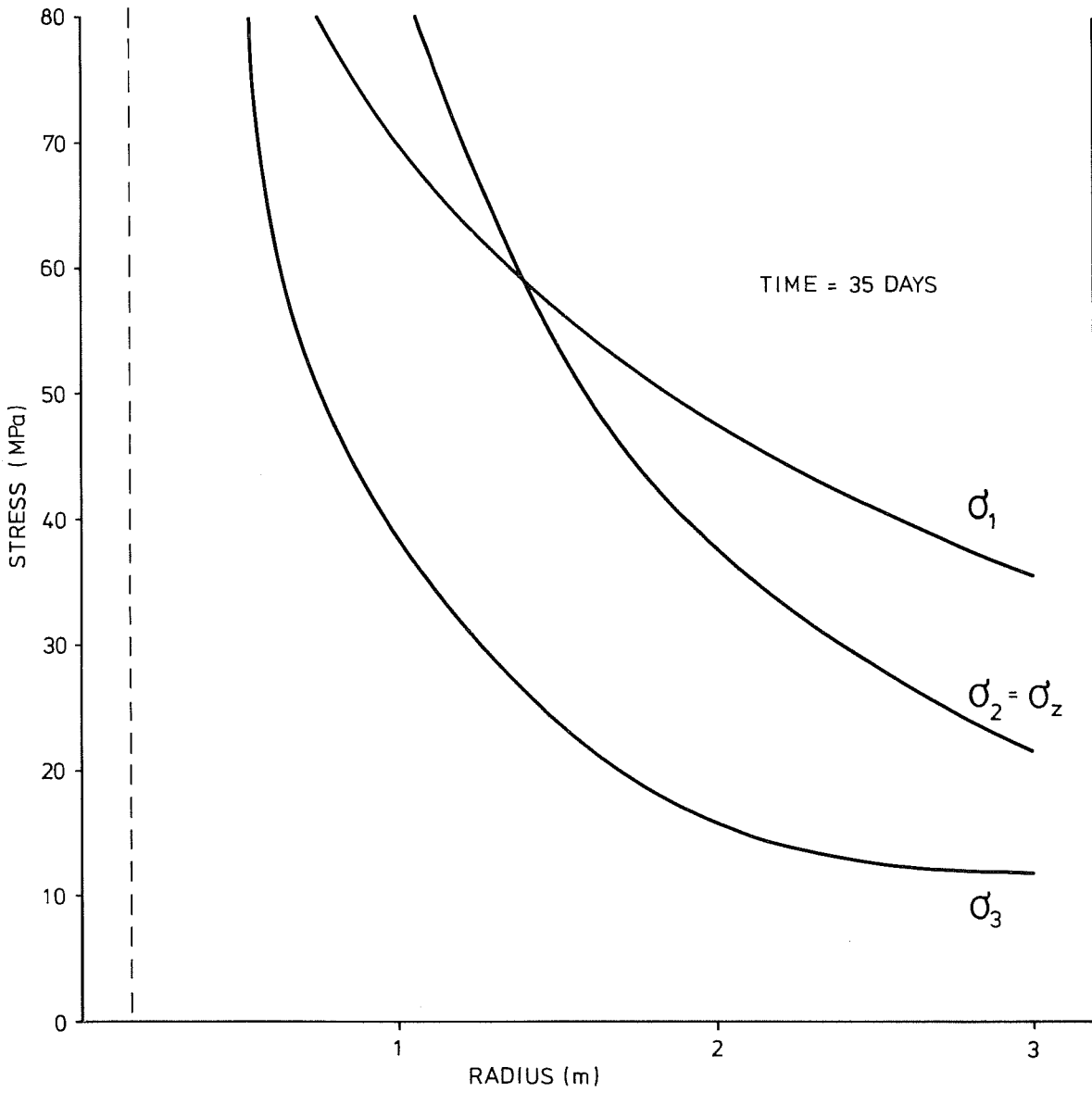
XBL 788-10242

Fig A.2.7 Principal, absolute stresses as a function of radius after 2 days heating.



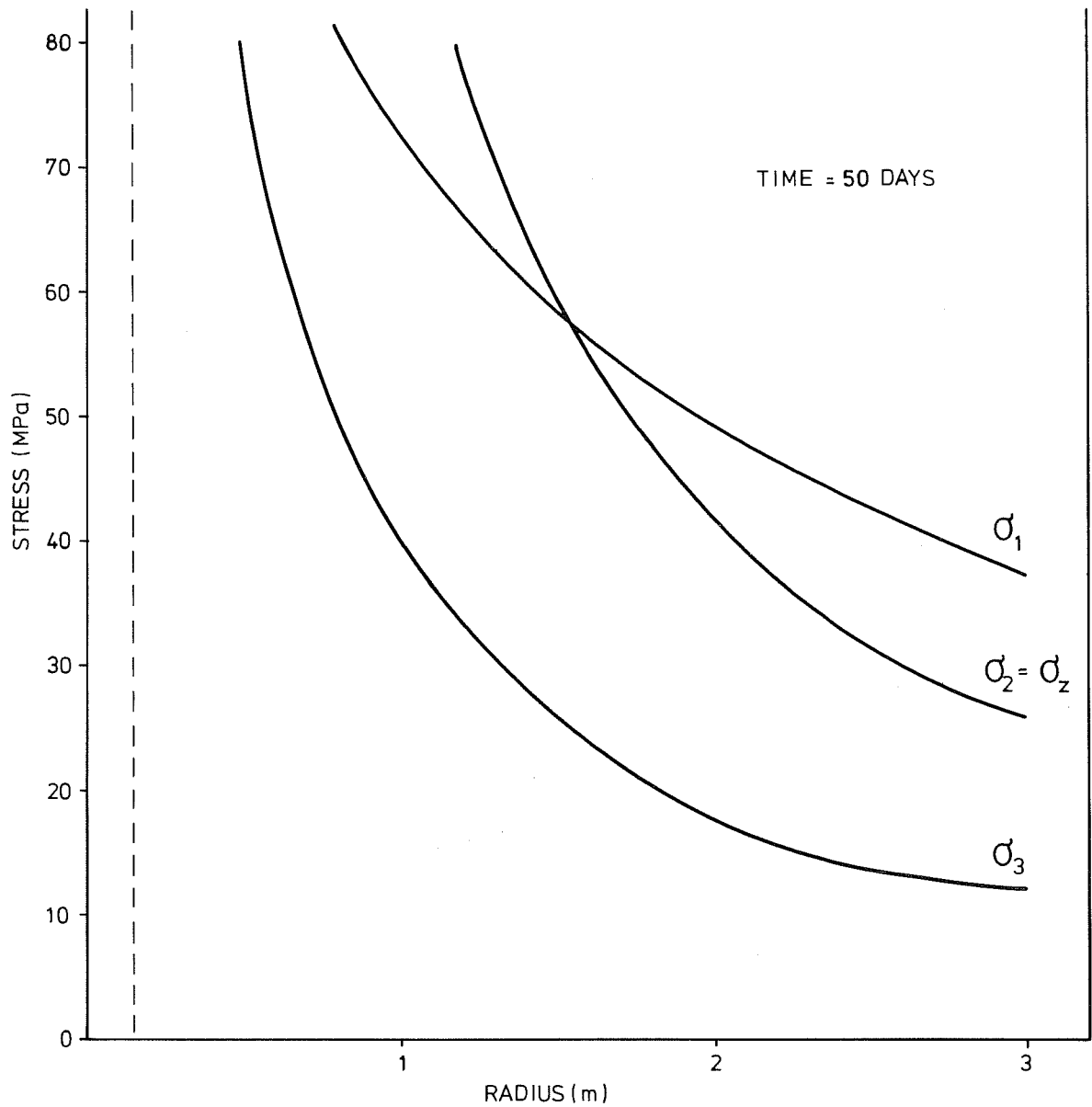
XBL 788-10243

Fig A.2.8 Principal, absolute stresses as a function of radius after 9 days heating.



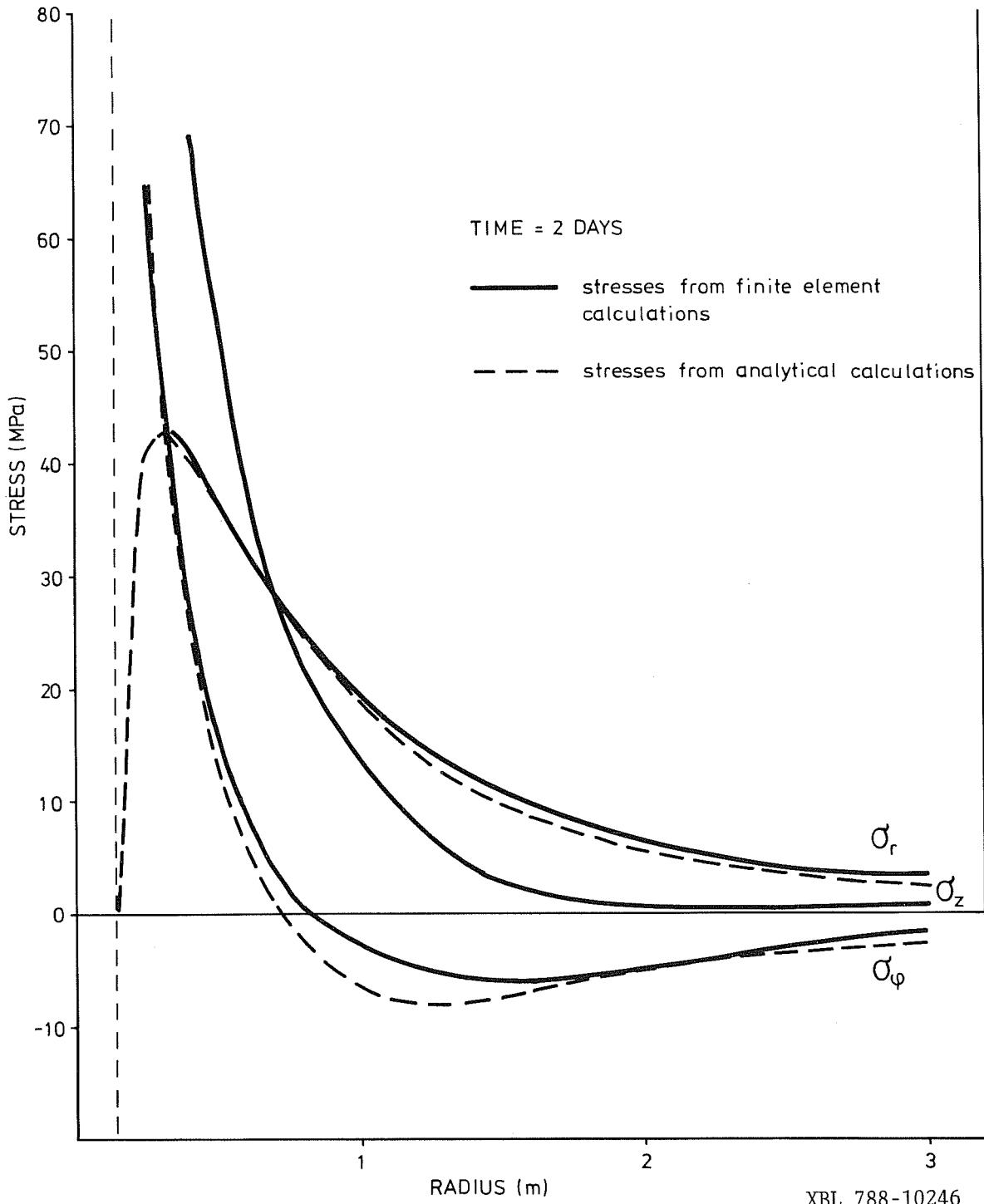
XBL 788-10244

Fig A.2.9 Principal absolute stresses as a function of radius after 35 days heating.



XBL 788-10245

Fig A.2.10 Principal, absolute stresses as a function of radius after 50 days heating.



XBL 788-10246

Fig A.2.11 Thermally induced, principal stresses after 2 days heating.

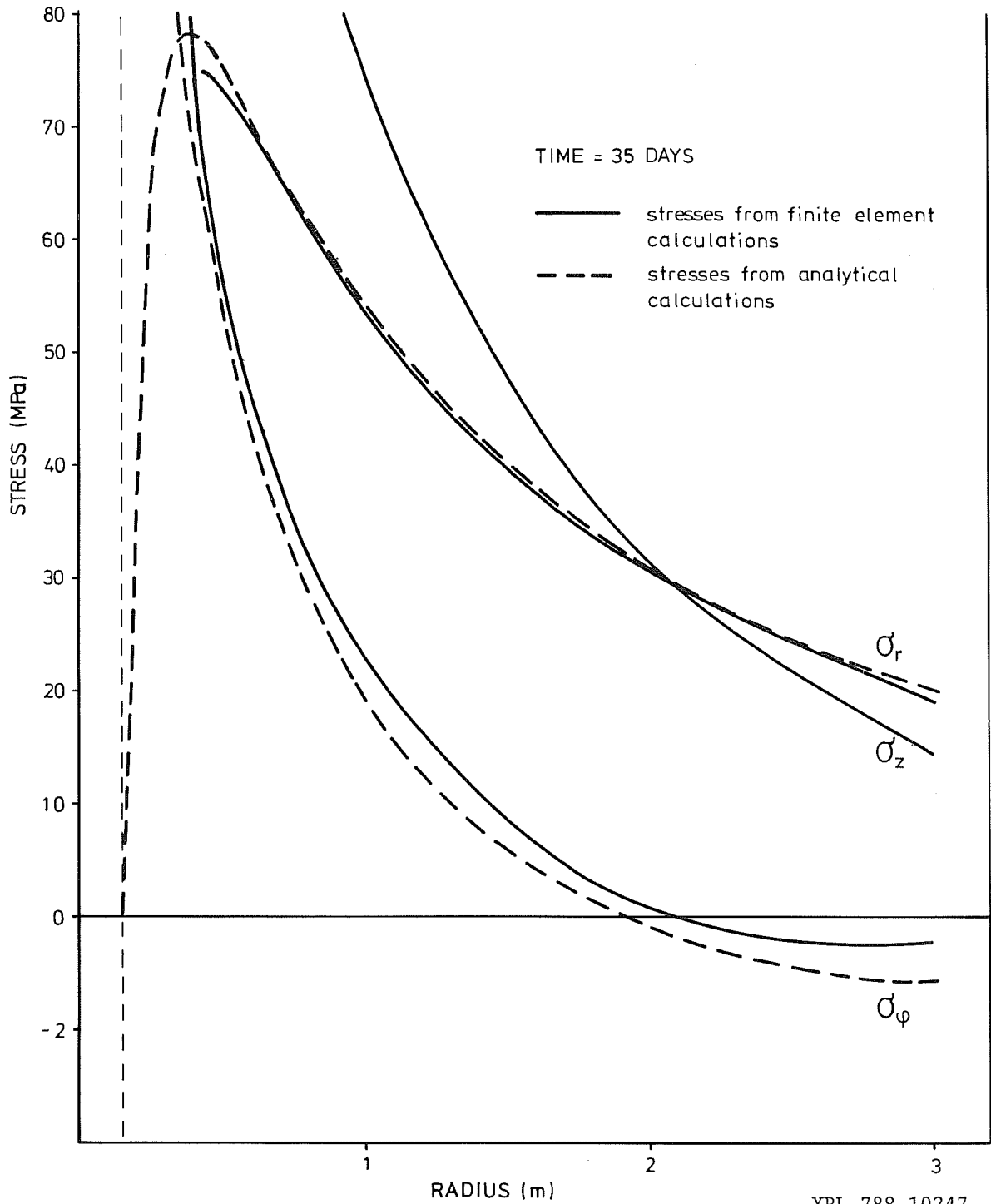


Fig A.2.12 Thermally induced, principal stresses after 35 days heating.

## REFERENCES

- [1] Axelsson, K., Fröjer, M: FEMFAB III. Dator program för strukturanalys med finit elementmetod. Chalmers Tekniska Högskola, Publikation 75:1.
- [2] Roark, R.J., Young, W.C: Formulas for Stress and Strain. Fifth edition, Mc-Graw-Hill, 1975.

IN SITU DETERMINATION OF THERMAL CONDUCTIVITY OF  
THE STRIPA GRANITE

Bengt Leijon

## INTRODUCTION

When the main heater was turned off after 68 days of heating at the test site in the Stripa mine, the decision was made to continue the temperature readings in order to study the cooling lapse. All measurements were cut off after 155 days since the cooling was almost complete. The temperature readings during the initial part of the cooling have been used with the intention of determining the in situ thermal conductivity of the Stripa granite. A mathematical model of the cooling lapse was set up, and the model parameters were varied so that best agreement with measured temperatures was obtained.

Laboratory tests on specimens, in order to determine the thermal conductivity, have been performed by Terra Tek, [4]. The main purpose of this study has therefore been to compare the laboratory tests with the in situ tests. Unfortunately, the decision to carry out the in situ evaluation of conductivity was made in a late stage of the test program. Hence, the way the temperature measurements were performed did not quite suit the purpose of determining thermal conductivity.

The mathematical and numerical work for this study has mainly been performed by Lennart Andersson and Leif Kussoffsky at the University of Luleå, Sweden.

## 1 THEORY

From the above mentioned laboratory tests, the relationship between thermal conductivity,  $\lambda$ , and temperature,  $T$ , is known to be a straight line. That is:

$$\lambda = \lambda_0 - \alpha \cdot T \quad \text{where}$$

$\lambda$  = conductivity at temperature  $T$

$\lambda_0$  = conductivity at temperature  $T = 0$

$\alpha$  = constant

The existence of such a linear relationship between temperature and thermal conductivity has been used as a fundamental assumption. Furthermore the following assumptions have been made:

1. The rock mass is homogeneous and isotropic
2. The specific heat of the rock is constant ( $c = 825 \text{ J/kg } ^\circ\text{C}$ , from [4])
3. The main heater is of infinite length. This approximation is discussed in more detail in a later section
4. Cooling is due to heat conduction only. No convection of ground water is considered in the analysis
5. The air-filled spacing between rock and heater is not considered. That is, perfect thermal contact between rock and heater is assumed-- which means that there is no temperature difference between the heater surface and the hole wall. (The temperature readings at  $r = 0.15 \text{ m}$  are taken at the heater surface.) However, the observed steady-state solution indicates that the thermal contact is not

very good. Hence, the effect of this assumption on the final results will be examined later

6. The heat transfer between the heater and the rock is assumed to be negligible after the heater has been turned off. This assumption will also be discussed later
7. Steady-state conditions are prevalent by the time of turning off the heater
8. The heater is turned off at exactly 06.00 a.m. day 69. This time is denoted as  $t = 0$ . The true time is not known since the turn off was partly uncontrolled and not well documented. However, it is reasonable to believe that the error is less than two hours

Mathematical model (see [3])

In a cylindrical coordinate system  $(r, \theta, z)$  a cylindrical, electric heater is situated at

$$\begin{aligned} r &\leq r_0 \\ 0 &\leq \theta \leq 2\pi \\ -a &\leq z \leq a \end{aligned}$$

The temperature  $T = T(r, t)$ , where  $t$  denotes time, for  $r_0 \leq r \leq r_\infty$  and  $z = 0$  is supposed to satisfy

$$\frac{\partial T}{\partial t} = \frac{1}{r} \frac{\partial}{\partial r} \left( \kappa \left( 1 - \frac{1}{\gamma} T \right) \frac{\partial T}{\partial r} \right) \quad (1)$$

where  $\kappa$  and  $\gamma$  are constants. The initial condition is supposed to be the steady-state solution with  $T$  specified at  $r = r_0$  and  $r = r_\infty$ . At  $t = 0$  the boundary conditions are changed according to

$$\frac{\partial T(r_0, t)}{\partial r} = 0$$

and

$$T(r_\infty, t) = f(t)$$

where  $f(t)$  is the observed temperature  $r = r_\infty$  at time  $t$ .

The substitution

$$u = \kappa \left(1 - \frac{1}{\gamma} T\right)$$

gives the standard equation

$$\frac{\partial u}{\partial t} = \frac{1}{r} \frac{\partial}{\partial r} \left( r u \frac{\partial u}{\partial r} \right) \quad (2)$$

The solution of this equation is known, [1] for certain boundary and initial conditions and obtained by the method of similarity variables. This method, however, does not seem to be appropriate for the present conditions.

The steady-state solution of (2) is

$$u = \sqrt{c_0 + c_1 \ln r} \quad (3)$$

In principle, the unknown constant  $\gamma$  in (1) can be determined from the observed steady-state solution (at  $t = 0$ ).

#### Model errors

Equation (1) is valid only for a cylindrical heater of infinite length, ( $a \rightarrow \infty$ ). A crude estimate of the error due to the finite value of  $a$  is easily obtained for the steady-state solution for the case when the material properties are independent of the temperature.

For a line source with constant source density,  $\tau_0$ , between  $z = -a$  and  $z = a$  and with zero temperature at infinity we get for  $z = 0$

$$T_a(r) = \frac{\tau}{2\pi} \ln \frac{a + \sqrt{r^2 + a^2}}{r}$$

On the other hand, for an infinitely long line source we get

$$T_\infty(r) = \frac{\tau}{2\pi} \ln \frac{c}{r}$$

where the constant  $c = 2a$ . The two expressions agree for  $r \rightarrow 0$ . Of course, the zero temperature condition cannot be satisfied in the latter case. The relative error at  $r = ka$  is then

$$\frac{T_a(ka) - T_\infty(ka)}{T(ka)} = \frac{\ln \frac{1 + \sqrt{k^2 + 1}}{2}}{\ln \frac{1 + \sqrt{k^2 + 1}}{k}}$$

From this we obtain:

k	relative error (%)
2	100
1	21
0.5	4

The true nature of the boundary condition at  $r = r_0$  is not known. The metal heater has much higher heat conductivity than the surrounding rock so that the cooling at the ends of the cylinder may be important for the temperature at  $r = 0, z = 0$ . Thus we do not know whether heat is leaving or entering the cylinder at  $r = r_0$  and  $z = 0$ . We have chosen to suppose the heat transfer at this point to be negligible,  $\frac{\partial T}{\partial r} = 0$ .

#### Numerical approximation

The differential equation is approximated by using a finite method, [2]. We have

$$\frac{\partial u}{\partial t} = \frac{1}{r} \frac{\partial}{\partial r} \left( r u \frac{\partial u}{\partial r} \right) = \frac{1}{r} u \frac{\partial u}{\partial r} + \frac{\partial u}{\partial r} \frac{\partial u}{\partial r} + u \frac{\partial^2 u}{\partial r^2},$$

$$r_0 \leq r \leq r_\infty, \quad t \geq 0,$$

$$\frac{\partial u(r_0, t)}{\partial r} = 0,$$

$$u(r_\infty, t) = f(t).$$

Let  $u_{i,j}$  be an approximate value for  $u(r_0 t, ih, jk)$ , where  $h = (r_\infty - r_0)/N$  is the steplength in  $r$  and  $k$  is the steplength in  $t$ . Further, let  $\Delta_t$ ,  $\tilde{\delta}_x$  and  $\delta_x^2$  be difference operators defined by

$$\Delta_t u_{ij} = u_{i,j+1} - u_{ij}$$

$$\tilde{\delta}_x u_{ij} = u_{i+1,j} - u_{i-1,j}$$

and

$$\delta_x^2 u_{ij} = u_{i-1,j} - 2u_{ij} + u_{i+1,j}$$

The difference approximation used is

$$\Delta_t u_{i,j} = \frac{k}{h^2} \left[ \frac{u_{ij}}{2(r_0/h+i)} \tilde{\delta}_x u_{i,j+1} + \frac{1}{4} (\tilde{\delta}_x u_{ij}) (\tilde{\delta}_x u_{i,j+1}) + u_{ij} \delta_x^2 u_{i,j+1} \right], \quad 0 \leq i \leq N, \quad j \geq 0,$$

$$\tilde{\delta}_x u_{0j} = 0, \quad j \geq 1,$$

$$u_{Nj} = f(jk), \quad j \geq 1.$$

This is a simple linear implicit scheme requiring the solution of a tridiagonal linear system of equations for each time step.

The initial solution is taken to be of the form (3), where the constants are chosen so that the solution matches the observed temperatures at the three innermost points.

## 2 RESULTS

Mean values of temperatures at radii 0.15 m, 0.85 m and 1.55 m were used as input data for the initial solution. As outer boundary conditions the temperature at actual time (mean of directions A, B and C) at radius 1.55 m was used. That is, only the three innermost points were taken into account.

The best agreement between computed temperature values and in situ measured values occurred for  $4.70 \leq \lambda_0 \leq 4.95$  (W/m °C). This value should be compared to the value from laboratory tests on rock specimens,  $\lambda_0 = 3.63$  W/m °C. Due to lack of temperature readings during the initial part of the cooling, it has not been possible to do any determination of the temperature dependency of  $\lambda$ . However it can be estimated that  $3.1 \cdot 10^{-3} < \alpha < 5.2 \cdot 10^{-3}$  (W/m °C<sup>2</sup>), ( $\alpha$ -value from laboratory tests is  $\alpha = 3.75 \cdot 10^{-3}$  (W/m °C<sup>2</sup>)). A variation of  $\alpha$  within this interval does not influence the computed value of  $\lambda_0$  very much.

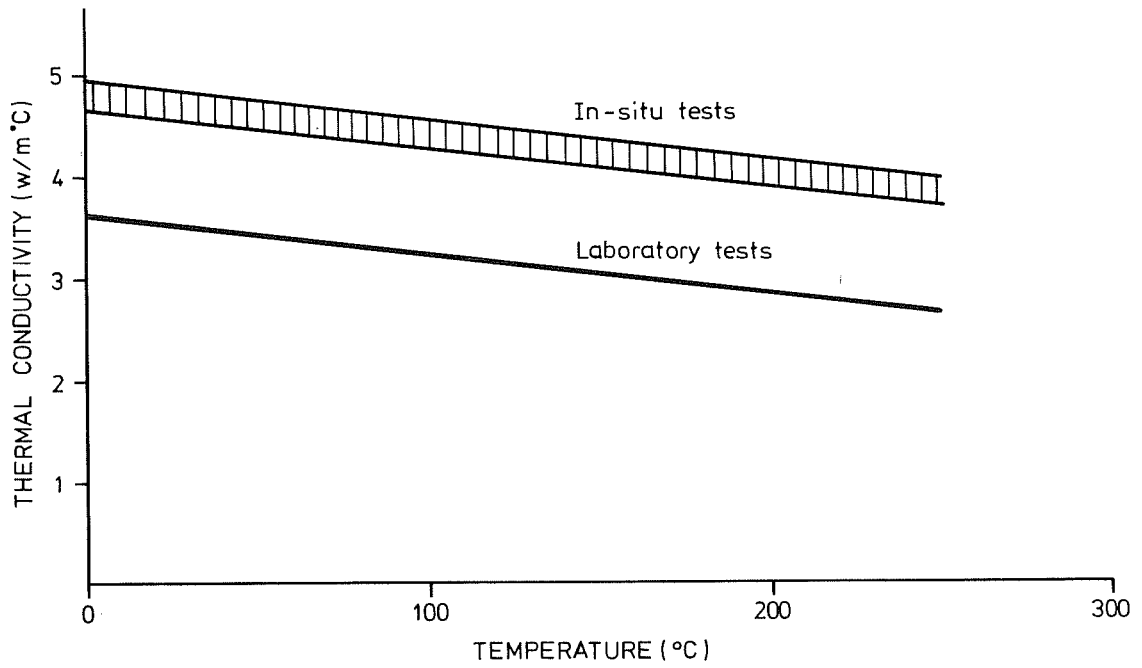
In order to estimate the error due to temperature differences between heater and rock, the temperature at  $r = 0.15$ , used in the initial solution, was varied within a wide range. No serious influence on computed  $\lambda_0$ -values occurred. The computed values and values from laboratory tests are shown in Fig A.3.1.

3

## CONCLUSION

It is reasonable to believe that the thermal conductivity of the rock mass will be volume dependent, since fractures will obstruct the heat conduction throughout the rock mass and decrease the conductivity. Thus, the rather high values, evaluated for conduction in situ can not be explained as a volume effect. The deviation seems too large to be explained as errors due to the mathematical model and the way it is used.

A possible explanation for the discrepancy is that heat is transferred due to convection of ground water. The numerical model does not include convection and the heat transport will thus appear as a false increase of thermal conductivity. However, the laboratory determined value,  $\lambda \sim 3.4 \text{ W/m } ^\circ\text{C}$ , used in Appendix I for prediction of temperatures during the heating phase, gave quite good agreement with in situ temperature readings. This indicates that the heating cycle has caused an increase of either thermal conductivity or water permeability.



XBL 788-10248

Fig A.III.1 Thermal conductivity from laboratory tests and in situ tests. The same temperature dependency has been assumed for both cases.

## 4 REFERENCES

- [1] Ames, W.F. Nonlinear Partial Differential Equations in Engineering, Academic Press, New York, 1965
- [2] Ames, W.F. Numerical Methods for Partial Differential Equations. Academic Press, New York, 1977
- [3] Courant, R. and Hilbert, D. Methods of Mathematical Physics. Interscience, New York, 1962
- [4] Pratt, H.R., Schrauf, T.W., Bills, L.A. and Hustrulid, W.A. Thermal and mechanical properties of granite, Stripa, Sweden. Terra Tek, Salt Lake City, USA, 1977

This report is part of a cooperative Swedish-American project supported by the U.S. Department of Energy and/or the Swedish Nuclear Fuel Supply Company. Any conclusions or opinions expressed in this report represent solely those of the author(s) and not necessarily those of The Regents of the University of California, the Lawrence Berkeley Laboratory, the Department of Energy, or the Swedish Nuclear Fuel Supply Company.

Reference to a company or product name does not imply approval or recommendation of the product by the University of California or the U.S. Department of Energy to the exclusion of others that may be suitable.

TECHNICAL INFORMATION DEPARTMENT  
LAWRENCE BERKELEY LABORATORY  
UNIVERSITY OF CALIFORNIA  
BERKELEY, CALIFORNIA 94720